Dimet

Ph.D. Program
Translational and Molecular Medicine

XXXII ciclo

Mitochondrial diseases related to mtDNA in childhood: genotype-phenotype correlation and characterization of novel phenotypes

Dottorando: Anna Ardissone

Tutor: Valeria Tiranti

Table of Contents

Chapter 1. General Introduction

Mitochondrial diseases (MD) are a group of rare inherited disorders characterized by extreme phenotypic heterogeneity often times with a rapidly progressive and devastating disease course.

MD alone are quite rare but, if taken as a whole, they are the most common genetic diseases in humans with a prevalence of about 1 out of 5000 individuals in the European population. Clinical manifestations of mitochondrial diseases are mainly related to ATP production in organs and tissues, especially where and when energy need is high, and this is the case for nerve cells and muscle fibers. This explains why mitochondrial disorders mainly involve central nervous system, skeletal muscle and heart.

However, mitochondrial pathology is, by definition, a multisistemic pathology involving many other tissues and / or organs such as liver, kidney, optic nerve, hematopoietic system, and endocrine system.

In childhood, clinical manifestations may include slowing or stopping of static-weight growth, psychomotor delay or regression, epilepsy, complex neurological signs, myopathy, optical atrophy and deafness.

In neurological terms, different clinical phenotypes may be distinguished (DiMauro et al 2012, Ardissone et al 2014): Leigh syndrome, Leucoencephalopathy, poliodystrophy (often associated with hepatic disease, as in Alpers disease).

From a medical standpoint, MD are often suspected on the basis of peculiar clinical presentations, but the diagnostic workup is often complex and difficult, requiring extensive clinical and laboratory evaluation. It can include careful clinical examination, instrumental and neuroimaging findings evaluation, bioumoral exams (e.g.. lactate in plasma and CSF, aminoacids, urin organic acids), immunohistochemical and histoenzymatic analyses, and biochemical investigation e.g. measurement of respiratory chain complex activity in cultured skin fibroblasts or skeletal muscle biopsy.

The classification of MD reflects the peculiar feature of the oxidative phosphorylation system of being formed by proteins encoded by two different genomes: mitochondrial genome (mtDNA) and nuclear genome (nDNA): most of the proteins required for the biogenesis, structure and function of mitochondria are encoded by genes contained in nDNA but 13 essential subunits of four of the five canonical respiratory-chain complexes are encoded by a physically separated, semi-autonomous, genome, the mtDNA (DiMauro et al 2003, Ghezzi et al 2012, Schon et al 2012). Unlike nDNA, which has a diploid organization (i.e. two copies) within the nucleus of somatic cells, and a haploid organization (i.e. one copy) in

gametes, mtDNA is present in multiple copies within the mitochondria of each cell. Human mtDNA is a circular, double-stranded molecule, 16,569 base pairs in size, which encodes 37 genes, including 22 tRNAs and 2 rRNAs encoding genes essential for mtDNA-specific translation of the 13 genes encoding as many respiratory chain subunits. In contrast to the double nuclear gene copies, that are called paternal and maternal alleles, present in human nuclei, there are hundreds of mtDNA molecules contained in each cell. In a normal individual, all the mtDNA molecules are identical, a condition called homoplasmy. Deleterious mtDNA mutations generally strike only a fraction of the mitochondrial genomes of an individual, leading to the coexistence in cells and tissues of two mtDNA populations, one normal and one mutated. This condition is called heteroplasmy. However, it is only when the mutated genomes reach a critical threshold over the normal genomes, that an effective reduction of OXPHOS activity occurs and thus the clinical manifestations of disease

Approximately 15–30% of disease causing-variants are found in the mtDNA (Ohtake et al., 2014;Tucker et al., 2010), whereas the majority of cases are caused by pathogenic variants in nDNA encode proteins necessary for mitochondrial maintenance and function (mtDNA replication and ex-pression), mitochondrial shape and dynamics (fission and fusion),Coenzyme Q10 (CoQ10) biosynthesis and the complex network con-trolling RC formation, activity and turnover (Herrmann et al., 2012;Calvo et al., 2016). In fact, all of these

genes should be considered as potential candidates for MD, and pathogenic variants in 309 of them have already been established to play a causative role (Stenton and Prokisch, 2018). However, a substantial fraction of patients suffering from MD are classified on the basis of clinical, neuroimaging and biochemical features, and lack a molecular diagnosis (Chinnery, 2000),despite the gold standard for definitive diagnosis is based on the identification of the underlying genetic defect. Recent advances in nextgeneration sequencing (NGS) technologies have become an invaluable tool to rapidly analyze known disease genes and to search for pathogenic variants in new candidate genes. NGS applications offer a wide range of approaches to screen patients with suspected MD, including targeted gene panel sequencing, clinical exome panel (~5.000 clinically relevant genes) and whole exome sequencing (WES).These technologies are contributing to fill the gap between clinical and biochemical mitochondrial disease diagnosis and their respective molecular genetic characterization (Legati et al., 2016).

Childhood phenotypes are often associated with nDNA mutations; using NGS we have identified causative genes of undefined cases and in collaboration with other centers we contributed to the definition of phenotype associated with the new identified disease genes.

The application of this technique has also been extended to the study of mtDNA: even if more than 100 mutations and deletions

in mtDNA have been described in association with an extremely heterogeneous spectrum of clinical presentations, only a few of them are associated with well-defined clinical syndromes in childhood. We performed a systematic evaluation of clinical, instrumental, metabolic and biochemical data of a large cohort of patients affected by the most common MD in childhood: Leigh syndrome. We analyzed in this population, genotype-phenotype correlation in nDNA and mtDNA gene associated cases in order to identify diagnostic clues for mtDNA related Leigh syndrome.

In genetically unresolved cases and various phenotypes (Leigh syndrome, leukodystropy..), we performed mtDNA screening using NGS technologies in order to assess, with high accuracy, point mutations and single or multiple large deletions, both in homoplasmic or heteroplasmic state. We identified both novel and known mutations associated to unexpected phenotype (i.e. CO3 gene). Our data better define and expand the phenotypic spectrum of mtDNA-MD in childhood.

Scope of the thesis

To identify the underlying molecular defects in patients clinically and biochemically suspected of MD, using a NGS strategy for mitochondrial diseases diagnosis studing both nDNA and mtDNA and define phenotype-genotype correlation.

References

- S. DiMauro, V. Emmanuele The clinical spectrum of Nuclear DNA-Related Mitochondrial Disorders
L.J. Wong (Ed.), Mitochondrial Disorders Caused by Nuclear Genes, Springer, New York (2012), pp. 3-26
- Anna Ardissone , Eleonora Lamantea, Federica Invernizzi , Silvia Genitrini, Isabella Moroni Graziella Uziel Mitochondrial diseases in childhood- Review Current Molecular Medicine 14(8), pp. 1069-1078
- S. DiMauro, E.A. Schon Mitochondrial respiratory-chain diseases N. Engl. J. Med., 348 (26) (Jun 26 2003), pp. 2656-2668
- D. Ghezzi, M. Zeviani Assembly factors of human mitochondrial respiratory chain complexes: physiology and pathophysiology Adv. Exp. Med. Biol., 748 (2012), pp. 65-106
- E.A. Schon, S. Dimauro, M. Hirano Human mitochondrial DNA: roles of inherited and somatic mutations
Nat. Rev. Genet., 13 (2012), pp. 878-890
- A. Ohtake, K. Murayama, M. Mori, H. Harashima, T. Yamazaki, S. Tamaru, Y. Yamashita, Y. Kishita, Y. Nakachi, M. Kohda, Y. Tokuzawa, Y. Mizuno, Y. Moriyama, H. Kato, Y. Okazaki Diagnosis and molecular basis of mitochondrial respiratory chain disorders: exome sequencing for disease gene identification Biochim. Biophys. Acta, 1840 (2014), pp. 1355-1359

- E.J. Tucker, A.G. Compton, D.R. Thorburn Recent advances in the genetics of mitochondrial encephalopathies Curr. Neurol. Neurosci. Rep., 10 (2010), pp. 277-285

- Herrmann et al., 2012 J.M. Herrmann, S. Longen, D. Weckbecker, M. Depuydt

Biogenesis of mitochondrial proteins Adv. Exp. Med. Biol., 748 (2012), pp. 41-64

-S.E. Calvo, K.R. Clauser, V.K. Mootha MitoCarta2.0: an updated inventory of mammalian mitochondrial proteins Nucleic Acids Res., 44 (2016), pp. D1251-D1257

-S.L. Stenton, H. Prokisch Advancing genomic approaches to the molecular diagnosis of mitochondrial disease Essays Biochem., 62 (3) (2018), pp. 399-408

- P.F. Chinnery Mitochondrial disorders overview M.P. Adam, H.H. Ardinger, R.A. Pagon, et al. (Eds.), Gene Reviews (Internet), University of Washington, Seatle, WA (2000)

- A. Legati, A. Reyes, A. Nasca, F. Invernizzi, E. Lamantea, V. Tiranti, B. Garavaglia, C. Lamperti, A. Ardissone, I. Moroni, A. Robinson, D. Ghezzi, M. Zeviani New genes and pathomechanisms in mitochondrial disorders unraveled by NGS technologies

Biochim. Biophys. Acta, 1857 (2016), pp. 1326-1335

Chapter 2

COA7 (C1orf163/RESA1) mutations associated with mitochondrial leukoencephalopathy and cytochrome c oxidase deficiency.

Martinez Lyons A, Ardissone A, Reyes A, Robinson AJ, Moroni I, Ghezzi D, Fernandez-Vizarra E, Zeviani M.

Journal of Medical Genetics 2016 Dec 53(12), pp. 846-849

Introduction

Cytochrome c oxidase (COX) is the terminal component of the mitochondrial respiratory chain (MRC). COX transfers four electrons from cytochrome c to oxygen. The energy liberated by this redox reaction sustains the translocation of four protons from the matrix to the intermembrane space (IMS) and contributes to the formation of the mitochondrial electrochemical gradient. In humans, COX deficiency can be either isolated or combined to defects in other MRC complexes. Phenotypes may vary[1] ,[2] from multisystem disorders to isolated myopathies or encephalopathies.[3] ,[4] Isolated COX deficiency may be caused by mutations in mitochondrial DNA (mtDNA) or nuclear DNA genes encoding structural COX subunits, but in

most cases is due to recessive mutations in nuclear genes encoding factors involved in COX biogenesis.[5] COA7 is a putative COX assembly factor containing five Sel1-like repeat domains (Interpro IPR006597), is conserved in animals, but neither in plants nor in fungi, and has been reported to localise in the mitochondrial IMS.[6] Here, we describe the first biallelic pathogenic *COA7* mutations in a patient with isolated COX deficiency and leukoencephalopathy, and show that the protein is localised in the inner mitochondrial compartment, predominantly in the matrix.

Case report

The proband is a 19-year-old woman, first child of healthy unrelated parents. Her family history was unremarkable. She was born at term after a normal pregnancy. The perinatal period was uneventful and her early development was referred to as normal, but after 1 year of age, psychomotor delay became evident. She started walking autonomously at 22 months, with poor balance and frequent falls. At 3 years of age, she developed a demyelinating sensorimotor neuropathy and a brain MRI disclosed supratentorial leukodystrophy. During her childhood, the clinical signs remained stable. At 10 years, her walking difficulties worsened, and limb weakness and tremor ensued. The neurological evaluation showed dysarthria, dysmetria, ataxic gait and hyporeflexia in the four limbs with muscle wasting. She was able to walk alone only for a few steps with an ataxic gait. Mild cognitive impairment was documented (IQ 75, WISC-R scale). Histological analysis of a

muscle biopsy showed hypo/atrophy of fibres. The clinical evolution was slowly progressive. At her last follow-up examination, at 19 years of age, she was able to walk alone only with ankle-foot orthotic aids and had developed a marked dorsal-lumbar scoliosis. Other clinical signs were stable. Neurophysiological studies confirmed worsening of her mixed axonal demyelinating peripheral neuropathy. Brain and spinal cord MRI showed mild extension of signal abnormalities and extensive cavitations in the cerebral white matter; the cerebellum and brainstem were spared but the spinal cord was thin with no obvious focal lesions (figure 1A). Plasma lactate was 2.9 mM (n.v. <2.1).

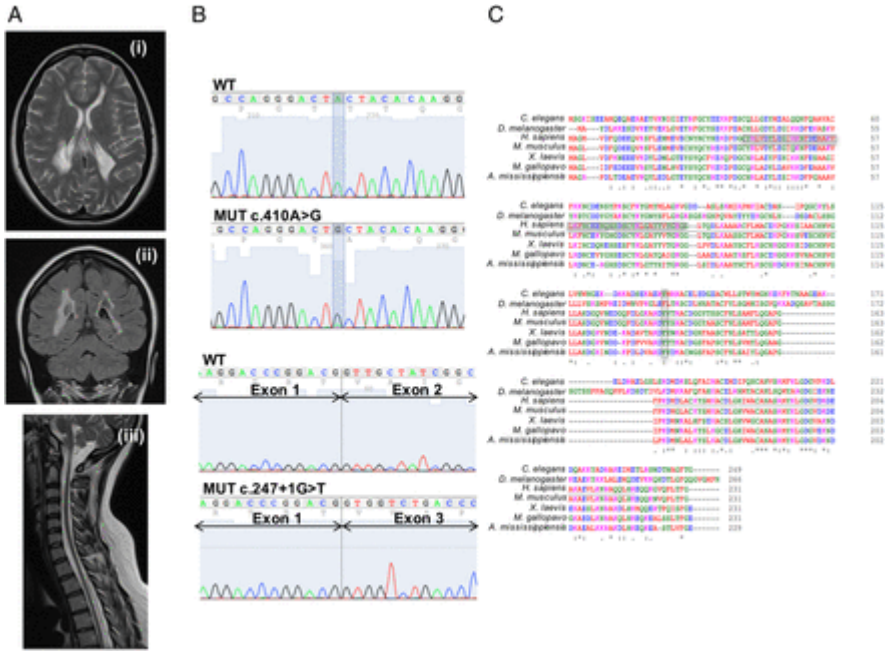

Figure 1

Clinical and genetic findings. (A) Transverse supratentorial (i), coronal (ii) and sagittal brain/spinal cord (iii) T2- fluid attenuated inversion recovery (FLAIR) MRI sequences. (B) Sanger sequence of the mutated regions in

cDNA from mutant fibroblasts. (C) Clustal W diagram. Boxed areas correspond to mutations. Sel1-like conserved domains are underlined.

Methods

Whole exome sequencing (WES) was performed as described.[7] Fibroblasts from skin biopsies were immortalised by lentiviral transduction using the pLOX-Ttag-iresTK vector (Tronolab, Addgene #12246). Primary and immortalised fibroblasts and HEK293T cells were grown in standard conditions. For mitochondrial localisation studies, mitochondria and mitoplasts were prepared and trypsin-digested as previously described.[8] ,[9] For membrane association studies, sonicated mitochondrial supernatants containing the soluble fractions were separated from the membrane-enriched pellets by ultracentrifugation. Membrane-containing pellets were treated with increasing ionic strength buffers, and for the final protein dissociation, they were suspended in equal volumes of isotonic buffer containing 0.2% SDS. These fractions were analysed by western-blot (WB) immunodetection, using several proteins as markers of distinct mitochondrial compartments.

The COA7 cDNA sequence was obtained from the IMAGE clone (ID: 4430419/IRATp970-0D0921D). PCR products were cloned into the lentiviral vector pWPXLd-ires-Puro^R (derived from pWPXLd, Tronolab, Addgene #12258). Lentiviral particle production and transduction of target cells were performed as recommended (https://www.addgene.org/tools/protocols/plko/#E).

Sodium dodecyl sulphate polyacrylamide gel electrophoresis (SDS-PAGE) and blue native gel electrophoresis (BNGE) were

performed as described.[10] Antibodies were purchased from Proteintech, Abcam and Sigma.

MRC and other enzymatic activities were measured as described.[11] ,[12]

Results

Biallelic mutations in COA7 are present in the proband

This study was approved by the Ethical Committee of the 'Carlo Besta' Neurological Institute, Milan, Italy, in agreement with the Declaration of Helsinki. Informed consent was signed by the parents of the patient. We ruled out the presence of pathogenic mutations in mtDNA by Sanger sequencing. WES[7] was then carried out. After standard filtering steps and assuming a recessive trait, we prioritised 13 genes with either one homozygous variant or two heterozygous variants. Of these 13 genes, the only one encoding a mitochondria-targeted protein was *COA7*,[6] which carried a (paternal) heterozygous nucleotide transition c.410A>G (NM_023077), p.Y137C and a (maternal) heterozygous G>T transversion affecting the first intronic nucleotide of the exon 2/intron 2 junction (c.287+1G>T). The two variants were not reported in the ExAc database (March 2016). The presence of both mutations was validated by Sanger sequencing.

COA7 mutations are associated with absence of the COA7 protein

Amplification of the patient *COA7* cDNA yielded two bands. The upper band, which had the same size as that amplified from control samples, showed the c.410A>G paternal missense

mutation. The lower band was originated from the maternal allele containing the c.287+1G>T-splicing mutation, which produces the deletion of the whole 141bp-long exon 2 of *COA7* (figure 1B). The missense mutation affects the highly conserved Tyr_{137}, which is replaced by a non-conservative Cys residue, whereas the splice site mutation produces the in-frame deletion of the 47 amino acids encoded by exon 2. This deletion spans almost all of the first conserved Sel1-like domain and half of the second (figure 1C).

Next, total protein lysates extracted from patient-derived cells were analysed by WB using a specific anti-COA7 antibody. No COA7 cross-reacting material was immunodetectable, and the amount of two COX structural subunits (MT-CO2 and MT-CO3) was reduced in the mutant sample, relative to control cells, whereas that of subunits belonging to complex I and complex III was normal (figure 2A).

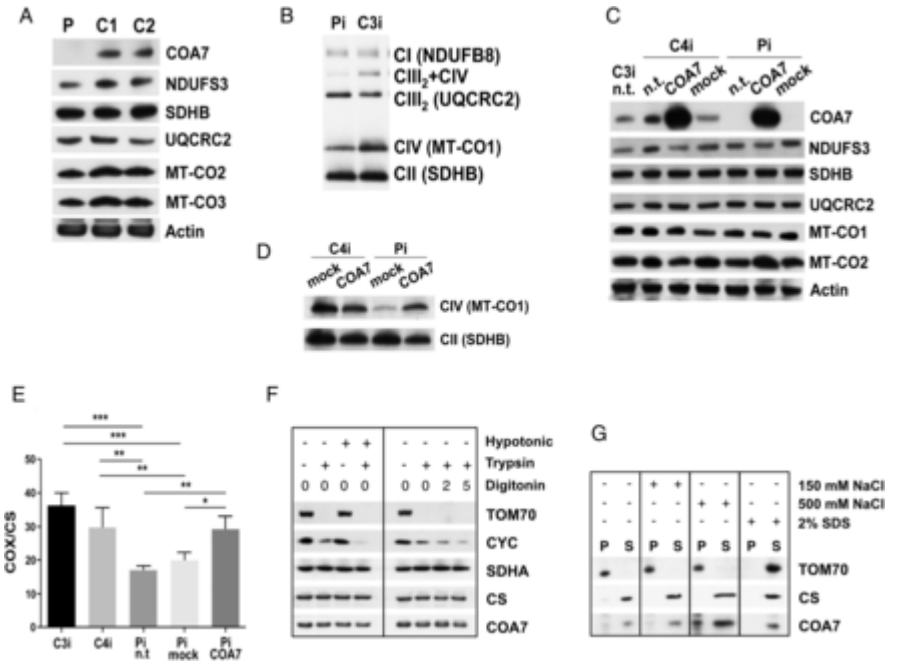

Figure 2

*Western blot (WB) immunodetection and enzymatic activities. (A) WB immunodetection of SDS-PAGE in primary fibroblasts. P, patient, C1 and C2, control cell lines. (B) WB immunodetection of BNGE in immortalised patient (Pi) and control (C3i) fibroblasts. Immunovisualised subunits are between brackets. (C) WB immunodetection of SDS-PAGE in immortalised patient fibroblasts (Pi) and a control (C4i). n.t., not transduced; mock, transduced with empty vector; COA7, transduced with COA7. (D) WB immunodetection of BNGE in COA7-transduced immortalised fibroblasts from patient (Pi) and a control (C4i). (E) Cytochrome c oxidase (COX)/citrate synthase (CS) activity in immortalised fibroblasts of two controls (C3i, C4i), and the patient (Pi). Vertical bars indicate SEM. Statistical analysis was by ANOVA (*p<0.05; **p<0.01; ***p<0.001). (F) WB immunodetection of SDS-PAGE of mitochondria and mitoplasts from HEK293T cells. (G) WB immunodetection of SDS-PAGE of soluble and membrane fractions from intact mitochondria. ANOVA, analysis of variance.*

COX activity and assembly are recovered after expression of wild-type COA7

In patient-derived immortalised fibroblasts, the levels of fully assembled cIV and of the $cIII_2$+cIV supercomplex were clearly lower relative to controls (figure 2B).

In order to test complementation, wild-type (wt) *COA7* (*COA7*^{wt}) was transduced in immortalised mutant fibroblasts. Robust overexpression of *COA7*^{wt} was detected in both mutant and wt transduced cells, and, in mutant cells, this was associated with the recovery of normal amount of MT-CO2 subunit (figure 2C) and of both COX assembly (figure 2D) and activity (figure 2E).

COA7 is localised in the mitochondrial matrix

To further characterise COA7, we isolated mitochondria from HEK293T cells and performed WB analysis in organellar and suborganellar fractions. Trypsin digestion was carried out in both intact mitochondria or after stripping off the outer mitochondrial membrane (mitoplasts), by either hypotonic shock or digitonin treatment. The outer membrane protein TOM70 was completely digested by trypsin in mitochondria and mitoplasts; the IMS protein cytochrome c was protected in mitochondria but progressively digested in mitoplasts, whereas the inner membrane protein succinate dehydrogenase subunit A (SDHA) (part of cII) and the matrix protein citrate synthase were protected from digestion in both mitochondria and mitoplasts, as was COA7 (figure 2F). Next, mitochondria were disrupted by sonication, and the ionic strength was increased by adding NaCl to soluble versus membrane fractions. As shown in figure 2G, COA7 was predominantly immunodetected in the supernatant, similar to citrate synthase, although a small

percentage was also detected in the pellet, before SDS treatment. Taken together, these results indicate that COA7 is predominantly localised in the mitochondrial matrix, although a small aliquot appears to be associated with the inner mitochondrial membrane.

Discussion

COA7 is involved in MRC biogenesis, as depletion by RNAi in cultured cells clearly affected COX assembly.[6] Here, we present the first pathological mutations in *COA7* in humans, associated with a severe, slowly progressive mitochondrial neurological disorder. We found biallelic mutations in one patient, according to the autosomal recessive mode of inheritance suggested by the patient's family tree. The *COA7* mRNA skipping of exon 2 in the maternal allele and the drastic amino acid change in the paternal allele suggested pathogenicity. Indeed, WB immunodetection showed the virtual absence of the protein in cultured cells. Furthermore, the expression of $COA7^{wt}$ restored COX assembly and activity in mutant cells.

Our case was diagnosed as a mitochondrial encephalopathy and peripheral neuropathy. Although the onset was in infancy, the clinical course was slowly progressive, as the patient has reached adulthood in relatively stable conditions. This could be related to a partially dispensable role of COA7 in COX biogenesis.

Finally, our suborganellar fractionation studies, supported by in vitro import results, indicate that COA7 localises in the mitochondrial inner compartment, mostly in the matrix, rather

than in the IMS, as previously proposed.[6] We suggest that the proposed localisation to the IMS was in fact the consequence of a incorrect interpretation of results similar to ours, that is, protection of COA7 from proteinase K-treated mitoplasts, thus indicating its localisation within the inner mitochondrial compartment.[6]

Future work is warranted to establish the interactions and partners of COA7, its mechanisms of action and the steps of its intervention during the formation of COX.

References

Shoubridge EA. Cytochrome c oxidase deficiency. Am J Med Genet
2001;106:46–52.

2 DiMauro S, Tanji K, Schon EA. The many clinical faces of cytochrome c oxidase
deficiency. Adv Exp Med Biol 2012;748:341–57.

3 Zeviani M, Carelli V. Mitochondrial disorders. Curr Opin Neurol 2007;20:564–71.

4 Zeviani M, Di Donato S. Mitochondrial disorders. Brain 2004;127(Pt 10):2153–72.

5 Rak M, Benit P, Chretien D, Bouchereau J, Schiff M, El-Khoury R, Tzagoloff A,
Rustin P. Mitochondrial cytochrome c oxidase deficiency. Clin Sci (Lond)
2016;130:393–407.

6 Kozjak-Pavlovic V, Prell F, Thiede B, Gotz M, Wosiek D, Ott C, Rudel T. C1orf163/

RESA1 is a novel mitochondrial intermembrane space protein connected to
respiratory chain assembly. J Mol Biol 2014;426:908–20.
7 Legati A, Reyes A, Nasca A, Invernizzi F, Lamantea E, Tiranti V, Garavaglia B,
Lamperti C, Ardissone A, Moroni I, Robinson A, Ghezzi D, Zeviani M. New genes
and pathomechanisms in mitochondrial disorders unraveled by NGS technologies.
Biochim Biophys Acta 2016;1857:1326–35.
8 Gai X, Ghezzi D, Johnson MA, Biagosch CA, Shamseldin HE, Haack TB, Reyes A,
Tsukikawa M, Sheldon CA, Srinivasan S, Gorza M, Kremer LS, Wieland T, Strom
TM, Polyak E, Place E, Consugar M, Ostrovsky J, Vidoni S, Robinson AJ, Wong LJ,
Sondheimer N, Salih MA, Al-Jishi E, Raab CP, Bean C, Furlan F, Parini R, Lamperti
C, Mayr JA, Konstantopoulou V, Huemer M, Pierce EA, Meitinger T, Freisinger P,
Sperl W, Prokisch H, Alkuraya FS, Falk MJ, Zeviani M. Mutations in FBXL4,
encoding a mitochondrial protein, cause early-onset mitochondrial
encephalomyopathy. Am J Hum Genet 2013;93:482–95.
9 Reyes A, He J, Mao CC, Bailey LJ, Di Re M, Sembongi H, Kazak L, Dzionek K,

Holmes JB, Cluett TJ, Harbour ME, Fearnley IM, Crouch RJ, Conti MA, Adelstein RS,
Walker JE, Holt IJ. Actin and myosin contribute to mammalian mitochondrial DNA
maintenance. Nucleic Acids Res 2011;39:5098–108.
10 Calvaruso MA, Smeitink J, Nijtmans L. Electrophoresis techniques to investigate
defects in oxidative phosphorylation. Methods 2008;46:281–7.
11 Tiranti V, Munaro M, Sandona D, Lamantea E, Rimoldi M, DiDonato S, Bisson R,
Zeviani M. Nuclear DNA origin of cytochrome c oxidase deficiency in Leigh's
syndrome: genetic evidence based on patient's-derived rho degrees transformants.
Hum Mol Genet 1995;4:2017–23.
12 Kirby DM, Thorburn DR, Turnbull DM, Taylor RW. Biochemical assays of respiratory
chain complex activity. Methods Cell Biol 2007;80:93–119.

Chapter 3

Novel mutations in IBA57 are associated with leukodystrophy and variable clinical phenotypes

Torraco A, Ardissone A, Invernizzi F, Rizza T, Fiermonte G, Niceta M, Zanetti N, Martinelli D, Vozza A, Verrigni D, Di Nottia M, Lamantea E, Diodato D, Tartaglia M, Dionisi-Vici C, Moroni I, Farina L, Bertini E, Ghezzi D, Carrozzo R.

Journal of Neurology 2017 Jan 264(1), pp. 102-111

Introduction

Leukodystrophies are heterogeneous disorders of the white matter, caused by a variety of genetic defects [1]. Mitochondria have been found to be essential for the white matter that is involved in several mitochondrial syndromes caused by defects of either mitochondrial DNA (mtDNA)

or nuclear genes encoding for respiratory chain complexes (RCC) subunits or assembly factors [2, 3]. Moreover, mutations in several nuclear genes involved in mtDNA maintenance, such as MPV17 and POLG, or, as recently reported, encoding for mitochondrial aminoacyl tRNA synthetases, such as DARS2, AARS2 and EARS2 may also affect the white matter [4–7].

A new class of mitochondrial diseases presenting with white matter abnormalities and multiple respiratory chain disorders has been classified as multiple mitochondrialdysfunction syndrome (MMDS). To date, there are four classes of MMDS: MMDS1 (#605711) due to mutations in NFU1 [8, 9], MMDS2 (#614299) with mutations in BOLA3 [9, 10], MMDS3 (#615330) associated with mutations in IBA57 [11] and MMDS4 (#616370) with mutations in ISCA2 [12]. Common features of all these MMDS are the involvement of a gene encoding for a protein implicated in the mitochondrial Fe/S cluster assembly process [13]. Here, we describe four patients carrying novel mutations in IBA57 (MIM# 615316) that encodes for a protein acting in the last steps of the mitochondrial Fe/S biogenesis pathway, involved in the insertion in recipient proteins of the cubane form of the Fe/S clusters, i.e., [4Fe-4S] clusters.

Interestingly, all patients presented white matter degeneration with a different severity degree, making this feature a hallmark that frequently occurs in MMDS.

Methods

Standard protocol approvals, registrations and patients consents The study was approved by the Ethical Committees of the Bambino Gesu` Children's Hospital, Rome, Italy, and the ''Besta'' Neurological Institute, Milan, Italy, in agreement with the Declaration of Helsinki. Informed consent was signed by the parents of the patients.

Biochemical and protein studies

RCC and citrate synthase activities were assayed on muscle homogenate using a previously reported spectrophotometric method [14]. Complex V activity (in the direction of ATP synthesis) was measured in fibroblast mitochondria of patients and age-matched controls, using reported spectrophotometric methods. Either succinate, malate or pyruvate malate were used as substrates [15]. The aketoglutarate dehydrogenase complex (KGDHc), pyruvic dehydrogenase complex (PDHc) and a-branched-chain keto acid dehydrogenase complex (BCKDHc) enzymatic activities were assayed essentially as previously described [16, 17].

For structural studies, fibroblast mitochondria were processed as described elsewhere [18] and 40–80 lg of proteins were loaded on linear 5–12 % gradient gel for first dimensional blue native gel electrophoresis (BNGE).

BNGE was later, either subjected to in-gel activity assay (IGA) as previously described [19] or processed for Western Blotting (WB) analysis. For SDS-PAGE, 35–45 lg of fibroblast mitochondria were loaded in a 12 % denaturing gel. WB of either BNGE or SDS-PAGE was performed by transferring

proteins onto polyvinylidene difluoride (PVDF) membrane and probed with specific antibodies.

Reactive bands were detected using Lite Ablot Extend Long Lasting Chemiluminescent Substrate (Euroclone, Pero (Mi), Italy). Densitometry analysis was performed using Quantity One software (BioRad, Hercules, CA, USA).

Antibodies

RCC subunits were detected using the following monoclonal antibodies purchased from MitoScience (Eugene, OR, USA): Complex I—NDUFS1, NDUFA9; complex II—SDHA, SDHB; complex III—UQCRC2, UQCRFS1; complex IV—COXIV; porin (VDAC). Anti-lipoic acid (Abcam), anti-mACO (Novus Biologicals), anti-ISCA1 (Abnova) antibodies were commercially available while anti-IBA57 and anti-ISCA2 antibodies were a kind gift of Dr. R. Lill.

Molecular studies

Genomic DNA was isolated from blood and cultured skin fibroblasts using QIAamp DNA mini kit (QIAGEN, Valencia, CA, USA). For Pt.1 and Pt.2 targeted resequencing was outsourced at the BGI-Shenzhen (BGIShenzhen, Shenzhen, China). A custom probe library was used for targeted enrichment (Agilent SureSelectXT Custom Kit) designed to capture coding exons and flanking intronic stretches (20 nt) of 1381 genes encoding for mitochondrial proteins (‘‘Mitoexome’’) [20], followed by deep sequencing using Illumina Hiseq technology, providing 255X effective mean depth. After excluding previously annotated single nucleotide changes occurring with high frequency in

populations (frequency[0.1 %), we prioritized variants predicted to have functional impact (i.e., nonsynonymous variants and changes affecting splice sites), taking into account a recessive inheritance model that together with the maternal transmission, represent the most common inheritance models of mitochondrial disorders. Particularly, only seven variants (four genes, ABCD1, GUF1, IBA57 and PPT1) for Pt.1, and four variants (two genes, PPM1J and IBA57) for Pt.2, were retained for further in silico predictions. After excluding those variants predicted as benign by both CADD, metaSVM algorithms, and after visual inspection of the alignments, IBA57 compound variants were selected as major pathogenic candidates. For Pt.3 and Pt.4, the coding exons and exon–intron boundaries of IBA57 were PCR-amplified using specific primers, cycle sequenced using BigDye chemistry 3.1 and run on an ABI 3130XL automatic sequencer (Applied Biosystems, Life Technologies

Results

Clinical features and Brain NMR findings

Pt.1 showed clinical signs since birth, whereas Pt.2, Pt.3 and Pt.4 presented disease onset after a normal psychomotor development and good health period. Pt.1, Pt.2 and Pt.4 developed a severe phenotype, followed by sudden death in Pt.1 and Pt.4. Only Pt.3, who presented a late onset, disclosed a slow neurological and general improvement and mild phenotype. Epilepsy was reported only in Pt.2 and Pt.3 several

years after disease onset. Treatment with riboflavin (100 mg/die) and CoQ10 (100 mg/die) was started in both patients.

Brain MRI showed a pattern of diffuse cavitating leukoencephalopathy where abnormalities were most prominent posteriorly and in the fronto-parietal regions including the upper part of the centra semiovalia under the pericentral cortex. Periventricular and deep white matter were prevalently affected with a variable involvement of the subcortical fibers. Only in Pt.3, who performed diffusion- weighted imaging (DWI) in the sub-acute stage, a high signal intensity suggesting diffusion restriction was detected in the non-cavitated white matter (Fig. 1n). In the acute phase, Pt.2 showed contrast enhancement in the affected deep white matter. Basal nuclei were always spared. Corpus callosum (Pt.1, Fig. 1a; Pt.2, Fig. 1i; Pt.3, Fig. 1m) and the posterior limb of internal capsulae (Pt.1, Fig. 1c; Pt.2, Fig. 1j; Pt.4, Fig. 1w) were involved in three cases at the first examination and in all at late MRI. At onset, three patients displayed the involvement of cerebellar white matter (Pt.1, Fig. 1b; Pt.2, not shown) and/or middle cerebellar peduncles (Pt.1, Fig. 1b; Pt.4, not shown); one patient (Pt.1) showed severe abnormalities in the brainstem (Fig. 1b) and upper cervical spinal cord as well.

In all patients, MRI follow-up showed an extension of signal abnormalities within hemispheric white matter and/or also in the corpus callosum, posterior arm of the internal capsulae, cerebellum, brainstem and cervical spinal cord (Fig. 1). In all patients but one (Pt.3) progressive rarefaction of the affected

white matter was seen with worsened of cavitations or appearance of small cysts (Fig. 1g, h, j, k, w, x). A variable degree of cerebral atrophy was observed in three patients (Pt.1, Fig. 1h; Pt.2, Fig. 1j, k, and Pt.3, Fig. 1r, s). In Pt.3, MRI showed appearance of signal abnormalities in the internal capsulae and of a small lesion in the cerebellar white matter. The patient had not brainstem abnormalities. Late cervical MRI demonstrated extensive signal abnormalities in the cervical spinal cord (Fig. 1t). In Pt.1, MRI showed new lesions in the thalami (Fig. 1g), red nuclei and increased signal abnormalities in the brainstem (Fig. 1e). In Pt.4, MRI follow-up has been performed in the sub-acute stage and showed mild progression of white matter involvement in the fronto-temporal regions, internal capsulae, middle cerebellar peduncles and brainstem. Signal abnormalities in the brainstem (Fig. 1v) and upper cervical spinal cord were noted. No atrophy was present. In Pt.2, late MRI showed disappearance of contrast enhancement in the affected white matter and involvement of long tracts within the brainstem and cervical spinal cord (Fig. 1l).

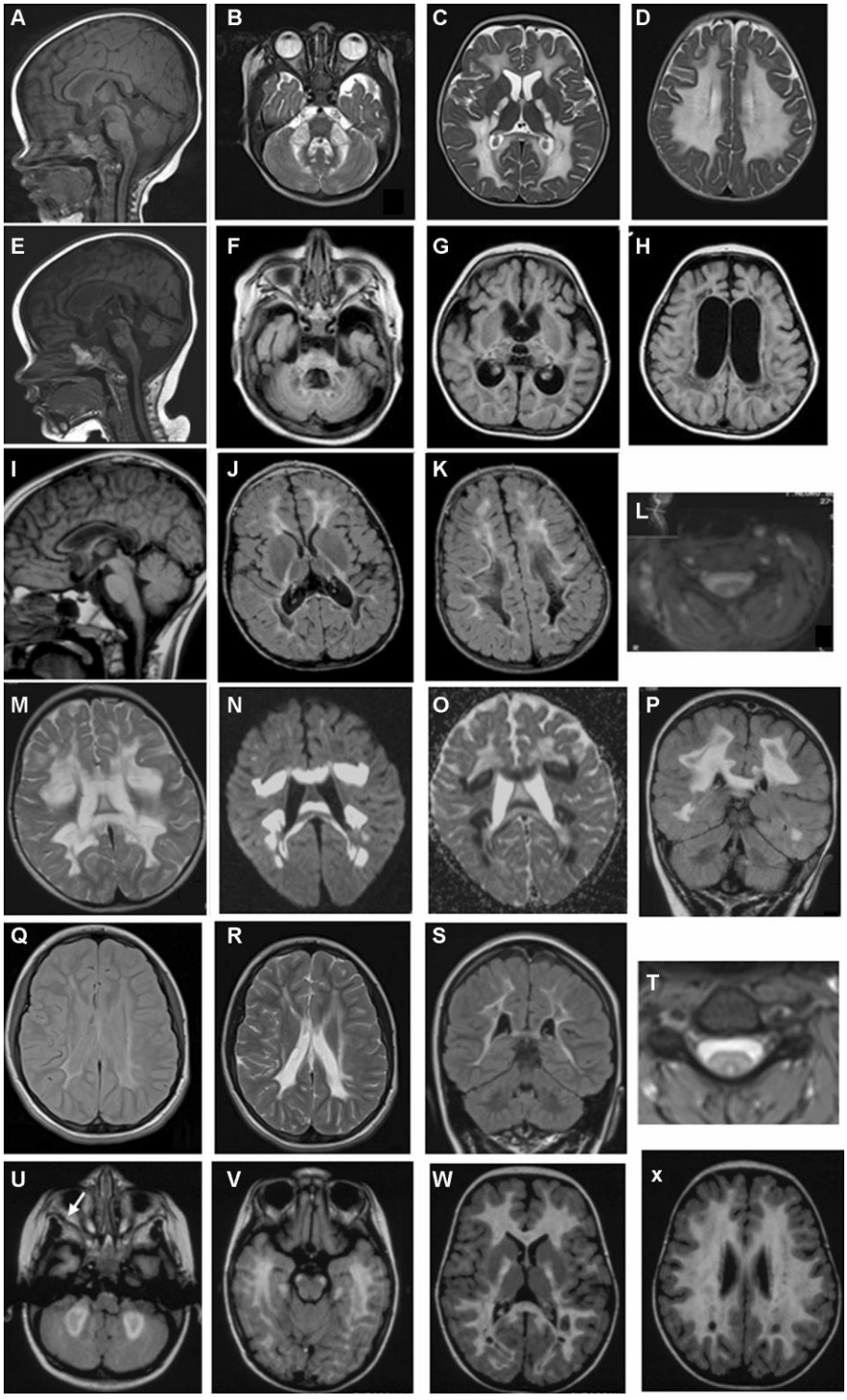
A
B
C
D
E
F
G
H
I
J
K
L
M
N
O
P
Q
R
S
T
U
V
W
x

Fig. 1 Pt.1: Sagittal T1-wi (a) and axial T2-wi (b–d) in the early stage; sagittal T1-wi (e) and axial FLAIR images (f–h) in the late stage. Hypointensities in the corpus callosum, brainstem and upper spinal cord (a). Signal abnormalities in the cerebral white matter also involved corpus callosum, posterior arm of the internal capsulae and middle cerebellar peduncles (b–d), cavitations in the internal capsulae (c). Marked white matter atrophy and cavitations with cystic degeneration (g, h). Additional lesions in brainstem (e), thalami (g) and corpus callosum and brainstem atrophy (e). Pt.2: Late MR, Sagittal T1-wi (i) Axial FLAIR images (j, k): diffuse leukoencephalopathy extended to the corpus callosum and posterior arm of the internal capsulae (i, j) cavitations marked posteriorly (j, k). Cervical MRI Axial T2-wi (l): signal abnormalities in the posterior column of the cervical spinal cord. Pt.3: Axial T2-wi (m–o), DWI (n), apparent diffusion coefficient (ADC) image, and coronal FLAIR image (p) in the acute phase; axial proton-density (q) and T2-wi (r), and coronal FLAIR image (s) in the late phase. Diffuse white matter signal abnormalities (m–o). Cavitations in the frontal (n) and parietal white matter (p); restricted diffusion in the non-cavitated white matter (n). White matter atrophy (q–s) U-fibers look spared (q). Additional hyperintensities in the cervical spinal cord (t). Pt.4: Late MR Axial
FLAIR images (u–x) diffuse involvement of hemispheric white matter extended to corpus callosum and internal capsulae (u–x). Rarefaction of the deep white matter (u, v) and appearance of small cysts (w, x); symmetric

Variants identification

A targeted resequencing was performed on Pt.1 and Pt.2. An in-house implemented pipeline, based on functional annotation (dbNSFP/WGSA framework), and recurrence in public (dbSNP142, 1000 Genomes, UK10K, ExAC) and inhouse databases combined filtering, was applied, leading to the identification of a single gene entry for both patients corresponding to IBA57 (NM_001010867.3; NP_00101086 7.1). In details, Pt.1 carried two heterozygous variants, c.586T[G (chr1:228174936) [p.W196G] and c.686C[T (chr1:228175128) [p.P229L], located in exon 2 and 3, respectively. Pt.2 presented

two heterozygous mutations, c.87ins_GCCCAAGGTGC (chr1: 228165903) [p.R30Afs*46] and c.313C[T (chr1:228166129) [p.R105W], both located in exon 1. Independently from theNGSstudy, a small cohort was screened by direct sequencing of the IBA57 gene, and two patients were positive. Pt.3 harbored a homozygous c.706C[T (chr1:228175148) [p.P236S] mutation in exon 3, whereas Pt.4 was compound heterozygous for the c.316A[G (chr1:228166132) [p.T106A] and c.757G[C (chr1:228175199) [p.V253L] variants located in exon 1 and 3, respectively (Supplementary Fig. 1). Sanger sequencing confirmed all the identified mutations, and for Pt.1, Pt.2 and Pt.3, their segregation within the families, being the parents heterozygous for a single IBA57 variant. DNA from Pt.4 parents was not available.

All variants were not reported in public (dbSNP142, ExAC, 1000 Genomes, UK10K) and in-house databases. Due to poor phylogenetic conservation of IBA57, all amino acids affected by the mutations found in our patients are not conserved in lower eukaryotes, but some of them result highly conserved amongst

vertebrates

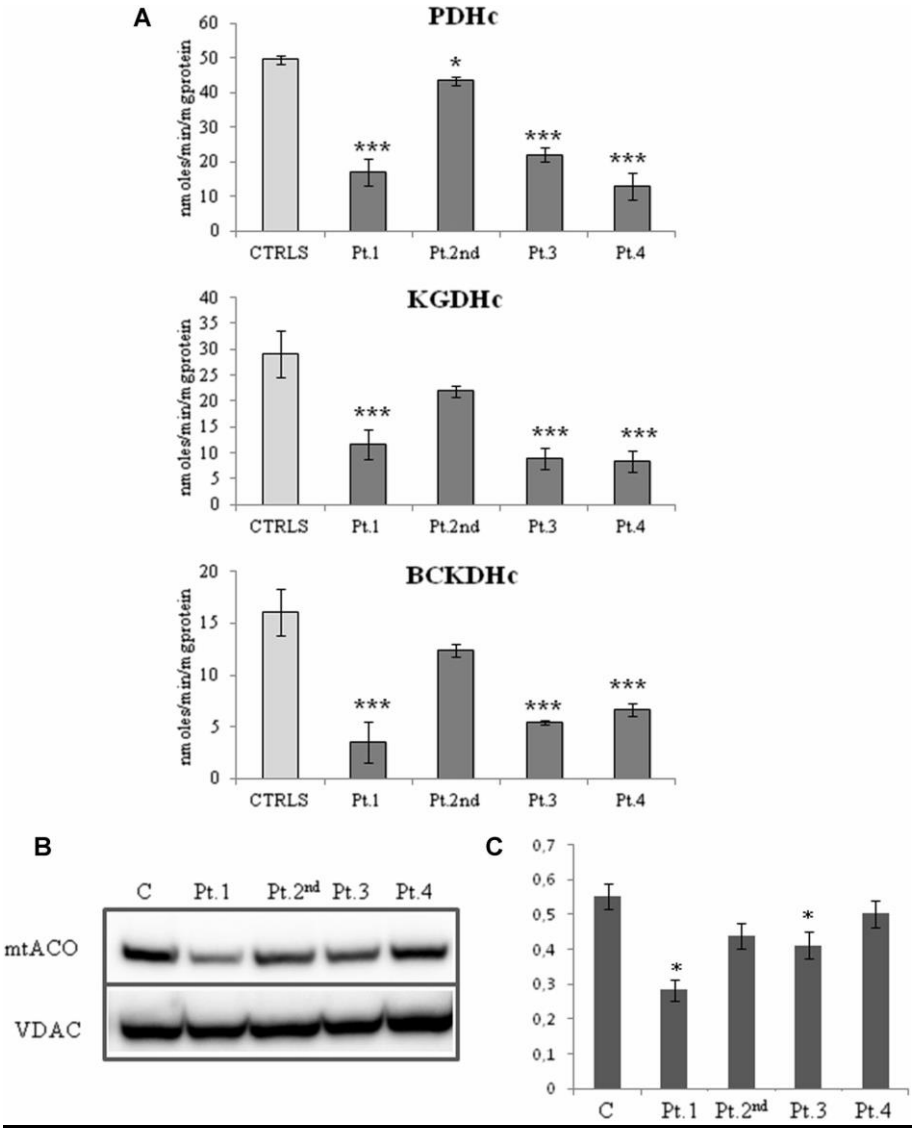

Fig. 2 a Effects of the mutations on the enzyme activities of three mitochondrial lipoylated dehydrogenases (PDHc, KGDHc, BCKDHc). The assays were performed on patients and control
mitochondria isolated from fibroblasts and following the NADH formation at 340 nm. The data represent the mean ± SD of three independent experiments in duplicate and were compared to the mean

Enzymatic findings

RCC activities of our patients, measured on either muscle specimens or fibroblast mitochondria, are summarized in supplementary Table 1. In our cohort, IBA57 deficiency was associated with severe impairment of the [4Fe-4S]cluster-containing enzymes in muscle specimen, i.e., RCCI or RCCII. Reduction of RCCII activity was reported also in fibroblasts mitochondria of Pt.2, derived from the first skin biopsy (Pt.1st) performed at thirty months of age, and of Pt.4, whereas RCC activities were normal in Pt.3 fibroblasts. Indirect evaluation of the OXPHOS status in patients fibroblasts by measuring the ATP synthesis, showed a severe decrease in Pt.1 with all substrates used. Conversely,ATP synthesis measured in Pt.2 fibroblasts derived from the second skin biopsy (Pt.2nd) appeared only moderately reduced. The latter result suggests an improvement of the biochemical profile of the patient in the timeframe between the two biopsies. Accordingly, also the activity of PDHc, KGDHc and BCKDHc, were all dramatically reduced in our patients, with the exception of Pt.2nd that showed a moderate reduction of PDHc (Fig. 2a). The expression of the mitochondrial aconitase (mACO) was significantly decreased in Pt.1 and Pt.3 whereas in the other patients it was normally expressed (Fig. 2b, c).

Western blotting analysis

WB analysis performed on fibroblasts mitochondria displayed a marked reduction of IBA57 in all patients compared to control cells, supporting the hypothesis that all mutations might have a

pathogenic role in the disease (Fig. 3a). This result is different from what was found in a previously reported IBA57 mutant patient affected by leukodystrophy, where the expression of the protein was close to control levels either in skeletal muscle or in fibroblasts [21].

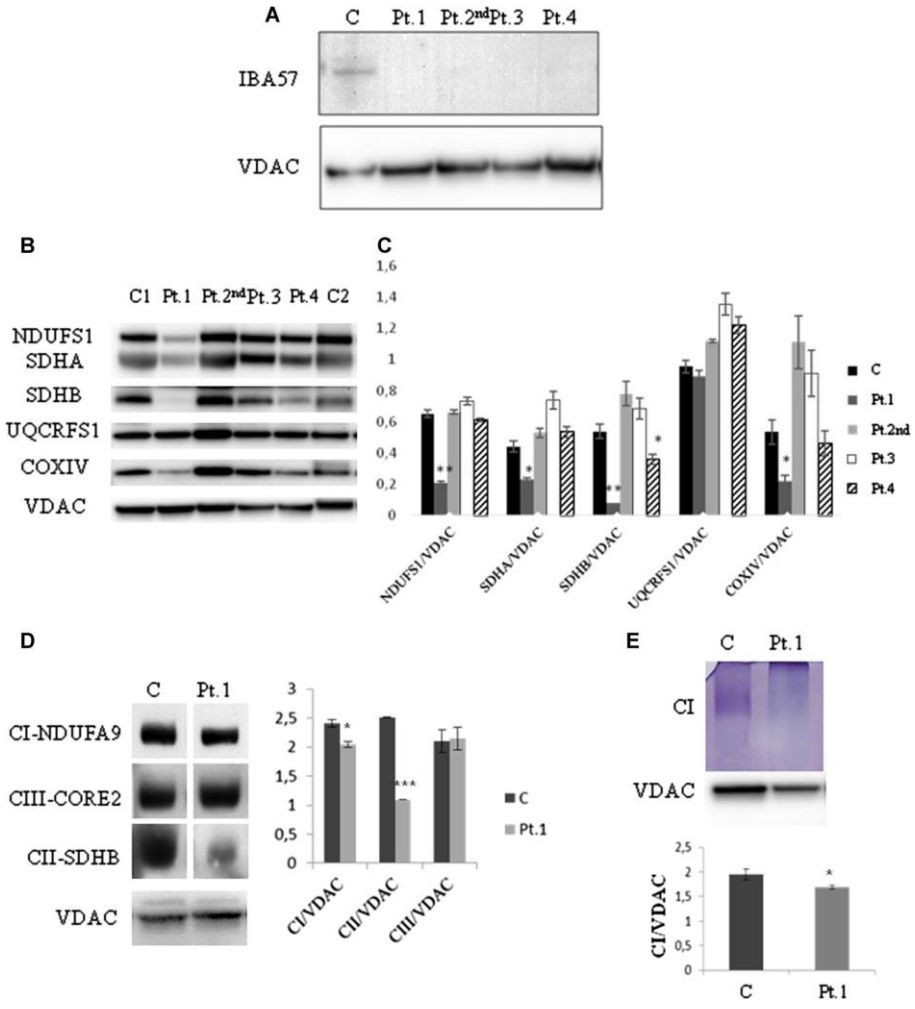

Fig. 3 a Fibroblasts mitochondria from control and patients cells were separated on a 12 % SDS-PAGE and reactive bands were probed with a specific antibody against IBA57. The mitochondrial

membrane protein VDAC was used for equal loading control. b Same samples were tested for the expression of the single subunits of the RCCI (NDUFS1), RCCII (SDHA, SDHB), RCCIII (UQCRFS1), RCCIV (COXIV). c The level of the different subunits of the RCC
reported in panel b was normalized against VDAC. Data are presented as a mean ± SD (n = 5 independent experiments).

SDS-PAGE of the single subunits of the RCC, using fibroblasts mitochondria, showed a severe reduction of RCCII (SDHB and SDHA) and a decrease of RCCI (NDUFS1) and RCCIV (COXIV) in Pt.1 (Fig. 3b, c). A decrease of SDHB was evident in Pt.4, whereas no other patients (Pt.2nd and Pt.3) showed a significant reduction of the RCC subunits (Fig. 3b, c), at least in fibroblasts mitochondria. As regards Pt.2, in accordance with the severe RCCII biochemical defect measured in muscle and fibroblasts homogenate of the first skin biopsy, WB analysis evidenced a dramatic decrease of SDHB in both tissues
(see Fig. 2 in Bugiani et al. [22]). The discrepancy between the results obtained in the two cultured fibroblast cell lines could be due to riboflavin supplementation (see ‘‘Discussion’’).

RCC assembly/stability studies, performed by BNGE on fibroblast mitochondria of the most affected patient (Pt.1), showed a severe decrease of RCCII amount and a slight decrease of RCCI, the latter confirmed also by in-gel activity assay (Fig. 3d, e).

When we indirectly evaluated the activity of lipoic acid synthetase (LIAS) by measuring the lipoylated proteins using an antibody against lipoic acid (LA), we found an altered lipoylation status that partially paralleled the reduction of the

corresponding enzyme activity. The lipoylation of the E2 subunit of KGDHc was reduced in all patients, while the lipoylated E2 subunit of PDHc was significantly reduced only in Pt.1 and Pt.2 (Fig. 4a, b).

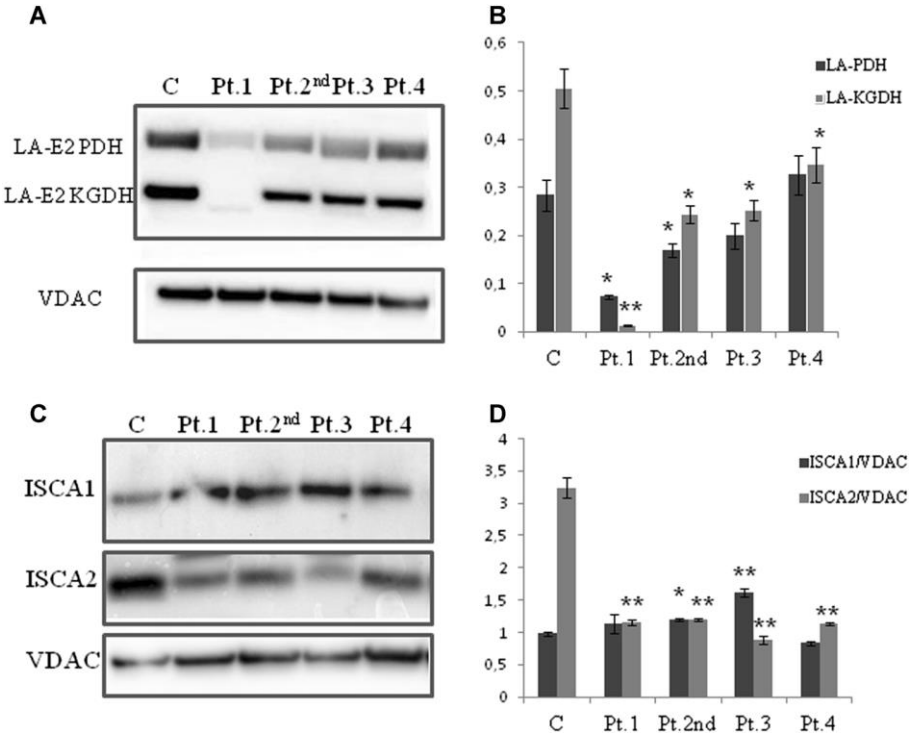

Fig. 4 a The lipoylated status of E2 subunit of PDH and KGDH was assayed by WB using a specific antibody against the E2 subunit of the lipoic acid (LA-E2). b The level of LA-E2 expression was normalized against VDAC. Data are presented as a mean ± SD (n = 3 independent
experiments). c The amount of ISCA1 and ISCA2 was evaluated by WB using specific antisera. d The indicated proteins were normalized to VDAC signal and data presented as a mean ± SD
(n = 3 independent experiments)

Previously reported studies performed in yeast have shown that a subset of proteins of the Fe/S cluster biogenesis, i.e., ISCA1, ISCA2 and IBA57, can interact amongst them [23]. We

evaluated the expression of ISCA1 and ISCA2 in our cohort of patients and found that ISCA1 was expressed in normal range in all our patients, with the exception of Pt.2 and Pt.3 where it resulted slightly overexpressed

(Fig. 4c, d). These results are in line with studies performed in HeLa cells where the silencing of IBA57 was associated to unchanged or increased expression of ISCA1 [24]. Contrariwise, when we evaluated ISCA2 expression, we found a drastic decrease of this protein in all patients (Fig. 4c, d).

Discussion

Herein, we report on four patients with an MRI profile of leukodystrophy and with novel mutations in IBA57. Our cohort defines a subset of patients characterized by similar MRI features, but with an heterogeneous disease course, ranging from fatal early onset (Pt.1 and Pt.4), as reported also by Debray et al. [21], to acute and severe psychomotor regression after the first year of life, followed by recovery of postural control and longer survival (Pt.3). In three patients, MRIs showed diffuse cavitating leukoencephalopathy that extended to the corpus callosum and particularly to the posterior arm of the internal capsulae. The cerebellum, brainstem and the cervical spinal cord were frequently involved as well. Late MRIs showed an extension of signal abnormalities and appearance or progression of infratentorial white matter involvement in the cerebellum, brainstem or cervical spinal cord. Brainstem may be spared (Pt.3). Moreover, a variable degree of cerebral atrophy was observed in three patients (Pt.1, Pt.3,and Pt.4).

Cavitating leukoencephalopathy has been reported in an increased number of infantile mitochondrial leukoencephalopathy and particularly in MMDS. The MRI pattern observed in our patients, characterized by cavitating leukoencephalopathy associated with posterior fossa structures and cervical spinal cord involvement, is similar to MRI features reported in MMDS4 related to ISCA2 mutations [12] and in one patient affected by MMDS3 related to IBA57 [21]. Lossos et al. [25] reported MRI features of IBA57 mutated patients presenting spastic paraplegia, and in these cases abnormalities were limited to few scattered foci of cavitating lesions and aspects of spinal cord atrophy that are generally found in patients with inherited spastic paraplegia. Leukodystrophy with cysts or cavitations has been described in MMDS1; however, differently from our MMDS3 patients, spinal cord and cranial posterior fossa were not involved [26, 27]. A similar MRI pattern together with spinal cord involvement has been reported in MMDS2 and in defects of an early acting component of the Fe/S cluster biogenesis, i.e., the glutaredoxin 5 [10].

IBA57 is a late-acting component of the Fe/S cluster machinery and assists the insertion of the [4Fe-4S] clusters in recipient enzymes that are selectively compromised in patients with mutations in IBA57. Although all of our patients presented markedly reduced levels of IBA57 in fibroblasts mitochondria, activity and amount of the [4Fe- 4S]-containing enzymes were variably affected. Interestingly, Pt.2 revealed a drastic recovery in the expression level of the RCCII subunit SDHB when we

compared the WB analysis performed on the first skin biopsy with the one performed on the second skin biopsy. It is conceivable that the therapeutic regimen of this patient, particularly the riboflavin supplementation, might have improved the stability and activity of those apo-flavoenzymes that contain FAD in their active sites [28], i.e., RCCII, PDHc, KGDHc and the BCKDHc. Indeed, Pt.2 has been already reported (referred as Pt.1 in Bugiani et al.) [22] as a RCCII deficient patient who was responsive to riboflavin treatment.

Pt.1 was the most affected patient, who beside the strong impairment of RCCII, displayed a reduction of the amount and activity of other enzymes containing [4Fe-4S], i.e., mACO, and of the lipoylated enzymes (PDHc, KGDHc and BCKDHc). Pt.1 showed also RCCIV involvement, although this complex lacks [4Fe-4S] clusters. RCCIV defect has been described in the skeletal muscle of two siblings with the neonatal form of IBA57 deficiency [11] and in a patient with a form of leukodystrophy associated with IBA57 mutation [21] but with almost normal amount of the protein. RCCIV was compromised also in HeLa cells and yeast depleted of IBA57. Taken together these data suggest that RCCIV involvement is likely in the most severe phenotypes, being the reduction of RCCIV not directly related to IBA57 amount but rather to indirect effects of IBA57 inactivation. The poor conservation of the gene amongst the species, demonstrate that is difficult to predict the impact of the novel mutations found in our cohort and to make a genotype/

phenotype correlation. Moreover, the insertion of [4Fe-4S] clusters affects such a high number of metabolic pathways that the outcome of the disease may be further complicated. Recent observations strengthen the role of the lipoic acid formation in the severity of the disease [29].

Indeed, several reported patients with mutations in genes encoding for other proteins involved in [4Fe-4S] delivery,i.e., NFU1, BOLA3 and ISCA2, and with reduced levels of protein-bound lipoic acid, share the same severe outcome of the disease [8, 12, 30]. In support of this hypothesis, we found in one of our mildest patients, Pt.2, just moderate reduction of the lipoylated enzymes. We cannot address whether riboflavin might have partially sustained the lipoylated enzymes activity in Pt.2 but the slight defects of these enzymes together with a recovery of RCCII activity may explain the better outcome of the patient.

In summary, this report expands the array of the genetic variation in IBA57 and defines a new subgroup of phenotypes recognizable from the MRI profiles of the patients.

Our report contributes to delineate MRI pattern related to IBA57-MMDS3, characterized by cavitating leukoencephalopathy extended to the corpus callosum, posterior arm of the internal capsulae, posterior fossa structures and cervical spinal cord. Finally, our findings strengthen the value of the MRI as non-invasive diagnostic tool above all in those cases associated with biochemical profile suggestive of MMDS in spite of variable clinical findings.

References

1. Vanderver A, Prust M, Tonduti D et al (2015) Case definition and
classification of leukodystrophies and leukoencephalopathies. Mol Genet Metab 114:494–500
2. Morato´ L, Bertini E, Verrigni D et al (2014) Mitochondrial dysfunction in central nervous system white matter disorders. Glia 62:1878–1894
3. Dallabona C, Abbink TE, Carrozzo R et al (2016) LYRM7 mutations cause a multifocal cavitating leukoencephalopathy with distinct MRI appearance. Brain 139:782–794
4. Taft RJ, Vanderver A, Leventer RJ et al (2013) Mutations in DARS cause hypomyelination with brain stem and spinal cord involvement and leg spasticity. Am J Hum Genet 92:774–780
5. Dallabona C, Diodato D, Kevelam SH et al (2014) Novel (ovario)
leukodystrophy related to AARS2 mutations. Neurology 82:2063–2071
6. Steenweg ME, Ghezzi D, Haack T et al (2012) Leukoencephalopathy
with thalamus and brainstem involvement and high
lactate ‘LTBL’ caused by EARS2 mutations. Brain 135:1387–1394
7. van Berge L, Hamilton EM, Linnankivi T et al (2014) Leukoencephalopathy with brainstem and spinal cord involvement
and lactate elevation: clinical and genetic characterization

and target for therapy. Brain 137:1019–1029
8. Cameron JM, Janer A, Levandovskiy V et al (2011) Mutations in
iron-sulfur cluster scaffold genes NFU1 and BOLA3 cause a fatal
deficiency of multiple respiratory chain and 2-oxoacid dehydrogenase
enzymes. Am J Hum Genet 89:486–495
9. Navarro-Sastre A, Tort F, Stehling O et al (2011) A fatal mitochondrial
disease is associated with defective NFU1 function in
the maturation of a subset of mitochondrial Fe-S proteins. Am J Hum Genet 89:656–667
10. Baker PR, Friederich MW, Swanson MA et al (2014) Variant non
ketotic hyperglycinemia is caused by mutations in LIAS, BOLA3 and the novel gene GLRX5. Brain 137:366–379
11. Ajit Bolar N, Vanlander AV, Wilbrecht C et al (2013) Mutation
of the iron-sulfur cluster assembly gene IBA57 causes severe
myopathy and encephalopathy. Hum Mol Gene 22:2590–2602
12. Al-Hassnan ZN, Al-Dosary M, Alfadhel M et al (2015) ISCA2 mutation causes infantile neurodegenerative mitochondrial disorder.
J Med Genet 52:186–194
13. Stehling O, Wilbrecht C, Lill R (2014) Mitochondrial iron-sulfur

protein biogenesis and human disease. Biochimie 100:61–77
14. Bugiani M, Invernizzi F, Alberio S et al (2004) Clinical and molecular findings in children with complex I deficiency. Biochim
Biophys Acta 1659:136–147
15. Rizza T, Vazquez-Memije ME, Meschini MC et al (2009) Assaying ATP synthesis in cultured cells: a valuable tool for the diagnosis of patients with mitochondrial disorders. Biochem Biophys Res Commun 383:58–62
16. Munujos P, Coll-Cantı´ J, Beleta J, Gonza´lez-Sastre F, Gella FJ
(1996) Brain pyruvate oxidation in experimental thiamin-deficiency
encephalopathy. Clin Chim Acta 255:13–25
17. Nakai N, Kobayashi R, Popov KM, Harris RA, Shimomura Y
(2000) Determination of branched-chain alpha-keto acid dehydrogenase
activity state and branched-chain alpha-keto acid
dehydrogenase kinase activity and protein in mammalian tissues.
Methods Enzymol 324:48–62
18. Nijtmans LG, Henderson NS, Holt IJ (2002) Blue native electrophoresis
to study mitochondrial and other protein complexes.
Methods 26:327–334
19. Zerbetto E, Vergani L, Dabbeni-Sala F (1997) Quantification of

muscle mitochondrial oxidative phosphorylation enzymes via histochemical staining of blue native polyacrylamide gels. Electrophoresis
18:2059–2064
20. Calvo SE, Compton AG, Hershman SG et al (2012) Molecular
diagnosis of infantile mitochondrial disease with targeted nextgeneration
sequencing. Sci Transl Med 4:118
21. Debray FG, Stu¨mpfig C, Vanlander AV et al (2015) Mutation of
the iron-sulfur cluster assembly gene IBA57 causes fatal infantile
leukodystrophy. J Inherit Metab Dis 38:1147–1153
22. Bugiani M, Lamantea E, Invernizzi F et al (2006) Effects of riboflavin in children with complex II deficiency. Brain Dev
28:576–581
23. Gelling C, Dawes IW, Richhardt N, Lill R, Mu¨hlenhoff U (2008)
Mitochondrial Iba57p is required for Fe/S cluster formation on aconitase and activation of radical SAM enzymes. Mol Cell Biol
28:1851–1861
24. Sheftel AD, Wilbrecht C, Stehling O et al (2012) The human mitochondrial ISCA1, ISCA2, and IBA57 proteins are required for [4Fe-4S] protein maturation. Mol Biol Cell 23:1157–1166
25. Lossos A, Stu¨mpfig C, Stevanin G et al (2015) Fe/S protein

assembly gene IBA57 mutation causes hereditary spastic paraplegia.
Neurology 84:659–667
26. Invernizzi F, Ardissone A, Lamantea E et al (2014) Cavitating
leukoencephalopathy with multiple mitochondrial dysfunction syndrome and NFU1 mutations. Front Genet 5:412
27. Nizon M, Boutron A, Boddaert N et al (2014) Leukoencephalopathy
with cysts and hyperglycinemia may result from
NFU1 deficiency. Mitochondrion 15:59–64
28. Carrozzo R, Torraco A, Fiermonte G et al (2014) Riboflavin responsive mitochondrial myopathy is a new phenotype of dihydrolipoamide dehydrogenase deficiency. The chaperon-like effect of vitamin B2. Mitochondrion 18:49–57
29. Uzarska MA, Nasta V, Weiler BD et al (2016) Mitochondrial Bol1 and Bol3 function as assembly factors for specific ironsulfur
proteins. Elife. doi:10.7554/eLife.16673
30. Ahting U, Mayr JA, Vanlander AV et al (2015) Clinical, biochemical,
and genetic spectrum of seven patients with NFU1
deficiency. Front Genet 6:123

Chapter 4

Not only dominant, not only optic atrophy: expanding the clinical spectrum associated with OPA1 mutations.

Nasca A, Rizza T, Doimo M, Legati A, Ciolfi A, Diodato D, Calderan C, Carrara G, Lamantea E, Aiello C, Di Nottia M, Niceta M, Lamperti C, Ardissone A, Bianchi-Marzoli S, Iarossi G, Bertini E, Moroni I, Tartaglia M, Salviati L, Carrozzo R, Ghezzi D.

Orphanet J Rare Dis. 2017 May 12;12(1):8

Background

Optic Atrophy 1 (OPA1, OMIM*605290) is a dynamin-related protein of the large GTPase superfamily that locates to the inner mitochondrial membrane and is involved in mitochondrial dynamics and mtDNA maintenance.

Pathogenic mutations in the *OPA1* gene have largely been associated with autosomal dominant optic atrophy (ADOA; OMIM#165500), a visual disorder associated with degeneration of retinal ganglion cells. Its prevalence is estimated at 1/50,000. Classical ADOA typically has early onset, before 10 years of age, and manifests with various levels of visual impairment: bilateral visual loss, dyschromatopsia, centrocecal scotomas and temporal optic disc atrophy. Up to 20% of *OPA1*-mutated patients also develop additional more complex neurodegenerative disorder with extra-ocular manifestations, including deafness [1], chronic progressive external

ophthalmoplegia, ptosis, ataxia, peripheral neuropathy and mitochondrial myopathy with multiple mtDNA deletions, leading to a syndromic disease sub-group known as 'ADOA plus' (OMIM#125250) [2, 3].

To date, over 300 mutations in *OPA1* have been identified and associated with ADOA and ADOA plus. Half of these variants are predicted to result in a truncated protein producing haploinsufficiency and are usually linked to the classical non-syndromic form of ADOA. The 'ADOA plus' phenotype is often associated with dominant missense mutations in *OPA1* [1]. In a few cases, the phenotype is due to compound heterozygous *OPA1* mutations preserving transcript expression [3], and suggestive of recessive or semi-dominant patterns of inheritance [3,4,5]. Recently, compound heterozygous mutations in *OPA1* have been associated with Behr syndrome (OMIM#210000), a disease characterized by the association of early-onset optic atrophy with spinocerebellar degeneration [6, 7]. Finally, the first homozygous *OPA1* mutation has just been reported, associated with fatal infantile mitochondrial encephalomyopathy, hypertrophic cardiomyopathy and optic atrophy [8]. The clinical spectrum of these emerging double-mutant *OPA1*-related disorders remains to be fully characterized.

We report here three patients with biallelic *OPA1* mutations: a boy showing an early-onset and severely progressive mitochondrial disorder and two girls showing a spastic ataxic

syndrome associated with sensory motor peripheral neuropathy, resembling Behr syndrome.

Methods

Molecular genetics

Total DNA was extracted from muscle, peripheral blood lymphocytes, fibroblasts from patients and relatives using standard methods. Sequencing of the entire mitochondrial DNA (mtDNA) was performed essentially as previously described [9]. mtDNA content was evaluated by real-time PCR-based quantification (ABI7000 Real-Time PCR System) using specific mtDNA probes (amplicons nt 867-928, 12835-12893) and a standard, single-copy autosomal gene (RNaseP) [10].

For Patients1 and 2, NGS library preparation, sequencing, alignment and variant calling were performed as recently described [11]. Filtering was carried out by applying a series of steps: low-quality variants were filtered out (Illumina Qscore threshold of 20); variants with a minor allele frequency (MAF) >1% in the 1000 Genomes Project (http://www.1000genomes.org), Exome Variant Server (http://evs.gs.washington.edu) and Exome Aggregation Consortium (ExAC: http://exac.broadinstitute.org) databases were discharged; finally, we focused on predicted missense, frame-shift, stop-gain or stop-loss, and splice-site variants.

For proband 3, targeted enrichment and massively parallel sequencing were performed on genomic DNA of the affected subject and their parents. Exome capture was carried out using SureSelect Human All Exon V.4 (Agilent). Sequencing data

analysis was performed using an in-house implemented pipeline which mainly takes advantage of the Genome Analysis Toolkit (GATK V.3.5) framework [12], as previously reported [13,14,15]. Quality filtering of variants were as previously reported [16], and high-quality variants were filtered against public (dbSNP146 and ExAC V.0.3) and in-house (approx. 600 population-matched WES) databases to retain private, rare (MAF <0.1%) and clinically associated variants, which were filtered to retain only those located in exons with any effect on the coding sequence, and splice site regions (variants located from −3 to +8 with respect to an exon-intron junction). Functional annotation of variants was performed using SnpEff V.4.2 and dbNSFP V.2.9 [17,18,19]. WES statistics are reported in Additional file 1. Functional impact of variants was analyzed by Combined Annotation Dependent Depletion (CADD) V.1.3 and dbNSFP Support Vector Machine (SVM) V.2.9 algorithms [18, 19]. Variant prioritization was performed by GeneDistiller [20]. All variants identified by NGS were validated by Sanger sequencing.

RNA was extracted from skin fibroblasts and 1 µg was used as template for reverse transcriptase PCR (RT-PCR) to obtain full-length cDNA. *OPA1* transcript was amplified and PCR products were sequenced in order to confirm genomic variants and unmask potential events of nonsense mediated decay.

Yeast studies

A hybrid gene was obtained by joining the 5' portion of the yeast *MGM1* gene (the orthologous of human *OPA1*), encoding

the mitochondrial targeting sequence and the transmembrane domain, to the 3' of the human *OPA1* cDNA using a sequential PCR protocol. Primers and conditions are available upon request. The resulting construct was then cloned into the pCM184 yeast expression vector. Individual mutants were generated by site-specific mutagenesis.

Yeast strains, media, growth conditions, and the whole procedure for selection of haploid cells have been previously reported in detail [21]. Briefly, a single copy of the *MGM1* gene was inactivated in wild type diploid W303 yeast by homologous recombination with a KANMX4 cassette. Heterozygous strains were transformed with either the wild type or one of the mutant constructs and, after sporulation, haploid yeast harboring the mutant *MGM1* gene and the plasmid of interest were selected and used for subsequent experiments.

Immunoblot analyses

Fibroblasts were pelleted and solubilized in RIPA buffer with protease inhibitors. 50 µg of proteins were loaded for each sample in 10% denaturing sodium-dodecyl sulfate polyacrylamide gel electrophoresis (SDS-PAGE).

The following antibodies were used: OPA1 (monoclonal antibody BD Biosciences), NDUFA9 (MitoSciences), MTCO2 (MitoSciences), porin/VDAC (MitoSciences), beta-tubulin/TUBB (Sigma-Aldrich), and HSP60 (Abcam).

Fluorescence microscopy

Skin fibroblasts from patients and controls were cultured in a 37 °C incubator with 5% CO_2, in either 25 mM glucose or 5 mM

galactose DMEM (Euroclone) supplemented with 10% FBS, 1% L-glutamine, and 0.2% sodium pyruvate. For visualization of the mitochondrial network, the mitochondrial fluorescent dye MitoTracker Red-CMXRos (Invitrogen) was added to the culture media at final concentrations of 50 nM for 30 min and then visualized by fluorescence microscopy. Images for P1 were acquired with a confocal microscope (Leica TSC-SP8) and for P3 with inverted microscope (Leica DMi8).

Biochemical studies

Complex V activity was measured in fibroblast mitochondria of P3 and age-matched controls, using reported spectrophotometric methods [22]. Either succinate (the direct substrate of complex II-succinate dehydrogenase), or malate and pyruvate + malate (which generate NADH, substrate of complex I-NADH dehydrogenase) were used as substrates. Cellular ATP content was assayed luminometrically using the ATPLite 1 Step (PerkinElmer, Boston) according to the procedure recommended by the manufacturer and using 2×10^4 cells. Aged matched controls have been used in three different experiments, either in a regular medium as well as in a galactose-supplemented medium (5 mM). Luminescence was measured using the EnSpire Multimode Plate Readers (PerkinElmer).

Electrophysiology studies

Electroretinogram (ERG): Retimax instrument (CSO, Firenze, Italy) was used for the full-field flash ERG and pattern VEP assessment in the protocol session. The cornea was

anesthetized with 1% dicaine. HKloops ring fiber electrodes were used to record ERGs. A small Ag/AgCl skin earth electrode was placed at the center of the forehead. Mesopic and photopic stimuli were used for recording sessions.

Visual evoked potential (VEP): Visual stimuli consisted of checkerboard patterns (a single check edge subtending 60 and 15 min of arc; contrast 99%; mean luminance 60 cd/m^2) generated on a monitor subtending 26° and reversed in contrast at the rate of two reversal per second. The stimulation was monocular, with full occlusion of the fellow eye. To maintain stable fixation, a small red target was (0.5°) was placed in the center of the stimulation field. VEPs were recorded by cup-shaped Ag/AgCl electrodes placed over the scalp two cm above the inion (Oz) with the reference in Fpz and the ground on the mastoid. The time-to-peak (in milliseconds) and peak-to-peak amplitude (in microvolts) of major VEP components (i.e. N75, P100 and N145) were measured.

Optical coherence tomography (OCT)

Peripapillar retinal nerve fiber layer (RNFL) thickness was measured with a spectral-domain (SD)-OCT (Optos SD-OCT, Glasgow, UK). All scans were done using an internal fixation target in the OCT device. The fast RNFL scan protocol consisted of three consecutive 360° circular scans with a diameter of 3.4 mm centered on the optic disc. Parameters including average RNFL thickness in four quadrants were generated automatically in the analysis report and compared to control values. Each sector was coded in green, yellow, or red

for RNFL measurement greater than the lower 95th percentile, less than the lower 95th percentile, or less than the lower 99th percentile range, respectively. All images had signal strength of at least 7. Images with motion artifacts were discarded and rescanned.

Results

Case reports

P1. The proband P1 (II-2) is a boy, second child from unrelated parents.

His older brother (II-1) was affected by a neurological disease for which a metabolic etiology was suspected but never confirmed. In II-1, psychomotor delay was reported since first age of life, and he never achieved sitting or standing position. At 9 months of age the presence of ptosis and ophthalmoparesis was depicted, with normal fundus exam. Neurological evaluation at the age 2.5 years showed poor somatic growth (10%ile), microcephaly (<3%ile), hypotonia, ataxia and mental retardation. The following exams resulted normal: plasma lactate, organic acids, amino acids, mucopolysaccharides, oligosaccharides; no brain MRI was available. The sibling II-1 died at age 2 years and 10 months with multiorgan failure during a septic shock due to paralytic ileus. No biological material was available from this individual.

P1 presented since first months with frequent vomiting and marked psychomotor delay: head control was acquired at 10 months, sitting at 2.5 years, standing at 5 years and first words at 3 years of age. He was firstly evaluated at 4 years in

another Hospital because of myoclonic epileptic seizures. Clinical examination showed a severe neurological impairment, characterized by absence of head control, poor eye contact and response to sounds, presence of nystagmus, and absence of language. Brain MRI (not available) depicted symmetrical hyperintense alterations in the putamina, cerebellar atrophy and presence of oedema in the occipito-parietal cortical areas. EEG showed poor organization of cerebral activity with the presence of sharp waves in occipital regions. Lactate levels were elevated in plasma (2800 mmol/L) and in CSF; the analysis of respiratory chain complexes and PDH complex on muscle biopsy resulted normal. The neurological conditions were subsequently referred stable, with good control of epilepsy, left hemiparesis and severe mental impairment. Fundoscopic examination at 5 years showed the presence of optic atrophy. At the age of 8 years, following an accidental head trauma, he developed an acute psychomotor regression; 5 months later was admitted to our Institute, showing poor height and growth, scarce response to pain stimuli, absence of postural control, marked hypotonia and absence of spontaneous movements. Hepatic function was markedly impaired; lactate and pyruvate levels were normal. EEG revealed the presence of theta-delta asymmetric activity (depressed on right hemisphere). Brain MRI showed the presence of bilateral, marked and swollen alterations in the mesencephalon, pons and subthalamic nuclei (Fig. 1a, b), associated with necrosis of putamina, and partially in caudate nuclei (Fig. 1c), thin corpus callosum, ventricular

enlargement and mild cerebellar atrophy (Fig. 1a, d); the presence of a cortical abnormality in the parietal and occipital right regions was also present. H-MRS showed a very high lactate peak, both in the abnormal and in the spared areas. A second MRI performed after 20 days was unchanged. Neurophysiological study showed the presence of severe axonal sensory neuropathy (absence of Sensory Action Potentials - SAPs, and normal Motor nerve Conduction Velocity - MCV, with mild reduction of Compound Muscle Action Potentials - CMAPs). Respiratory chain complexes and PDH complex activities resulted normal in muscle and fibroblasts. In the following days he developed respiratory failure requiring artificial ventilation and subsequently a severely progressive impairment of clinical conditions with sepsis and a multiorgan failure leading to decease. Parents refused autopsy. Neurological and neuro-ophthalmological evaluations were normal in both parents.

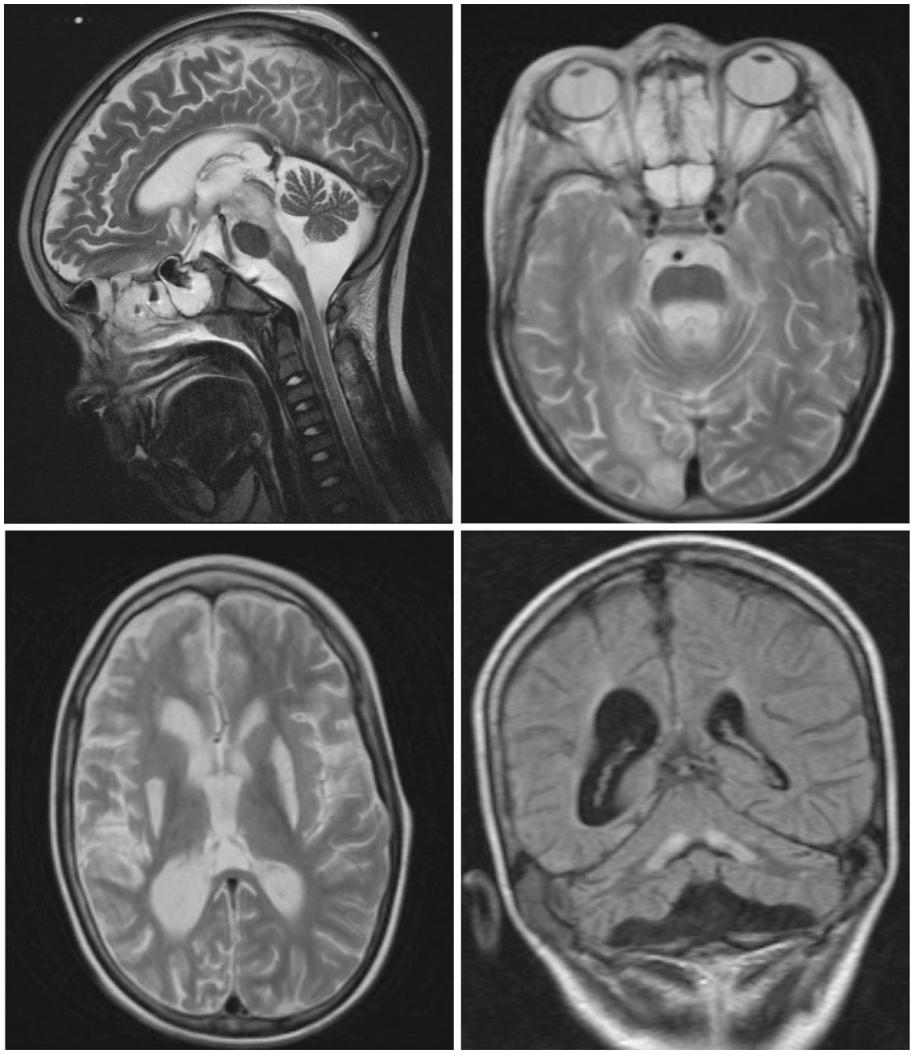

Fig. 1

MRI findings of proband 1. **a**, **b**: sagittal and axial T2-weighted sections showing the presence of bilateral hyperintense alterations in the mesencephalon, pons and subthalamic nuclei, all markedly swollen; **c**: axial T2-weighted image showing bilateral necrosis of putamina and left caudate nuclei; **d**: coronal T1-weighted image showing cerebellar atrophy, dentate nuclei hyperintensity and ventricular enlargement

P2. The proband P2 is the only child of unrelated parents of Italian origins. Family history was negative: mother presents severe myopia without optic atrophy or any neurological sign. P2 was born at term after an uncomplicated pregnancy and delivery. Psychomotor development was referred normal. Between ages 4 and 6 years, she presented worsening of her visual acuity. Bilateral optic neuropathy was diagnosed with normal ERG but altered VEPs. She underwent to ophthalmologic follow-up (instrumental data not available). She arrived at our observation at 14 years of age. Neurological evaluation showed mild bilateral ptosis and strabismus, dysdiadochokinesia, dysmetria, mild ataxia and pes cavus; tendon reflexes were absent. Cognitive functions were normal. Fundoscopy and VEPs confirmed optic atrophy; ERG was normal; SAPs and BAEPs showed central conduction abnormalities. Brain MRI disclosed optic nerves and chiasm atrophy. Electroneuronography revealed an axonal sensory neuropathy. Electroencephalography was normal. Plasmatic lactate levels were normal. Treatment with idebenone (135 mg/die) was started. Neurological and ophthalmologic follow-up, six months after diagnosis, were stable.

P3. The proband P3 is a 12 year old girl, who was born at term by dystocic delivery; she was the second child of healthy consanguineous parents. The eldest brother was healthy. She acquired autonomous ambulation at 14 months of age, but parents reported that she had always been unsteady, and had delayed speech development. At 4 years she began to present

psychomotor regression, ataxia and deficient motor coordination. At 4 years the neurological examination showed an ataxic-spastic gait, nystagmus, dysmetria and dysarthria. She performed a first brain MRI which showed abnormal hyperintensities of the periventricular and centrum semiovale white matter areas in T2-weighted images bilaterally (Additional file 2). Electrophysiological examinations showed bilateral absence of the V wave at Brainstem Auditory Evoked Potentials (BAEPs), and Nerve Conduction Studies (NCS) disclosed an axonal sensory-motor neuropathy (decreased CMAP and SAP amplitudes with conduction velocities at the lower level of controls range). Phytanic and pristanic acids, VLCFA, Vitamin E, hexosaminidase A and B levels were in the normal range. One year later, the neurological conditions worsened with increased spasticity in her legs and unsteadiness during walking and postural changes. NCS showed a progressive decrease of CMAP amplitudes compared to previous values; VEP and ERG were normal. A second MRI performed at 8 years of age showed T2-hyperintense abnormal signals corresponding to both putaminal nuclei, associated with mild global cerebellar atrophy, while the abnormal areas of T2 hyperintensities of the white matter had disappeared (Additional file 2). Mutations in *FXN, ATM* and *PLA2G6* were ruled out by Sanger sequencing. At age 10 years the neurological examination was stable; repeated flash VEP showed slightly delayed latencies bilaterally, whereas OCT was reported as normal. The last neurological evaluation at age 12 years

showed an ataxic-spastic syndrome with distal muscular atrophy of upper and lower limbs. A deep ophthalmological examination was performed: OCT revealed a mild reduction of retinal nerve fiber layer in both eyes whereas flash ERG and pattern VEP responses (60' stimuli) were in the normal range. However, an amplitude reduction of VEP response was found for 15' stimuli: abnormalities in VEP 15' responses, which mainly reflect macular fibers responses contributing to the temporal quadrant of the optic nerve, are quite typical of OPA1-related optic neuropathy.

Genetic studies

Because of the clinical presentation suggesting a mitochondrial disorder, we first investigated the mitochondrial DNA (mtDNA) in our proband P1. The complete sequencing of mtDNA revealed the presence of two homoplasmic variants: the m.11778G > A change in *MTND4*, known to be associated with Leber's hereditary optic neuropathy (LHON), and the m.3337G > C change in *MTND1.* The latter is expected to cause the p.Val11Leu substitution, affecting a poorly conserved amino acid residue (with leucine present in chicken). Bioinformatics tools for pathogenicity predicted a neutral effect for this amino acid change. Both variants were homoplasmic also in the mother's DNA. The quality/quantity of the DNA extracted from the proband's muscle was not enough to perform Southern blot analysis. Since the LHON mutation was unlikely the main cause of the disease in P1, his DNA was subjected to targeted resequencing of a panel containing >100 nuclear genes

associated with mitochondrial disorders. After filtering steps to remove common polymorphisms (>1% in public database) and variants with probably neutral effect (synonymous changes, intronic variants >20 bases far from exons), 6 variants remained. Because the pedigree was suggestive for a recessive trait, we focused on the only gene with bi-allelic variants: *OPA1*. Two heterozygous calls were present: a 5 nucleotide deletion c.190_194del (NM_130837.2), predicting a truncated protein product (p.Ser64Asnfs*7), and a previously annotated missense c.1311A > G change (p.Ile437Met). Direct sequencing validated the two variants and confirmed their occurrence in trans, with the missense change on the maternal allele and the frame-shift change on the paternal allele (Fig. 2a). The c.190_194del was absent in public variant databases, whereas the c.1311A > G change is reported with a frequency of 0.06% in ExAc database. The latter corresponds to c.1146A > G, p.I382M based on transcript NM_015560.2, used in the past as reference isoform, and has been already reported in other bi-allelic cases [5, 23].

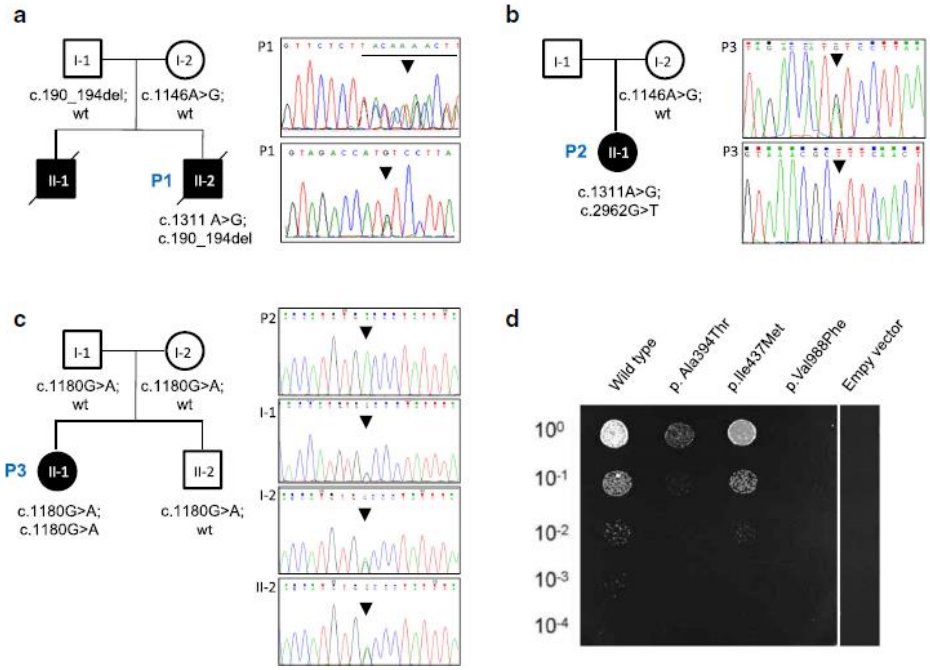

Fig. 2

Genetic and yeast studies. **a**, **b**, **c**: Pedigrees and electropherograms showing the mutations found in this study: families of proband P1 (panel **a**), proband P2 (panel **b**) and proband P3 (panel **c**). **d**: Strains lacking *MGM1* and transformed with either wt *OPA1* hybrid allele or individual mutants p.Ala394Thr, p.Val988Phe, p.Ile437Met or empty vector were grown on YP medium supplemented with glycerol. Cells were plated after serial dilutions. Picture was taken after 4 days of growth. Numbering of amino acids in the yeast hybrid genes refers to the corresponding human counterpart (NM_130837.2; NP_570850.2)

Targeted sequencing and variant filtering in P2 led to the identification of two heterozygous *OPA1* variants: c.2962G > T (p.Val988Phe), and the recurrent c.1311A > G substitution (p.Ile437Met). Both variants were confirmed by Sanger sequencing; the mother harbored the c.1311A > G, the paternal DNA was not available for genotyping (Fig. 2b).

In P3 data annotation of WES data predicted 13229 high-quality variants having functional impact (*i.e.*, non-synonymous, indels and splice site changes). Among them, 338 private and rare changes were retained for further analyses. Variants were prioritized on the basis of the functional relevance of genes, taking into account both dominant and recessive inheritance models. Only changes predicted to be deleterious by CADD V.1.3 (score >15.0) or dbNSFP SVM V.2.9 (radial score >0.0) algorithms were considered as candidates. Variant filtering and prioritization allowed to identify a missense homozygous variant in *OPA1*, c.1180G > A (NM_130837.2), predicting the p.Ala394Thr amino acid substitution, as the best candidate underlying the trait, which fitted with the documented consanguinity in the family (Fig. 2c). Consistently, no suggestive disease gene candidate with a functionally relevant *de novo* heterozygous variant was identified in the proband (Additional file 1).

Yeast studies

Yeast lacking *MGM1* cannot grow on non-fermentable carbon sources and develop a petite phenotype [24]. Human *OPA1* per se cannot complement yeast *MGM1* deletion mutants [24]. We therefore employed a hybrid gene comprised of the 5' portion of *MGM1* (encoding the targeting sequence and the transmembrane domain) and the 3' portion of human *OPA1* (from exon 6 to the stop codon). Haploid yeast lacking *MGM1* and expressing either the wild-type hybrid gene or individual mutants, were plated at seriate dilutions in medium

containing glycerol as sole carbon source (YPD). The wild type hybrid gene restored growth in YPD. Conversely, yeast expressing the p.Ala394Thr displayed a marked reduction of respiratory growth, the p.Val988Phe mutation virtually abolished the activity of the mutant allele, while the defect observed with the p.Ile437Met mutant was milder, evident only at the 10^{-3} dilution (Fig. 2d).

Characterization of fibroblasts carrying *OPA1* mutations

The *OPA1* transcript levels, assessed by quantitative RTPCR in P1, were comparable in patient's and control samples and cDNA sequencing indicated that the two alleles were similarly expressed, excluding major mRNA decay of the allele with the premature stop codon. Nevertheless, Western blot analysis on whole cell lysates of primary fibroblasts from P1 showed a clear reduction in the amount of all OPA1 isoforms (Fig. 3a). Given the known role of OPA1 in mitochondrial fusion, to evaluate the functional consequences of the identified *OPA1* variants we assessed the mitochondrial network in fibroblasts. Fibroblasts grown in either standard glucose- or galactose-medium were stained with a mitochondrial dye (Mitotracker Red) and examined by fluorescence microscopy. In patient's cells we found increased fragmentation of the mitochondrial network compared with controls (Fig. 3b, Additional file 4), in agreement with the expected reduced fusion caused by dysfunctional OPA1. In addition to the role in mitodynamics, OPA1 has been reported to act in the maintenance of mitochondrial genome integrity [25]. In total DNA extracted from fibroblasts we

quantified the amount of mtDNA by quantitative PCR. In P1, the mtDNA content was partly but significantly lower than controls (≈40% of the mean control value, Fig. 3c). Notably, the reduction in mtDNA levels (≈35% of the mean control value) was confirmed in DNA extracted from patient's muscle (Fig. 3c). Similarly, in P3 cells the amount of OPA1 was reduced and the mitochondrial network appears fragmented; as for P1, the latter phenomenon was more evident in medium supplemented with galactose (Additional file 4 and Additional file 5). In the fibroblasts mitochondria of P3 the rate of ATP synthesis was found to be slightly reduced, with respect to the control mean values, when succinate was used, whereas a significant reduction was evident when malate and pyruvate + malate were used as substrates (Additional file 6A). The ATP content in P3 fibroblasts was normal respect to controls in regular medium but significantly reduced in galactose medium reflecting the lower efficiency of ATP production by OXPHOS in stress condition (Additional file 6B). No cells were available from P2.

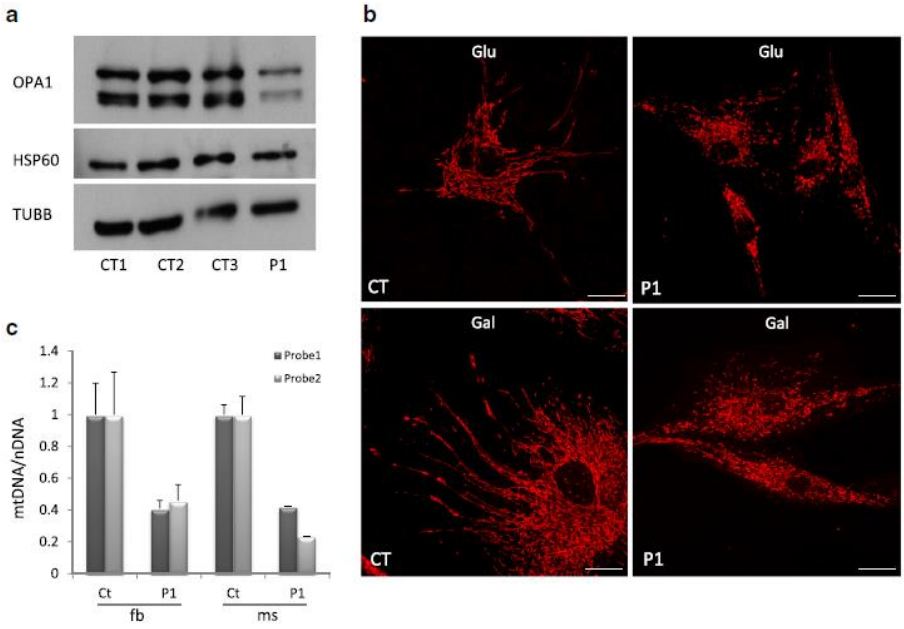

Fig. 3

Characterization of fibroblasts from proband 1. **a**: OPA1 protein amount in patient's (P1) and control (CT1, CT2 and CT3) fibroblasts, obtained using an anti-OPA1 antibody. Anti-TUBB and anti-HSP60 antibodies were used as loading controls. **b**: Representative images of mitochondrial morphology (obtained with Mitotracker *red*) in fibroblasts from proband 1 (P1) and a control (CT), grown either in glucose or galactose medium. Scale bar: 20 µm. **c** Quantification of mtDNA amount in fibroblasts (fb) and skeletal muscle (ms) from proband 1 (P1) and controls. (Ct). The bars represent the amount of mtDNA normalized to nuclear DNA (nDNA), compared to the mean value of controls (=1). Two different probes for mtDNA were used. Data are represented as mean + SD

Discussion

Compound heterozygous mutations in *OPA1* have been rarely reported, usually associated with ADOA plus phenotype [5, 6, 7, 23, 26]. A table summarizing genetic and clinical

features of these cases is reported as Additional file 7. The p.Ile437Met missense variant, although not causing a phenotype *per se*, has been recently suggested to contribute consistently in modulating the phenotype in *OPA1* compound heterozygous subjects [23].

The biallelic *OPA1* variants found in two of our patients combine a classic *OPA1* haploinsufficiency mutation (i.e. a frameshift change in P1 and a missense change, acting as a null allele in yeast, in P2), which can determine dominant isolated optic atrophy with reduced penetrance, and the missense mutation p.Ile437Met, considered hypomorphic or with very low potential pathogenicity since apparently it was not able to lead to clinical symptoms in heterozygous or even homozygous state [23]. Instead, in P3 we found a homozygous p.Ala394Thr change; this is the second case of homozygous missense mutation in *OPA1* reported to date, after the description of a patient with a severe fatal cardiomyopathy associated with the p.Leu589Arg mutation [8].

In accordance with a recessive mode of inheritance, the parents of our probands, each carrier of one heterozygous *OPA1* variant, displayed no symptoms, with the exception of a mother harboring the p.Ile437Met variant and presenting a severe myopia; this genotype-phenotype association was previously reported [5]. Reduced penetrance of dominant mutations, typical of ADOA, may also explain the segregation in the families but it is unlikely given the severe phenotype of these patients.

The effect of the missense mutations on growth of the yeast model seems to correlate with the clinical presentation in biallelic *OPA1* mutant patients; the presence of a virtually null allele (p.Val988Phe found in P2) plus a mildly compromised allele (p.Ile437Met found in P1 and P2) or the presence of a homozygous mutation with an intermediate effect (p.Ala394Thr found in P3) probably cause a similar overall impairment in OPA1 function, resulting in the disease observed in our patients.

From a medical point of view, the most striking aspect of this study is the extremely severe presentation of P1, with an infantile lethal outcome. The same course was reported in the older brother, albeit the genetic diagnosis was not possible because of lack of available DNA. We therefore cannot exclude the presence of a different genetic defect that was the primary cause of the disease in this subject, or even in our proband. However, the extensive genetic analysis with sequencing of >100 genes associated with mitochondrial disorders makes unlikely the latter hypothesis. It is possible that additional genetic factor may have exacerbated the phenotype caused by the *OPA1* mutations. Interestingly, P1 showed two homoplasmic changes in his mtDNA. The mutation m.11778G > A in *MTND4* is a well-known cause of LHON, a mitochondrial disorder that leads to bilateral subacute visual failure. Rarely patients harboring the m.11778G > A show a LHON-plus phenotype; nevertheless visual impairment remains the most common presenting feature, although neurologic

features have been documented in several cases, including movement disorders, multiple sclerosis–like illnesses, peripheral neuropathy, and seizures [27]. Haplogroup J has been shown to increase the penetrance of this mutation [28], but our proband belonged to haplogroup T1. However, the low penetrance of the m.11778G > A in females is compatible with the homoplasmic status of the unaffected mother. The other change found in mtDNA, m.3337G > C/p.Val11Leu in *MTND1,* is not phylogenetically conserved, is predicted benign but it is not present in Mitomap database (http://www.mitomap.org). Valine 11 is located at the beginning of the first α-transmembrane helix of ND1 protein, and the change with leucine is not predicted to alter the transmembrane domain. Despite both mtDNA variants affected respiratory complex I, its activity was normal in patient's samples. All these considerations did not suggest a primary pathogenic role for the two identified mtDNA variants but did not exclude a synergistic effect together with the *OPA1* mutations, worsening the clinical phenotype in our patient.

Amongst the published patients with biallelic *OPA1* mutations (Additional file 7), the severe neonatal-onset disorder characterized by severe optic atrophy, ataxia, hypotonia, gastrointestinal dysmotility and dysphagia, described in two siblings by Schaaf et al. [5], is the closest to the clinical presentation of P1 and his brother. Conversely the phenotype reminiscent of the Behr syndrome, reported in 4 cases by Bonneau et al. [6], was similar to that observed in P2 and P3.

However, optic atrophy was evident in all the other *OPA1*-mutant subjects, being often the first and main symptom; in contrast, in our patients overt optic atrophy was observed later compared to most of the other neurological signs (P1 and P3) or not reported (P1's brother and P3, untill 10 years of age). Moreover, the rapidly progressive course of P1 is reminiscent of Leigh syndrome rather than of DOA-plus or Behr syndrome. Infantile lethal outcome due to *OPA1* mutations has been described for the first time very recently: a homozygous *OPA1* mutation has been found in two sisters with fatal infantile mitochondrial encephalomyopathy, hypertrophic cardiomyopathy and optic atrophy [8]. No evidence of heart involvement was reported in our patients, but a multiorgan failure, including gastrointestinal and hepatic impairment, was observed in P1, confirming that OPA1 proper functioning is crucial not only for the optic nerve but also for several other tissues/organs. Clinical features in P3 were particularly misleading for an *OPA1* related condition, with manifestations of early onset progressive spastic ataxia and sensory motor polyneuropathy, in the absence of optic atrophy. The MRI was likewise peculiar, showing early MRI abnormal hyperintensities of the white matter suggesting a leukodystrophy followed serially by a disappearance of white matter abnormalities and appearance of bilateral abnormalities in the putamen.

Conclusions

Our report confirms the broad complexity in the phenotypic spectrum associated with recessive *OPA1* mutations that

ranges from non-syndromic phenotypes overlapping with those caused by dominant *OPA1* mutations to severe fatal encephalopathy resembling typical mitochondrial diseases. Moreover, our findings suggest that bi-allelic *OPA1* mutations should be considered in disorder where optic atrophy is not obvious (or even absent).

OPA1 mutations should not be considered only for dominant trait or only for optic atrophy phenotypes.

References

1.

Amati-Bonneau P, Guichet A, Olichon A, Chevrollier A, Viala F, Miot S, Ayuso C, Odent S, Arrouet C, et al. OPA1 R445H mutation in optic atrophy associated with sensorineural deafness. Ann Neurol. 2005;58:958–63.

2.

Amati-Bonneau P, Valentino ML, Reynier P, Gallardo ME, Bornstein B, Boissiere A, Campos Y, Rivera H, de la Aleja JG, et al. OPA1 mutations induce mitochondrial DNA instability and optic atrophy 'plus' phenotypes. Brain. 2008;131:338–51.

3.

Yu-Wai-Man P, Griffiths PG, Gorman GS, Lourenco CM, Wright AF, Auer-Grumbach M, Toscano A, Musumeci O, Valentino ML, et al. Multi-system neurological disease is common in patients with OPA1 mutations. Brain. 2010;133:771–86.

4.

Pesch UEA, Leo-Kottler B, Mayer S, Jurklies B, Kellner U, Apfelstedt-Sylla E, Zrenner E, Alexander C, Wissinger B. OPA1

mutations in patients with autosomal dominant optic atrophy and evidence for semi-dominant inheritance. Hum Molec Genet. 2001;10:1359–68.

5.

Schaaf CP, Blazo M, Lewis RA, Tonini RE, Takei H, Wang J, Wong L-J, Scaglia F. Early-onset severe neuromuscular phenotype associated with compound heterozygosity for OPA1 mutations. Molec Genet Metab. 2011;103:383–7.

6.

Bonneau D, Colin E, Oca F, Ferre M, Chevrollier A, Gueguen N, Desquiret-Dumas V, N'Guyen S, Barth M, et al. Early-onset Behr syndrome due to compound heterozygous mutations in OPA1. Brain. 2014;137:e301.

7.

Carelli V, Sabatelli M, Carrozzo R, Rizza T, Schimpf S, Wissinger B, Zanna C, Rugolo M, La Morgia C, et al. 'Behr syndrome' with OPA1 compound heterozygote mutations. Brain. 2015;138:e321.

8.

Spiegel R, Saada A, Flannery PJ, Burte F, Soiferman D, Khayat M, Eisner V, Vladovski E, Taylor RW, et al. Fatal infantile mitochondrial encephalomyopathy, hypertrophic cardiomyopathy and optic atrophy associated with a homozygous OPA1 mutation. J Med Genet. 2016;53:127–31.

9.

He L, Chinnery PF, Durham SE, Blakely EL, Wardell TM, Borthwick GM, Taylor RW, Turnbull DM. Detection and

quantification of mitochondrial DNA deletions in individual cells by real-time PCR. Nucleic Acids Res. 2002;30:e68.
10.
Gai X, Ghezzi D, Johnson MA, Biagosch CA, Shamseldin HE, Haack TB, Reyes A, Tsukikawa M, Sheldon CA, et al. Mutations in FBXL4, encoding a mitochondrial protein, cause early-onset mitochondrial encephalomyopathy. Am J Hum Genet. 2013;93:482–95.
11.
Legati A, Reyes A, Nasca A, Invernizzi F, Lamantea E, Tiranti V, Garavaglia B, Lamperti C, Ardissone A, et al. New genes and pathomechanisms in mitochondrial disorders unraveled by NGS technologies. Biochim Biophys Acta. 2016;1857:1326–35.
12.
McKenna A, Hanna M, Banks E, Sivachenko A, Cibulskis K, Kernytsky A, Garimella K, Altshuler D, Gabriel S, et al. The genome analysis toolkit: a MapReduce framework for analyzing next-generation DNA sequencing data. Genome Res. 2010;20:1297–303.
13.
Cordeddu V, Redeker B, Stellacci E, Jongejan A, Fragale A, Bradley TE, Anselmi M, Ciolfi A, Cecchetti S, et al. Mutations in ZBTB20 cause Primrose syndrome. Nat Genet. 2014;46:815–7.
14.
Niceta M, Stellacci E, Gripp KW, Zampino G, Kousi M, Anselmi M, Traversa A, Ciolfi A, Stabley D, et al. Mutations impairing GSK3-mediated MAF phosphorylation cause cataract,

deafness, intellectual disability, seizures, and a down syndrome-like facies. Am J Hum Genet. 2015;96:816–25.
15.
Sferra A, Baillat G, Rizza T, Barresi S, Flex E, Tasca G, D'Amico A, Bellacchio E, Ciolfi A, et al. TBCE mutations cause early-onset progressive encephalopathy with distal spinal muscular atrophy. Am J Hum Genet. 2016;99:974–83.
16.
Flex E, Niceta M, Cecchetti S, Thiffault I, Au MG, Capuano A, Piermarini E, Ivanova AA, Francis JW, et al. Biallelic mutations in TBCD, encoding the tubulin folding cofactor D, perturb microtubule dynamics and cause early-onset encephalopathy. Am J Hum Genet. 2016;99:962–73.
17.
Cingolani P, Platts A, le Wang L, Coon M, Nguyen T, Wang L, Land SJ, Lu X, Ruden DM. A program for annotating and predicting the effects of single nucleotide polymorphisms, SnpEff: SNPs in the genome of Drosophila melanogaster strain w1118; iso-2; iso-3. Fly (Austin). 2012;6:80–92.
18.
Kircher M, Witten DM, Jain P, O'Roak BJ, Cooper GM, Shendure J. A general framework for estimating the relative pathogenicity of human genetic variants. Nat Genet. 2014;46:310–5.
19.
Dong C, Wei P, Jian X, Gibbs R, Boerwinkle E, Wang K, Liu X. Comparison and integration of deleteriousness prediction

methods for nonsynonymous SNVs in whole exome sequencing studies. Hum Mol Genet. 2015;24:2125–37.
20.
Seelow D, Schwarz JM, Schuelke M. GeneDistiller--distilling candidate genes from linkage intervals. PLoS One. 2008;3:e3874.
21.
Cassandrini D, Cilio MR, Bianchi M, Doimo M, Balestri M, Tessa A, Rizza T, Sartori G, Meschini MC, et al. Pontocerebellar hypoplasia type 6 caused by mutations in RARS2: definition of the clinical spectrum and molecular findings in five patients. J Inherit Metab Dis. 2013;36:43–53.
22.
Rizza T, Vazquez-Memije ME, Meschini MC, et al. Assaying ATP synthesis in cultured cells: a valuable tool for the diagnosis of patients with mitochondrial disorders. Biochem Biophys Res Commun. 2009;383:58–62.
23.
Bonifert T, Karle KN, Tonagel F, Batra M, Wilhelm C, Theurer Y, Schoenfeld C, Kluba T, Kamenisch Y, et al. Pure and syndromic optic atrophy explained by deep intronic OPA1 mutations and an intralocus modifier. Brain. 2014;137:2164–77.
24.
Nolli C, Goffrini P, Lazzaretti M, Zanna C, Vitale R, Lodi T, Baruffini E. Validation of a MGM1/OPA1 chimeric gene for functional analysis in yeast of mutations associated with dominant optic atrophy. Mitochondrion. 2015;25:38–48.

25.
Elachouri G, Vidoni S, Zanna C, Pattyn A, Boukhaddaoui H, Gaget K, Yu-Wai-Man P, Gasparre G, Sarzi E, et al. OPA1 links human mitochondrial genome maintenance to mtDNA replication and distribution. Genome Res. 2011;21:12–20.
26.
Lee J, Jung SC, Hong YB, Yoo JH, Koo H, Lee JH, Hong HD, Kim SB, Chung KW, Choi BO. Recessive optic atrophy, sensorimotor neuropathy and cataract associated with novel compound heterozygous mutations in OPA1. Mol Med Rep. 2016;14:33–40.
27.
Paquay S, Benoit V, Wetzburger C, Cordonnier M, Meire F, Charon A, Roland D, Van Coster R, Nassogne MC, Maystadt I. Uncommon Leber “plus” disease associated with mitochondrial mutation m.11778G > A in a premature child. J Child Neurol. 2014;29:NP18–23.
28.
Carelli V, Achilli A, Valentino ML, Rengo C, Semino O, Pala M, Olivieri A, Mattiazzi M, Pallotti F, et al. Haplogroup effects and recombination of mitochondrial DNA: novel clues from the analysis of Leber hereditary optic neuropathy pedigrees. Am J Hum Genet. 2006;78:564–74.

Chapter 5

Neurologic Phenotypes Associated With Mutations in RTN4IP1 (OPA10) in Children and Young Adults.

Charif M, Nasca A, Thompson K, Gerber S, Makowski C, Mazaheri N, Bris C, Goudenège D, Legati A, Marrofian R, Shariati G, Lamantea E, Hopton S, Ardissone A, Moroni I, Giannotta M, Siegel C, Strom TM, Prokisch H, Vignal-Clermont C, Derrien S, Zanlonghi X, Kaplan J, Ham CP, Leruez S, Procaccio V, Bonneau D, Reynier P, White FE, Hardy SA, Barbosa IA, Simpson MA, Vara R, Perdomo Trujillo Y, Galehdari H, Deshpande C, Haack TB, Rozet JM, Taylor RW, Ghezzi D, Amati-Bonneau P, Lenaers G.

JAMA Neurology 2018 Jan 75(1), pp. 105-113

Introduction

Mitochondrial inherited diseases are frequent causes of neurologic disorders that may consist of either isolated symptoms (eg, optic neuropathy, deafness, and myopathy) or complex syndromes (eg, Leigh syndrome, mitochondrial encephalomyopathy with lactic acidosis and stroke-like episodes, and neurogenic weakness with ataxia and retinitis pigmentosa) associated with many debilitating symptoms and these diseases and often lead to premature death because of severe encephalopathies.[1,2] Recently, the first mutations in the *RTN4IP1* (OMIM 610502) were described in individuals with

isolated recessive optic atrophy-10 (OPA10) in 3 families with a founder effect as well as in 2 sisters from an unrelated family, who were affected with a syndromic form associating the optic atrophy with cerebellar ataxia, mild intellectual disability, and seizures.[3] The *RTN4IP1* gene encodes a mitochondrial targeted protein[4] with a quinone oxidoreductase activity, involving 2 domains—an amino-terminal region with an alcohol dehydrogenase GroES-like signature (ADH_N) and a carboxy-terminal domain including a zinc-binding motif (ADH_Zinc). Mutations in this gene were not reported to affect mitochondrial network morphologic features, as is frequently the case in cells from individuals with dominant optic atrophy,[5,6] but result in a mild deficit in mitochondrial complexes I and IV enzymatic activities.[3] Together, these data led us to consider *RTN4IP1* sequence integrity in cohorts of individuals with inherited optic atrophy and complex I deficiency by using either targeted or whole-exome sequencing. In this article, we report on the identification of 11 novel families with *RTN4IP1* mutations and describe their association with various neurologic phenotypes.

Methods

Genetic Investigations

All patients were born from asymptomatic parents, except the mother from family 2, who showed symptoms unrelated to the disease of the 2 affected daughters. In consanguineous families (families 1 to 5 as well as 7 and 8), we anticipated identifying homozygous mutations. In the 4 nonconsanguineous simplex

families (families 6, 9, 10, and 11), we considered both recessive and dominant de novo mutations, especially in family 6, in which the affected girl was born to a father in his 50s. After extraction of genomic DNA from peripheral blood cells, we found homozygous or biallelic mutations in *RTN4IP1* by resequencing panels of genes dedicated to the molecular diagnosis of inherited optic neuropathies (panel of 17 genes, families 1-5) or to mitochondrial inherited diseases (panel of 219 genes, family 9) or by whole-exome sequencing (performed at the Imagine Institute for family 6; at the Helmoltz Zentrum München for families 7, 10, and 11; and at the Beijing Genomics Institute for Family 8). We analyzed the results by applying various prioritization filters, which are described elsewhere.[7,8] All identified nucleotide substitutions were absent or had a frequency lower than 1 in 1000 in public databases. Classification of mutation pathogenicity was performed according to the American College of Medical Genetics and Genomics criteria.[9] The Iranian mutation was absent in ethically and geographically matched 450 exomes. With Sanger sequencing using primers, which are described elsewhere,[3] we confirmed the identified mutations and tested the carrier status of the unaffected relatives when their DNA was available. This study was approved by the institutional review boards of Angers University Hospital in Angers, France; Neurological Institute “Besta” in Milan, Italy; Technical University of Munich in Munich, Germany; and King’s College in London, England. Written informed patient consent was obtained from each participant in

this study or from the parents of participants who were younger than 18 years, according to approved protocols of the different institutions involved in this study and the Declaration of Helsinki.[10] This study was conducted from May 1, 2014, to June 30, 2016.

Biochemical and Cellular Studies of Fibroblasts and Muscle Biopsies

Biochemical measurement of individual oxidative phosphorylation complex activities was performed by standard spectrophotometric assays[11] in muscle homogenate and digitonin-treated skin fibroblasts. Assessments of RTN4IP1 abundance and the mitochondrial network structure of *RTN4IP1*-mutated and control fibroblast cell lines were performed according to the process described in Angebault et al.[3] Quadruple immunofluorescence analysis and assessment of the assembly of the respiratory chain complexes of muscle biopsy specimens were performed according to the process described in Rocha et al.[12] Blue native polyacrylamide gel electrophoresis on skeletal muscle samples was performed as described in Alston et al.[13]

Results

Patient Presentations

Family 1

A teenaged boy was the first child born to Romany consanguineous parents. His sister and brother were healthy. Strabismus was detected at age 3 years and operated on at age 6 years. Nystagmus was present at age 6 years and was

stable. His bilateral visual acuity was 20/250, and fundus examination revealed a temporal pale papilla. Optical coherence tomography (OCT) confirmed the optic atrophy. Magnetic resonance images (MRIs) of the brain were normal.

Family 2

Two girls—a preteen and a teenager—born to Romany consanguineous parents had optic atrophy and a visual acuity of 20/200 and 20/500, respectively. Their sister and brother were healthy. Their brain MRIs were normal. The mother had photophobia, a mild right ptosis, and balance disorder.

Family 3

This teenaged boy born to Romany consanguineous parents presented at age 4 years with progressive bilateral visual loss leading to visual acuity of 20/100 bilaterally. Visual evoked potential (VEP) showed cortical conduction delay with amplitude change, OCT confirmed the bilateral optic atrophy, and a brain MRI was normal. He had a healthy sister.

Family 4

This young man in his 20s born to Romany consanguineous parents presented with bilateral visual acuity loss (20/400) at age 5 years. The VEP and OCT confirmed the presence of a bilateral optic atrophy.

Family 5

This girl younger than 10 years was born to consanguineous Maghrebian parents and diagnosed at the age of 6 with an optic atrophy. She had a visual acuity of 3/20 bilaterally and a red-green dyschromatopsy, but she had no nystagmus.

Family 6

This girl younger than 10 years was the last and only affected child of 4 children born to an unrelated Mauritius father of Irish/Pakistani descent and a mother of Indian descent. There was no family history of visual deficiency. At conception, her father was almost 60 years old and her mother was in her early 30s. The girl was born full term after an uneventful pregnancy and delivery. The perinatal period was unremarkable. At age 2 years, she presented with strabismus, but the diagnosis of optic neuropathy was made at age 5 years when she experienced a sudden and severe decrease in visual acuity—from 20/32 OU to 20/400 OD and 20/200 OS in a 3-month period.

Ophthalmological examination revealed bilateral temporal optic atrophy at the fundus, loss of optic nerve fibers and normal macula at the OCT, severely altered VEP with normal electroretinogram, and dyschromatopsia with red-green axis. Neurologic examination and cerebral and medullar MRI were strictly normal.

Family 7

This boy was born at term after a normal pregnancy by vaginal delivery to healthy, consanguineous parents from Pakistan. A younger and an older brother were healthy. Postnatal adaption and early development were reported as normal. As a toddler, he had a first seizure during an infection with a high temperature. Two weeks after this acute episode, twitching of the eyes and the mouth were observed. Sixteen months later, the first generalized tonic-clonic seizure occurred. Thereafter,

he had seizures every 2 to 3 months that did not respond well to medication. Subsequently, he lost already acquired skills, such as chewing and expressive language (single words). On physical examination in the preteen years, his weight was 22.9 kg (<third centile), length was 116 cm (<third centile), and head circumference was 53 cm (21st centile). He was severely intellectually impaired, nonverbal, and unable to stand or walk unaided. A hearing impairment was suspected clinically, but no pediatric audiologic examination had been performed. Extensive laboratory testing was unremarkable, and only the plasma lactate concentration was elevated (28.8 mg/dL [to convert to millimoles per liter, multiply by 0.111]). Results of a brain MRI and cranial ultrasonography were normal. Testing of the *POLG* (OMIM *174763) gene did not reveal any pathogenic variants. No optic atrophy was mentioned in the results from cardiac MRI, and no explicit ophthalmologic examination was performed.

Family 8

The woman in her 30s was from a consanguineous family from south Iran. She has 3 sisters and 1 brother, all of whom are healthy. She was hypotonic at birth but otherwise was normal. All her growth measurements were within the normal range. She had psychomotor delay with walking difficulty characterized by unsteady ataxic gaits, poor balance, and frequent falls. She could not walk without assistance, and this condition got worse gradually; in her midteens, she had lost the ability to walk and

became wheelchair-bound and bedridden. Her lower limbs were spastic, and she experienced severe pain in her lower legs.

She has poor language skills and speaks only single words. She displays severe intellectual disability, cannot live independently, and requires close supervision and support with self-care activities. Vertical nystagmus was noticed in infancy, and in her preteen years, her vision started to decline gradually, which eventually led to loss of vision in her mid-20s. Ophthalmologic examination showed progressive bilateral optic atrophy associated with nystagmus, photophobia, and color vision impairment. She experienced her first seizure suddenly before age 5 years. In her childhood, she experienced seizure only once a day, every 2 to 3 months, but this increased to be more severe with 5 to 6 attacks every 2 to 3 months that were not responsive to medication. Her bouts of seizure only remitted in her mid-20s. Currently, her seizure is under control with low doses of medication. Brain MRI and OCT have not been performed for this patient.

Family 9

This patient was a boy younger than 10 years and was the second child born to healthy, unrelated Italian parents. His family history was unremarkable. He was born at term after a regular pregnancy and had a normal perinatal period. During his first year of life, his parents noticed poor visual contact and delay in head control. First instrumental examinations were performed before 1 year of age: fundus examination disclosed bilateral optic atrophy, and a brain MRI showed normal findings.

Clinical evolution confirmed psychomotor developmental delay: sitting position at older than 1 year, supported deambulation from age 5 years, and babbling at age 2 years (no other language skills were reported). At age 3 years, he presented with generalized seizures that became drug resistant in the following years and were associated with multifocal and subcontinous abnormalities on the electroencephalogram (EEG). Serial brain MRI disclosed bilateral T2 hyperintensities in the subthalamic nucleus and in the nucleus dentate and brainstem, brainstem auditory evoked potential revealed the absence of a v wave, and elevated serum lactate (2.9 mmol/L; reference range, 0.5-2.1 mmol/L) and serum pyruvate (150 µmol/L; reference range, 40-140 µmol/L) levels were detected. A mitochondrial disease was suspected, a muscle biopsy was performed, and the result of a respiratory chain analysis was normal. Analysis of the *POLG*, *MTATP6* (OMIM +516060), *OPA1* (OMIM *605290), *SCA1* (OMIM 164400), *SCA2* (OMIM 183090), and *SCA6* (OMIM 183086) genes were negative for pathogenic variants.

This patient arrived for our observation before age 10 years. Results of a clinical examination showed spastic tetraparesis and dystonia at the upper limbs, with deambulation possible only with support and severe cognitive impairment (which was impossible to test). Fundus oculi confirmed bilateral optic atrophy, visual and brainstem auditory evoked potentials disclosed marked multisystem central abnormalities, and

neuronography showed sensitive axonal neuropathy. A brain MRI disclosed T2 hyperintensities in the thalami as well as abnormalities in the subthalamic and dentate nuclei and in the brainstem. The lactate level (32.4 mg/dL; reference range, 5.2-18.9 mg/dL) and pyruvate level (1.7 mg/dL; reference range, 0.4-1.2 mg/dL [to convert to micromoles per liter, multiply by 113.56) were elevated in plasma; amino acid serum levels and urinary organic acid levels were normal. Treatment with thiamin hydrochloride, coenzyme Q 10, and riboflavin was started, but no clinical benefits were observed. Clinical evolution was stable except for worsening of epilepsy. The spectrophotometric determination of mitochondrial respiratory chain complex activities displayed an isolated reduction of complex I normalized to citrate synthase (12.6; reference range, 16-34) in skin fibroblasts. No further material from muscle biopsy was available.

Family 10

This boy was the first born after a normal pregnancy by vaginal delivery to nonconsanguineous Italian parents. In his first months of life, the first signs noticed were eyelid myoclonia with inconsolable stridor on awakening, impaired eye-to-eye contact, hypotonia, and developmental delay. At age 4 months, concomitant to the first vaccination, he manifested fever and seizures consisting of eyelid myoclonias and partial tonic-clonic fits that rapidly spread into generalized myoclonic epileptic refractory status. Later, his condition led to drug-resistant partial seizures and myoclonic status. An EEG showed a burst-

suppression pattern. He developed a severe psychomotor delay with hypotonia and scarce visual contact. Results of a brain MRI were normal in the first few months of life but revealed severe cerebral atrophy with an increase in lactate at spectroscopy as he approached 1 year. Visual function investigation showed evidence of mild pale papilla, normal photopic, and absent (impossible to test) scotopic responses on an electroretinogram. Visual evoked potentials showed cortical conduction delay with amplitude change. Extensive metabolic and molecular workup did not reveal alteration in values for serum, cerebrospinal fluid, or urine amino acids; urine organic acids; sulfitest; clinitest; cerebrospinal fluid neurotransmitters; serum very-long-chain fatty acid; congenital defects of glycosylation; biotinidase; and copper and ceruloplasmin dosage. Comparative genomic hybridization array, *CDKL5* (OMIM *300203) and *ARX* (OMIM *300382) expression, and *POLG* sequence and karyotype were normal. Pyruvate dehydrogenase complex activities were normal on examination of skin and muscle biopsy specimens as was palmitoyl protein thioesterase 1 dosage on fibroblasts. Analysis of mitochondrial respiratory chain complexes showed an isolated complex I reduction in muscle (value normalized to citrate synthase activity, 6.5; reference range, 13-28) and skin fibroblasts (value normalized to citrate synthase activity, 12.2; reference range, 13-30). The boy died of cardiorespiratory failure before age 5 years.

Family 11

This girl was the second child born to unrelated parents. There were decreased fetal movements during the pregnancy but no anomalies on the antenatal scans. She was born at term (birth weight, 4 kg; length, 59 cm; and head circumference, 36 cm) and was discharged home at 2 days but readmitted at age 1 week for poor feeding and stridor. Her weight gain was very poor, and nasogastric feedings were started at 3 weeks. Investigations showed persistently elevated plasma lactate levels (3.0 mmol/L). At age 3 weeks, she developed eye-rolling movements and was not as responsive; she was referred to a specialist center for further investigation. An elevated plasma lactate level (28.8 mg/dL) was noted at admission along with a raised alanine level (6.59 mg/dL [to convert to micromoles per liter, multiply by 112.2); the urinary organic acid profile was nonspecific; and results of very-long-chain fatty acids, acylcarnitine profile, and liver function tests were all normal. Brain MRI findings showed symmetrical T2 high-signal change with associated swelling in the posterolateral aspect of both putamina suggestive of a mitochondrial disorder . She had progressive stridor, and bronchoscopy showed short aryepiglottic folds and collapsing arytenoids. She had a tracheostomy. She developed frequent apneas, and her EEG showed an abnormal attenuated background with slow waves and low-voltage spikes and spike-and-wave discharges that were seen independently over the left centrotemporal and right posterior quadrants and suggestive of focal left temporofocal

epilepsy. Her clinical status deteriorated progressively, and she died before age 1 year.

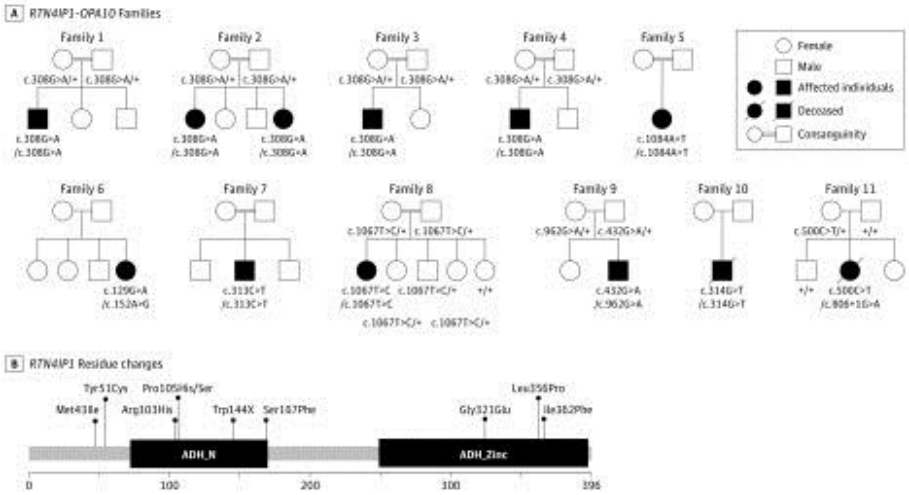

Figure 1.

Pedigree of the RTN4IP1 (OPA10) Families, Segregation of the Mutations, and Alterations of the Protein Primary Structure

A, Pedigrees show the affected cases in the 11 families and the segregation of the mutations. Black symbols indicate affected patients. B, Localization of RTN4IP1 residue changes in the protein: the primary structure of RTN4IP1 protein (domains and amino acid positions) is described in the figure with all of the pathogenic mutations reported in this study. ADH_N indicates alcohol dehydrogenase GroES-like domain; ADH_Zinc, zinc-binding dehydrogenase domain.

Molecular Investigations

Using a dedicated gene panel covering all *RTN4IP1* exons, we sequenced DNA from 300 patients with suspected inherited optic neuropathies that were negative for *OPA1* mutations and the 3 main Leber hereditary optic neuropathy mutations. Five cases from consanguineous families (families 1-4) were identified with the homozygous c.308G>A mutation (Figure 1A) on a unique haplotype (described in Angebault et al[3]), leading

to the p.Arg103His residue change. These cases were all of Romany origin, suggesting a high prevalence of this mutation in that population. A patient with a homozygous c.1084A>T mutation (p.Ile362Phe) in a consanguineous Maghrebian family (family 5; Figure 1A) was also identified. The p.Arg103His and p.Ile362Phe mutations affect each of the 2 oxidoreductase conserved domains, ADH_N or ADH_Zinc, respectively (Figure 1B), and are considered to be deleterious according to the SIFT, Polyphen, and MutationTaster programs and the American College of Medical Genetics and Genomics criteria. A patient born to nonconsanguineous parents from Mauritius (family 6) was found to be compound heterozygous for the unreported c.129G>A (p.Trp51Cys) and c.152A>G (p.Met43Ile) mutations, which affect evolutionary conserved amino acids upstream of the ADH_N domain and are considered to be deleterious. All of these individuals presented severe, isolated, early-onset optic atrophy (Figure 2) and stable low visual acuity

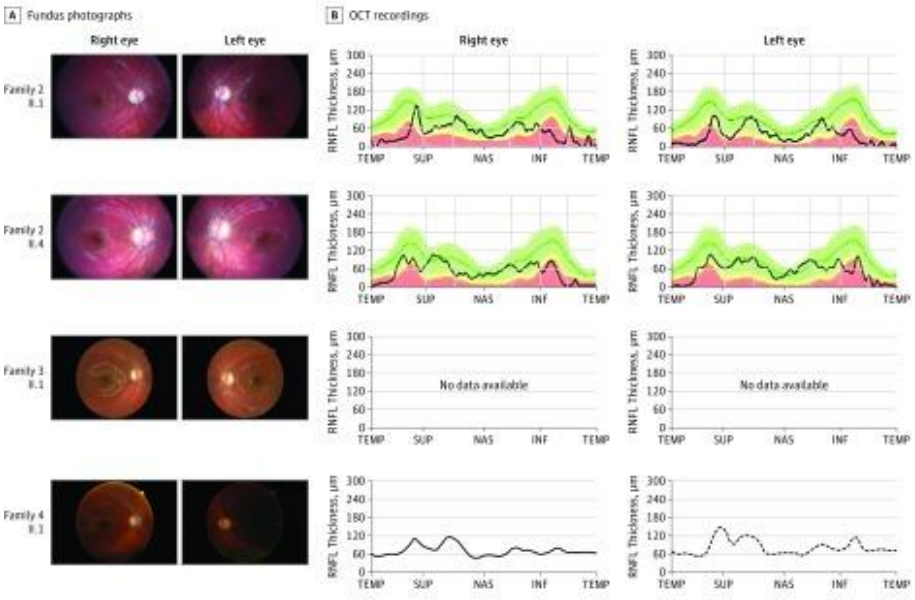

Figure 2.

Ophthalmological Examination of *RTN4IP1 (OPA10)* Patients

Eye fundus of the right and left eyes from indicated patients (A) and the corresponding optical coherence tomographic (OCT) recordings (B) are shown, when available. INF indicates inferior; NAS, nasal; RNFL retinal nerve fiber layer; SUP, superior; and TEMP, temporal.

Using a resequencing panel of 219 mitochondrial genes or by whole-exome sequencing, we identified novel pathogenic *RTN4IP1* mutations in 5 individuals with severe early-onset encephalopathy associated with optic atrophy (Figure 1A). Three homozygous mutations were found in families: c.313C>T in family 7, c.314C>A in family 8, and c.1067T>C in family 10. These mutations are anticipated to change a proline to either a serine or lysine (p.Pro105Ser/Lys) in the ADH_N domain or a leucine to a proline (p.Leu356Pro) in the ADH_Zinc domain, thus possibly destabilizing the protein

structure or impairing its function (Figure 1B). In the 2 heterozygous composite cases from families 9 and 11 (Figure 1A), 1 mutated allele led to a loss of function corresponding to either a stop codon (p.Tyr144*) or to a splicing defect (de novo c.806 + 1G>A mutation), while the other mutated allele induced a rare damaging missense mutation (p.Gly321Glu or p.Ser167Phe, respectively). All these changes altered either of the 2 conserved ADH enzymatic domains of RTN4IP1 (Figure 1B). In these affected individuals, a core of common symptoms was identified that consisted of optic atrophy (although not investigated by an ophthalmologist in family 7), seizures, and various severity of global developmental delay as reported in a previous study.[3] In addition, in the most affected cases (families 9-11), the associated clinical features were deafness, brain MRI abnormalities stridor, and abnormal EEG, all of which eventually led to premature death. In these cases, we disclosed a complete absence of RTN4IP1 protein in fibroblasts and muscle biopsy (Figure 3A and C), which was associated with the fragmentation of the mitochondrial network (Figure 3B) in fibroblasts from the index cases of families 9 and 10 and with the drastic effect on *NDUFB8* (OMIM *602140) (complex I) protein levels and mitochondrial complex I assembly in the muscle biopsy from the index case of family 11 (Figure 3C). Furthermore, increased lactate concentrations in blood and brain were revealed by MRI spectroscopy in these severely affected patients.

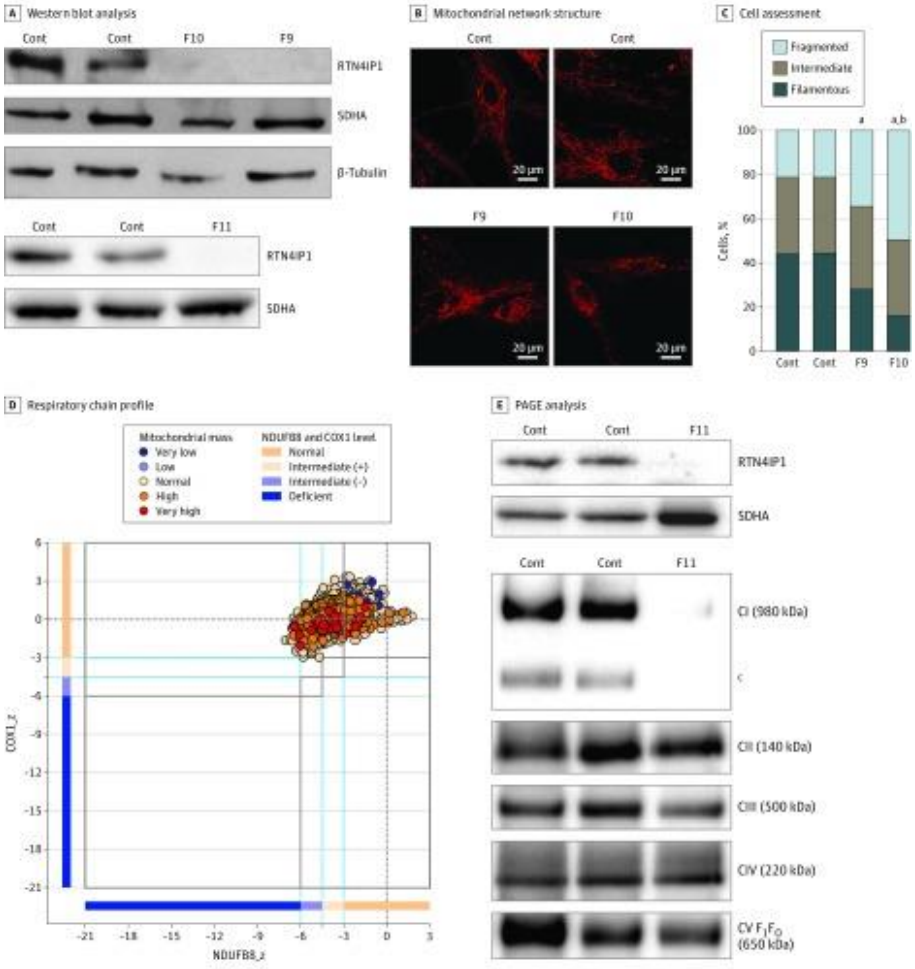

Figure 3.

Association of Decreased RTN4IP1 Levels With Mitochondrial Network Structure Muscle of Severely Affected Patients

A, Western blot analysis of RTN4IP1 protein levels in fibroblasts from controls (Cont) and *RTN4IP1* index cases of families 9 (F9), 10 (F10), and 11 (F11). Succinate dehydrogenase and β-tubulin antibodies were used as loading Cont. B, Assessment of mitochondrial network structure from 2 Cont fibroblast cell lines and from fibroblasts of the index cases of F9 and F10 (MitoTracker stain; Thermo Fisher Scientific). C, Assessment of the percentage of cells presenting a fragmented, intermediate, or filamentous network. D, Respiratory chain profile following quadruple oxidative phosphorylation immunofluorescence analysis of cryosectioned muscle from the index case of F11, confirming the presence of fibers lacking complex I

(NDUFB8) protein but with normal complex IV (COX1) expression. (Experimental procedures per the protocols of Rocha et al.) Each dot represents the measurement from an individual muscle fiber, color coded according to its mitochondrial mass. Gray dashed lines indicate SD limits for the classification of fibers; lines next to x- and y-axes, the levels (SDs from the average of Cont fibers after normalization to porin/VDAC1 levels) of NDUFB8 and COX1, respectively; and _*z*, the *z* score for COX1 or NDUFB8. (For formulas and full description of statistics involved, see the Methods section of Rocha et al.) Blue dotted lines indicate the mean expression level observed in respiratory normal fibers. E, One-dimensional blue native polyacrylamide gel electrophoresis (PAGE) (4%-16% gradient) analysis showing a specific complex I assembly defect in skeletal muscle from the index case of F11 and age-matched Cont. Individual oxidative phosphorylation complexes were detected by immunoblotting using subunit-specific antibodies (complex I [C1] [NDUFB8], CII [SDHA], CIII [UQCRC2], CIV [COX1], and CV [ATP5A]). Complex V comprises the F_1 and F_O subcomplexes. F_1F_O denotes that the band is the complete assembled form of adenosine triphosphate synthase (CV). [a]*P* < .001 compared with Cont. [b]*P* < .05 compared with F9. [c]Indicates the presence of an additional, partially assembled CI intermediate also detected with the NDUFB8 antibody, absent in the patient sample, and likely corresponding to the approximately 650-kDa Iβ subcomplex of the hydrophobic membrane arm.

Discussion

A large spectrum of neurologic features, ranging from isolated optic atrophy to severe early-onset encephalopathy, can be associated with biallelic mutations in *RTN4IP1*. A first group of nonsyndromic cases comprised patients who presented severe, early optic atrophy with stable, low visual acuity but no additional symptoms . Their clinical presentations overlapped with those of previously reported families[3]; the common Romany origin and the shared p.Arg103His mutation confirm a founder effect in this ethnic group and a strict genotype-phenotype correlation for this variant. Nevertheless, the same

phenotype was observed in 2 cases (families 5 and 6) with different origins and mutations. In family 6, heterozygous composite mutations affecting amino acids 43 and 51 located out of the 2 conserved ADH domains might interfere with the structure of the mitochondrial targeting sequence, which is predicted to encompass amino acids 1 to 49. In the syndromic cases, harboring various novel mutations, a core of common symptoms consisted of optic atrophy, seizures, and various severity of mental and growth retardation as already reported in the last family of our previous study.[3] Nevertheless, the most severely affected individuals presented features of deafness, brain MRI abnormalities, stridor, and abnormal EEG findings, which were systematically associated with drastically reduced RTN4IP1 abundance, complex I activity, and assembly and increased lactate concentrations in blood, revealing a major impairment of the oxidative phosphorylation function, which is reported for many diseases with complex I defect, such as the Leigh syndrome.[14-16]

Most novel *RTN4IP1* mutations affect either of the 2 conserved enzymatic domains of RTN4IP1 protein, but there is no evident correlation between the severity of the clinical presentation and the affected domain. For instance, mutations affecting very close amino acids (ie, Arg103 and Pro105) led to highly different phenotypes. However, analysis of amino acid changes reveals that, in nonsyndromic cases, mutations in ADH domains led to conservative changes, substituting arginine to histidine (2 positively charged residues) and isoleucine to phenylalanine (2

hydrophobic residues). Similarly, the 2 mutations affecting the N-terminal domain located upstream of the ADH_N domain, changed methionine to isoleucine and tyrosine to cysteine, which are also conservative.

Conversely, in syndromic individuals, all the missense mutations change the biochemical properties of the residues, probably destabilizing the protein structure, often by introducing or deleting a proline. Two other mutations found in the most severe cases are predicted to cause the truncation of the protein; thus, these alterations are likely more deleterious on RTN4IP1 activity or structure than those leading to isolated optic atrophy. Nevertheless, the mitochondrial function of RTN4IP1 remains poorly described, particularly the characterization of its enzymatic activity, prompting future pathophysiological challenges.

The gradual severity associated with the different mutations in a single gene is a phenomenon increasingly reported in the past few years, particularly for mitochondrial diseases affecting primarily the central nervous system. *RTN4IP1* is the third gene responsible for recessive isolated optic atrophy, after the identification of *TMEM126A* (OMIM *612988) and *ACO2* (OMIM *100850),[17,18] and is the most frequently mutated, as we have now reported a total of 9 *RTN4IP1* families with this restricted ophthalmological presentation, whereas only 5 were reported with *TMEM126A* mutations and 1 with *ACO2* mutations. Auditory neuropathy and encephalopathy associated with cerebellar ataxia have also been reported in association with

the optic nerve atrophy in individuals bearing mutations in *TMEM126A* and *ACO2*.[17,18] In this respect, many other syndromic presentations with recessive or dominant traits involve an alteration of the optic nerve, and an increasing number of mild mutations in causative genes that manifest syndromic disorders have been shown to be responsible for isolated optic atrophy,[19-21] emphasizing the frailty of the retinal ganglion cells to mitochondrial dysfunction. This finding is further highlighted by the spectrum of complex I diseases that can result either in isolated optic neuropathy, such as Leber hereditary optic neuropathy, or in severe syndromic diseases, such as Leigh syndrome, which leads to clinical presentations quite similar to those described here.

Limitations

This study has several limitations. First, deep-intronic variants were not screened in our sample of individuals with isolated or syndromic optic neuropathies, possibly leading to an underestimation of *RTN4IP1* involvement. Second, biochemical and mitochondrial investigations were not performed in all affected individuals, limiting the correlation that could be drawn between clinical and biochemical phenotypes.

Conclusions

We expect that future works will identify novel mutations in tens of genes that will illustrate a spectrum of clinical presentations, ranging from isolated optic atrophy to very complex and severe syndromes, as exemplified here for *RTN4IP1*. In this respect, there is a need to generate novel databases that aggregate

genotype-phenotype associations for genes involved in inherited mitochondrial diseases, such as the one we designed for *OPA1*-related isolated and syndromic optic neuropathies.[22]

References

1. DiMauro S. Mitochondrial diseases. *Biochim Biophys Acta*. 2004;1658(1-2):80-88.

2. Munnich A, Rustin P. Clinical spectrum and diagnosis of mitochondrial disorders. *Am J Med Genet*. 2001;106(1):4-17.

3. Angebault C, Guichet PO, Talmat-Amar Y, et al. Recessive mutations in *RTN4IP1* cause isolated and syndromic optic neuropathies. *Am J Hum Genet*. 2015;97(5):754-760.

4. Hu WH, Hausmann ON, Yan MS, Walters WM, Wong PK, Bethea JR. Identification and characterization of a novel Nogo-interacting mitochondrial protein (NIMP). *J Neurochem*. 2002;81(1):36-45.

5. Lenaers G, Hamel C, Delettre C, et al. Dominant optic atrophy. *Orphanet J Rare Dis*. 2012;7:46.

6. Chao de la Barca JM, Prunier-Mirebeau D, Amati-Bonneau P, et al. *OPA1*-related disorders: diversity of clinical expression, modes of inheritance and pathophysiology. *Neurobiol Dis*. 2016;90:20-26.

7.
Legati A, Reyes A, Nasca A, et al. New genes and pathomechanisms in mitochondrial disorders unraveled by NGS technologies. *Biochim Biophys Acta*. 2016;1857(8):1326-1335.
8.
Colin E, Daniel J, Ziegler A, et al; FREX Consortium. Biallelic variants in *UBA5* reveal that disruption of the UFM1 cascade can result in early-onset encephalopathy. *Am J Hum Genet*. 2016;99(3):695-703.
9.
Richards S, Aziz N, Bale S, et al; ACMG Laboratory Quality Assurance Committee. Standards and guidelines for the interpretation of sequence variants: a joint consensus recommendation of the American College of Medical Genetics and Genomics and the Association for Molecular Pathology. *Genet Med*. 2015;17(5):405-424.
10.
World Medical Association. World Medical Association Declaration of Helsinki: ethical principles for medical research involving human subjects. *JAMA*. 2013;310(20):2191-2194.
11.
Bugiani M, Invernizzi F, Alberio S, et al. Clinical and molecular findings in children with complex I deficiency. *Biochim Biophys Acta*. 2004;1659(2-3):136-147.
12.
Rocha MC, Grady JP, Grünewald A, et al. A novel immunofluorescent assay to investigate oxidative

phosphorylation deficiency in mitochondrial myopathy: understanding mechanisms and improving diagnosis. *Sci Rep*. 2015;5:15037.

13.

Alston CL, Howard C, Oláhová M, et al. A recurrent mitochondrial p.Trp22Arg *NDUFB3* variant causes a distinctive facial appearance, short stature and a mild biochemical and clinical phenotype. *J Med Genet*. 2016;53(9):634-641.

14.

Angebault C, Charif M, Guegen N, et al. Mutation in *NDUFA13/GRIM19* leads to early onset hypotonia, dyskinesia and sensorial deficiencies, and mitochondrial complex I instability. *Hum Mol Genet*. 2015;24(14):3948-3955.

15.

Fassone E, Rahman S. Complex I deficiency: clinical features, biochemistry and molecular genetics. *J Med Genet*. 2012;49(9):578-590.

16.

Lebre AS, Rio M, Faivre d'Arcier L, et al. A common pattern of brain MRI imaging in mitochondrial diseases with complex I deficiency. *J Med Genet*. 2011;48(1):16-23.

17.

Metodiev MD, Gerber S, Hubert L, et al. Mutations in the tricarboxylic acid cycle enzyme, aconitase 2, cause either isolated or syndromic optic neuropathy with encephalopathy and cerebellar atrophy. *J Med Genet*. 2014;51(12):834-838.

18.

Hanein S, Perrault I, Roche O, et al. *TMEM126A*, encoding a mitochondrial protein, is mutated in autosomal-recessive nonsyndromic optic atrophy. *Am J Hum Genet*. 2009;84(4):493-498.

19.

Charif M, Roubertie A, Salime S, et al. A novel mutation of *AFG3L2* might cause dominant optic atrophy in patients with mild intellectual disability. *Front Genet*. 2015;6:311.

20.

Klebe S, Depienne C, Gerber S, et al. Spastic paraplegia gene 7 in patients with spasticity and/or optic neuropathy. *Brain*. 2012;135(pt 10):2980-2993.

21.

Rouzier C, Bannwarth S, Chaussenot A, et al. The *MFN2* gene is responsible for mitochondrial DNA instability and optic atrophy “plus” phenotype. *Brain*. 2012;135(Pt 1):23-34.

22.

Ferré M, Caignard A, Milea D, et al. Improved locus-specific database for OPA1 mutations allows inclusion of advanced clinical data. *Hum Mutat*. 2015;36(1):20-25.

Chapter 6

Compound heterozygous missense and deep intronic variants in NDUFAF6 unraveled by exome sequencing and mRNA analysis.

CataniaA, Ardissone A, Verrigni D,LegatiA, Reyes A, Lamantea E, Diodato D, Tonduti D, Imperatore V, Pinto AM, Moroni I, Bertini E, Robinson A, Carrozzo R, Zeviani M, Ghezzi D.

Journal of Human Genetics 2018 May 63(5), pp. 563-568

Introduction

Leigh syndrome is an early onset progressive neurodegenerative disease with an invariably devastating clinical course. The neuropathology of Leigh syndrome is characterized by bilateral, symmetrical necrotic lesions in deep gray matter structures. The most common cause of Leigh syndrome is a defect in oxidative phosphorylation.[1] The NADH dehydrogenase (ubiquinone) complex I assembly factor 6 (*NDUFAF6,* previously known as *C8ORF38*) gene encodes a mitochondrial protein, highly conserved across eukaryotes, which plays an essential role in the early assembly stages of mitochondrial respiratory chain complex I.[2] Biallelic missense mutations within *NDUFAF6* have been associated with cases of Leigh syndrome due to mitochondrial complex I deficiency.[3–5] In a very recent paper about molecular and enzymatic assays for diagnosis in Leigh syndrome cases, *NDUFAF6* was one of the

most frequently mutated nuclear genes and was invariably associated with reduced complex I activity.[6]

Recently, Bianciardi et al.[7] described a patient presenting Leigh syndrome and mitochondrial complex I deficiency associated with a pathogenic heterozygous missense variant in *NDUFAF6* (c.532G>C:p.A178P) and an almost monoallelic expression of the mutated allele at transcriptional level; an autosomal recessive model of inheritance was hypothesized, but the second pathogenic mutation remained unidentified.[7] Upon identification in our laboratory of two siblings and a singleton unrelated subject, all affected by Leigh syndrome and harbouring the same heterozygous missense mutation (c.532G>C:p.A178P), here we provide evidence that the second allelic mutation consists of a deep intronic variant present in all affected individuals, including the previously published case.[7] Through mRNA analysis we demonstrated that the identified intronic mutation is responsible for the formation of an alternative splice site, leading to altered mRNA splicing.

2. Materials and Methods

Informed consents for biological sample collection and genetic studies were obtained from all the subjects involved in the study (Siblings A1 and A2 and their parents; patient B, previously described by Bianciardi et al.[7]; patient C and his parents), in agreement with the Declaration of Helsinki.

Extraction of genomic DNA from peripheral blood was performed using standard methods. A targeted-NGS using a custom panel containing genes responsible for mitochondrial

disorders[8] was performed on DNAs from patients A1 and B, while clinical exome sequencing using a commercial kit with genes associated with inherited diseases (TrusightOne, Illumina) was performed in patient C. Whole exome sequencing (WES) analysis and variant calling/prioritization were conducted on DNAs from patients A1 and A2, as previously described.[8] Libraries were prepared with the Nextera Rapid Exome Capture kit (FC-140-1001, Illumina), and sequencing was performed on an Illumina MiSeq platform. Variants identified by NGS were validated by Sanger sequencing and resolved on a 3130xl Genetic Analyzer (Applied Biosystems).

The identified mutations were validated by employing the following pairs of primers, respectively:

Exon 3b F: 5'-ATTTTGAGGTGGTGATTTCAAAG-3'; R: 5'-GGAAGGCTTTAGTGGTAAACTGG-3';

Exon 5 F: 5'-AATGGAAACCTATGGGCTAGAG-3'; R: 5'-TGAGCTTCTTGAAGTGGGATG-3'.

For RNA purification and cDNA retrotranscription we used RNeasy mini kit (QIAGEN) and GoTaq 2-Step RT-qPCR System (Promega), respectively, according to the manufacturers' protocols.

For cDNA amplification (from exon 3 to exon 7) and sequencing we used the following primer pair:

3F: 5'-CTGAGAAAACAATTGGACTGATG-3'; 7R: 5'-TCTCACATTTTTATCTTGGTTCCTC-3'.

For deep sequencing of *NDUFAF6* transcript, PCR products were processed with Nextera XT DNA sample preparation kit

(Illumina). Next Generation Sequencing (NGS) was performed on an Illumina MiSeq instrument. Filtered reads were then aligned using BWA and visualized with Integrating Genomics Viewer (IGV).

Tag SNPs were selected using the SNPinfo web server (https://snpinfo.niehs.nih.gov), based on the HapMap CEU (Utah residents with Northern and Western European ancestry) and Tuscani populations. Specific primers were designed (available upon request) and SNPs were assessed by Sanger sequencing. Information about SNPs frequencies was obtained from public databases: dbSNP, Genome Aggregation Database (gnomAD).

For the nonsense-mediated mRNA decay (NMD) assay, patients and control fibroblasts were grown in complete DMEM and incubated for 12 h with puromycin (100 µg/ml). Total RNA was extracted after 4 and 8 hours of recovery in puromycin free medium from treated and untreated paired cultures.

3. Results

3.1. Case reports

We report an Italian family in which two siblings were diagnosed with Leigh syndrome (Family A, Fig. 1A). The older sibling (patient A1) presented psychomotor regression at 21 months of age; neurological evaluation at 30 months showed ataxic gait and fine tremor. Cognitive functions were preserved. He presented a Leigh syndrome pattern at brain MRI. Biochemical analysis showed an isolated respiratory chain complex I deficiency in muscle and fibroblasts (42% and 38% of the

controls' mean, respectively). The disease was slowly progressive: at 4½ years he presented with drooling, dysarthria, dysmetria, tremor, severe ataxic gait and hypertonia. His younger sister (patient A2) showed psychomotor delay at the age of 12 months and then limb dysmetria, trunk titubation, and ataxic gait. Cognitive functions were preserved. MRI disclosed a Leigh syndrome pattern. Plasma lactate and pyruvate levels were slightly increased. A detailed clinical description of these cases is reported in the supplementary material.

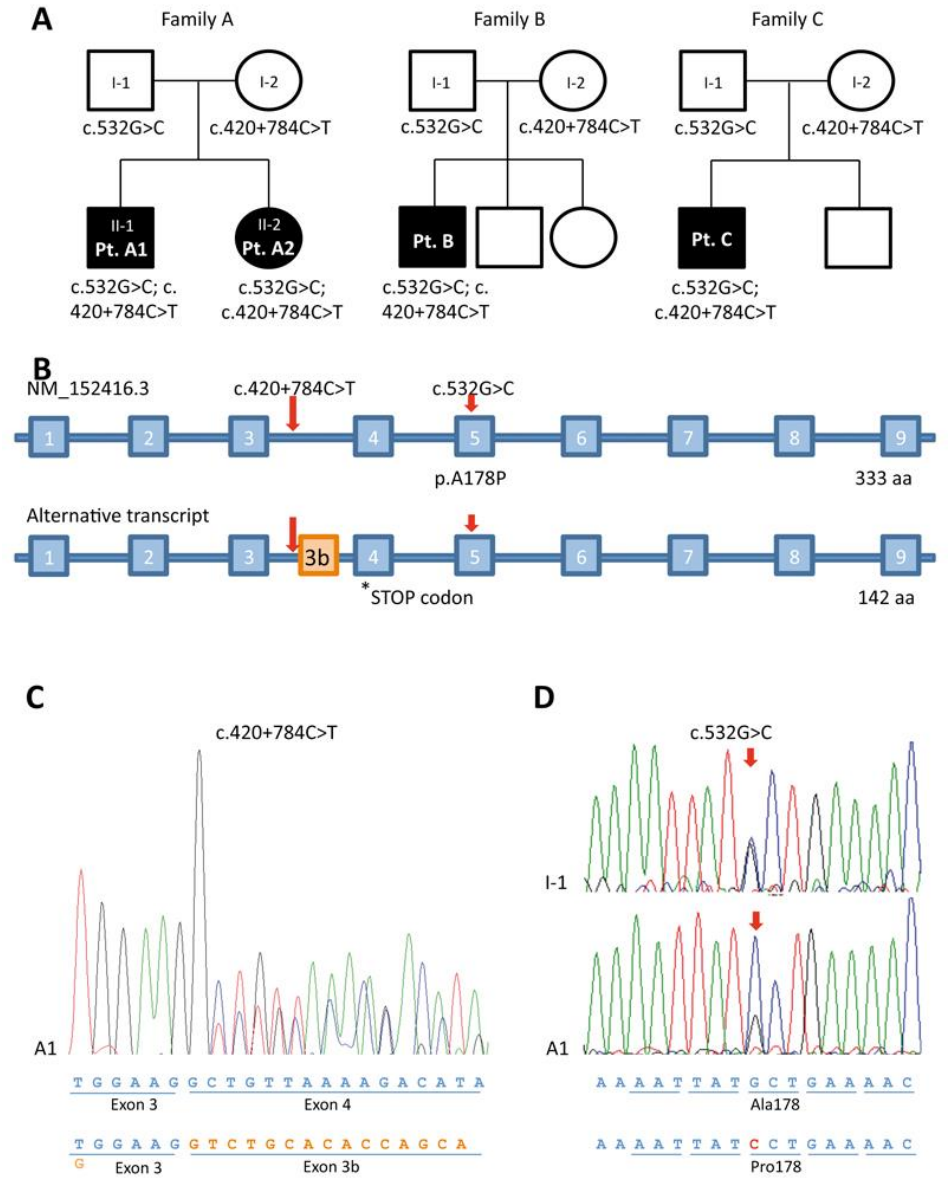

Figure 1

Pedigrees and genetic studies

A. Pedigrees of the families A, B, C showing the identified *NDUFAF6* variants. Black symbols indicate the affected siblings.

B. Schematic structure of *NDUFAF6* NM_152416.3 transcript (upper panel) and alternative splicing isoform (bottom panel). The retention of a string of 124

nucleotides located within intron 3 (exon 3b, orange box) generates a premature stop codon within exon 4 (arrow).

C. Sanger sequence of *NDUFAF6* cDNA obtained from patient A1 blood RNA, showing two distinct sequences starting from the end of exon 3, that correspond to the NM_152416.3 transcript (junction exon 3-exon 4) and an alternative transcript retaining exon 3b (junction exon 3-exon 3b).

D. Sanger sequence of *NDUFAF6* cDNA obtained from blood samples of patient A1 (bottom panel) and his father (I-1, upper panel), showing a region within exon 5 which encompasses the heterozygous missense mutation.

Patient B was described in detail by Bianciardi et al.[7] Briefly, he developed motor and language disturbances by the age of 3.5 years progressing to severe gait impairment, dysartria and early occurrence of dystonic movements. Brain MRI showed necrotic damage of the putamina, gradually extending to dentate nuclei and anterior caudate nuclei. Evaluation of mitochondrial respiratory chain revealed decreased complex I activity on fibroblasts (~25% of the controls' mean), while enzymatic activity was normal on muscle homogenate.

Patient C is an 11 year-old Italian boy, first child of unrelated parents. Psychomotor developmental milestones were referred as normal. He presented at 5 years of age with gait unsteadiness and motor coordination problems. These symptoms gradually worsened, configuring over time an extrapyramidal syndrome; cognitive function were preserved. Brain MRI disclosed involvement of the putamen bilaterally, stable over time. Extensive metabolic screening was normal as well as mtDNA analysis. A detailed clinical description of this case is reported in the supplementary material.

3.2. Molecular studies

WES was performed on patients A1 and A2. Variants annotation and filtering steps focused on variants shared by both siblings and affecting mitochondrial genes led to the identification of the heterozygous missense variant c.532G>C:p.A178P in *NDUFAF6* (NM_152416.3) in both siblings; the same mutation (rs201088736) had been already reported as pathogenic by Bianciardi et al.[7] Analysis of WES data also revealed the presence of an additional heterozygous intronic variant (NM_152416.3:c.420+784C>T) in *NDUFAF6* in both affected siblings (Fig. 1A-B). It corresponds to rs749738738 in dbSNP database, and is reported with an extremely low allele frequency (0.003% in gnomAD). The missense and the intronic variants, validated by Sanger sequencing, were inherited from the unaffected father and mother, respectively (Fig. 1A).

In order to assess the effects of the intronic variant, RNA was extracted from fresh blood samples of family A members and retrotranscribed into cDNA. Through amplification and sequencing of the *NDUFAF6* transcript (Fig. 1C-D), we detected an additional transcript in samples of both siblings and their mother : this corresponded to alternative splicing isoforms (e.g. ENST00000520757.1 or XM_005250791.1), retaining an extra 124 nucleotide-long exon (exon 3b; Fig. 1B) and predicted to undergo premature non-sense mediated decay on public databases, because of the creation of a premature stop codon. Interestingly, the alternative splicing acceptor site is placed 11 nucleotides downstream the rs749738738 variant and *in*

silico predictions gave higher scores for creating an acceptor site to the mutant sequence .

We also assessed and eventually confirmed the presence of the same intronic variant on DNA of patient B, already reported to be heterozygous for the paternally inherited c.532G>C:p.A178P mutation.[7] In accordance with a recessive pattern of transmission, segregation analysis confirmed a maternal origin for the intronic variant.

Similarly, direct sequencing revealed the c.420+784C>T intronic variant in an additional case, patient C, in which an independent genetic analysis using a clinical exome panel had identified the c.532G>C:p.A178P heterozygous variant. The two variants were inherited from the parents (Fig. 1). Increased expression of the alternative splicing isoform of the transcript (retaining exon 3b) was confirmed on RNA purified from patient B's fibroblasts as well.

A further analysis of *NDUFAF6* transcripts using an NGS approach confirmed that, although expressed at low levels also in control subjects, the alternative isoform is overrepresented in the samples from individuals harboring the intronic variant (patients A1 and B, and the mother of siblings A1 and A2) compared to subjects lacking this variant (control subjects and the father of siblings A1 and A2) (Fig. 2).

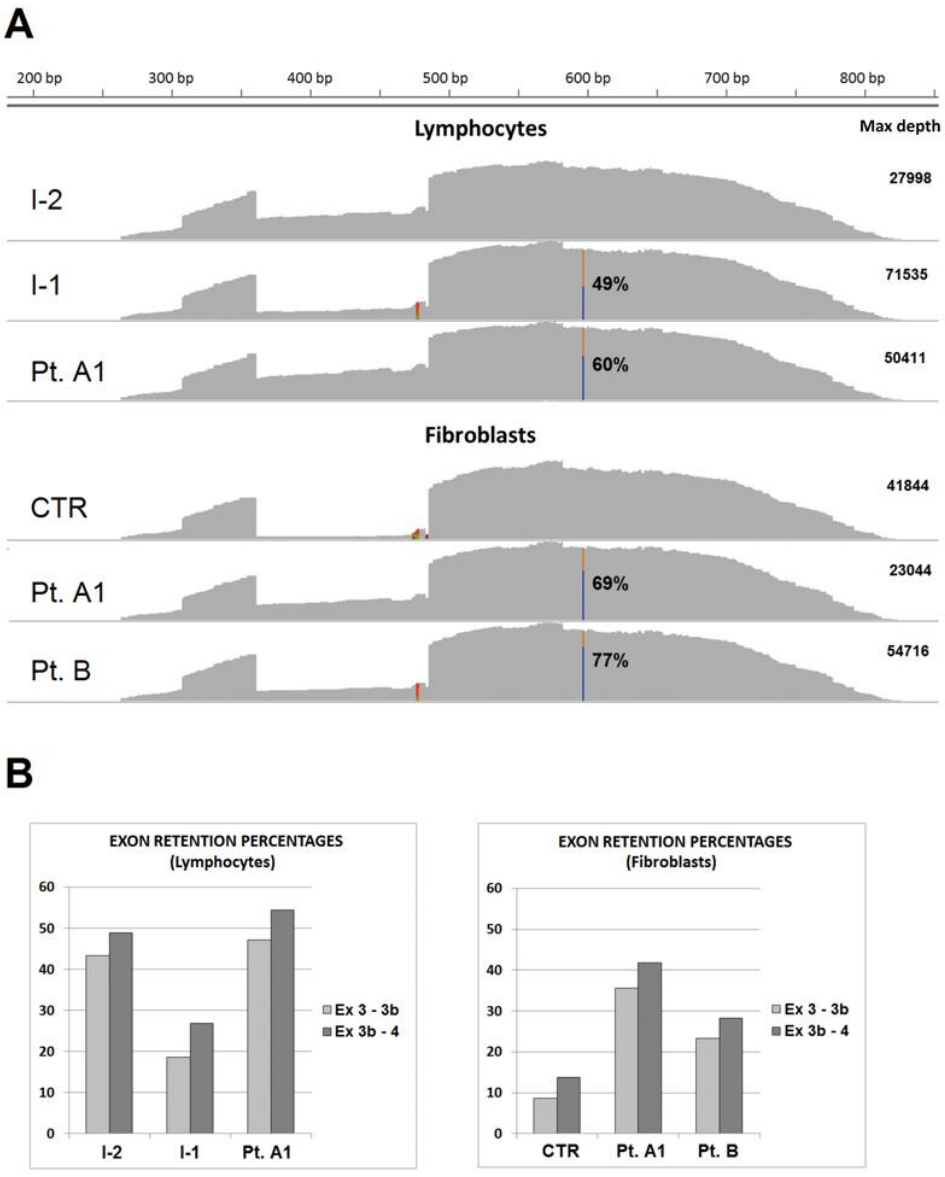

Figure 2

NGS coverage analysis A. Profiles of depth of coverage obtained through NGS on *NDUFAF6* transcript PCR products. RNA was extracted from lymphocytes of Patient A1 (Pt. A1) and his parents (I-1; I-2), and from fibroblasts of patients A1, B and a control sample (CTR).

B. Quantification of exon 3b retention. Graphs of the coverage ratio (in percentage) between the *NDUFAF6* alternative isoform containing exon 3b and the canonical isoform, calculated for all the samples analyzed by NGS (the two bars correspond to the junctions exon 3-exon 3b and exon 3b-exon 4).

Notably, in the patients we observed a predominant expression of the mutated allele harboring the missense mutation c.532G>C in fibroblasts and, partly, in blood (Fig. 1D, Fig. 2). A non-sense mediated decay (NMD) assay performed on fibroblasts from both patients A1 and B and a control individual did not show any detectable difference in RNA sequence profiles between treated and untreated samples.

The identification of two extremely rare variants in three unrelated families from Italy displaying a similar clinical presentation raised the possibility of unreported/unknown relationship between the families and common founder alleles. All the families originate from Southern Italy, although from different regions (2 from Campania, 1 from Abruzzo). We performed a haplotype analysis using 7 tagSNPs present in the *NDUFAF6* genomic region. All the patients showed the same haplotype indicating that they likely harbor common *NDUFAF6* alleles rather than having had independent mutational events. Analysis of the variants identified by targeted-NGS confirmed this finding, with shared *NDUFAF6* haplotypes amongst patients; however it revealed a quite different variants profile in surrounding genes present on chromosome 8 suggesting not recent founder occurrence.

4. Discussion

We identified compound heterozygous missense and deep intronic variants in three different families with a typical recessive *NDUFAF6*-related disease characterized by Leigh syndrome. Complementation studies, previously performed on patient B,[7] already proved that *NDUFAF6* impairment was the cause of the disease. In accordance with *in silico* predictions, our transcript data suggest that the intronic variant promotes the alternative splicing event, thus enhancing expression of the non-functional altered isoform of the gene at the expense of the canonical one.

An NMD assay, together with the amplification of the aberrant transcript in standard conditions, excludes the hypothesis of a relevant NMD involvement on the alternative *NDUFAF6* isoform, at least in fibroblasts. Nevertheless, several *NDUFAF6* transcripts which could be variably expressed in different tissues have been reported[2] and may be differently affected by the intronic variant and otherwise subjected to NMD. In line with this hypothesis, different expression of the two alleles was reported by Bianciardi et al.[7] in blood, fibroblasts, urine and brush RNA samples from patient B. These data could thus suggest the existence of trans-splicing factors which determine a tissue-specific switch between the alternative spliced isoform and the canonical isoform.

The fact that we identified three unrelated cases with the same, peculiar combination of extremely rare *NDUFAF6* variants may be casual. Otherwise we may speculate that one of these

variants is hypomorphic (possibly the splicing variant which allows the formation of a quote of wild type transcript) and does not lead to disease, at least Leigh syndrome, in the homozygous state but only when associated with a severe mutation which in turn is too deleterious/embryolethal in the homozygous state. Homozygosity or various compound heterozygosity of splicing defect, missense changes or nonsense mutations have been found in the previously reported patients with *NDUFAF6* mutations[3–6], and the affected nucleotides are located throughout the gene hampering an easy identification of obvious genotype-phenotype correlations.

The clinical presentation of the *NDUFAF6*-mutant cases here reported is a Leigh syndrome with early childhood onset (1-5 years) and stable or slowly progressive course, associated with isolated cerebellar or extrapyramidal signs depending on affected cerebral structures; cognitive involvement and seizures were not detected/reported. MRI pattern was characterized by striatal and dentate nuclei involvement. Patient C presented isolated putamina involvement that was stable over time, and a relatively mild phenotype compared to other patients. Only in patient A2 putamen alterations were not observed, but she performed a single MRI at disease onset and additional data about radiological course were not available.

Reports on mutations located outside the coding regions and associated with human diseases are rapidly growing. In this study we confirmed that WES data analysis should take into account all rare variants, including those with poorly predictable

effect on transcript/protein. Moreover we underline that mRNA analysis is a complementary strategy, extremely useful to integrate WES and demonstrate the deleterious impact of identified variants, especially those affecting splicing and stability of transcripts.

References

[1] Dahl H-H. Getting to the nucleus of mitochondrial disorders: identification of respiratory chain-enzyme genes causing Leigh syndrome. Am J Hum Genet. 1998;63:1594–1597.

[2] McKenzie M, Tucker EJ, Compton AG, Lazarou M, George C, Thorburn DR, Ryan MT. Mutations in the gene encoding C8orf38 block complex I assembly by inhibiting production of the mitochondria-encoded subunit ND1. J Mol Biol. 2011;414:413–426.

[3] Pagliarini DJ, Calvo SE, Chang B, Sheth SA, Vafai SB, Ong S-E, et al. A mitochondrial protein compendium elucidates complex I disease biology. Cell. 2008;134:112–123.

[4] Kohda M, Tokuzawa Y, Kishita Y, Nyuzuki H, Moriyama Y, Mizuno Y, et al. A comprehensive genomic analysis reveals the genetic landscape of mitochondrial respiratory chain complex deficiencies. PLoS Genet. 2016;12:e1005679.

[5] Fang F, Liu Z, Fang H, Wu J, Shen D, Sun S, et al. The clinical and genetic characteristics in children with mitochondrial disease in China. Sci China Life Sci. 2017;60:746–757.

[6] Ogawa E, Shimura M, Fushimi T, Tajika M, Ichimoto K, Matsunaga A, et al. Clinical validity of biochemical and

molecular analysis in diagnosing Leigh syndrome: a study of 106 Japanese patients. J Inherit Metab Dis. 2017;40:685–693

[7] Bianciardi L, Imperatore V, Fernandez-Vizarra E, Lopomo A, Falabella M, Furini S, et al. Exome sequencing coupled with mRNA analysis identifies NDUFAF6 as a Leigh gene. Molec Genet Metab. 2016;119:214–222.

[8] Legati A, Reyes A, Nasca A, Invernizzi F, Lamantea E, Tiranti V, et al. New genes and pathomechanisms in mitochondrial disorders unraveled by NGS technologies. Biochim Biophys Acta. 2016;1857:1326–1335.

Chapter 9

KARS-related diseases: progressive leukoencephalopathy with brainstem and spinal cord calcifications as new phenotype and a review of literature.

Ardissone A, Tonduti D, Legati A, Lamantea E, Barone R, Dorboz I, Boespflug-Tanguy O, Nebbia G, Maggioni M, Garavaglia B, Moroni I, Farina L, Pichiecchio A, Orcesi S, Chiapparini L, Ghezzi D Orphanet J Rare Dis. 2018 Apr 4;13(1):45.

Background

KARS encodes lysyl- transfer ribonucleic acid (tRNA) synthetase, which catalyzes the aminoacylation of tRNA-Lys in the cytoplasm and mitochondria [1]. Mitochondrial and cytoplasmic aminoacyl–tRNA synthetases (aaRSs) are encoded by distinct nuclear genes, with the exception of KARS and GARS (glycyl–tRNA synthetase) which are present in both cellular compartments [2, 3].

Mutations in *aaRSs* genes have been linked to a growing number of neurological and systemic disorders with heterogeneous phenotype. Eleven families/sporadic patients and 18 different mutations in *KARS* have been reported to date. Phenotype is heterogeneous ranging from early onset encephalopathy [4–7] to isolated peripheral neuropathy [8] or nonsyndromic hearing impairment [9]. Recently, late onset

leukoencephalopathy [10] and cardiomyopathy [11, 12] have been reported.

A progressive leukoencephalopathy with brainstem and spinal cord calcifications was previously described as a distinct entity in a singleton patient [13] and in two siblings [14]. We report the clinical, biochemical and molecular findings of 2 unreported patients presenting a similar clinical and radiological picture. Genetic analysis performed on them and in the patient previously described [13] revealed the presence of biallelic mutations in *KARS* in all three subjects. Review of *KARS* mutant patients published to date will also be discussed.

Methods

All procedures followed were in accordance with the ethical standards of the responsible committee on human experimentation (institutional and national) and with the Helsinki Declaration of 1975, as revised in 2000. Written informed consent was obtained from all individuals or caregivers.

Genetic analysis

Genomic DNA was extracted from peripheral blood by standard methods. Whole exome sequencing was performed on DNA from patient A, while patient B and C were analyzed using a targeted next generation sequencing (NGS) custom panel containing genes responsible for mitochondrial disorders (Additional file 1). Variants filtering was performed as previously described [15]. Variants identified by WES were validated by

Sanger sequencing and resolved on a 3130xl Genetic Analyzer (Applied Biosystems).

Biochemical studies in skeletal muscle and fibroblasts

Mitochondrial respiratory chain (MRC) activities of complexes I to IV were measured by spectrophotometric methods in supernatants of 800 × g muscle homogenates or in digitonin treated fibroblasts [16]. The activities were normalized to citrate synthase activity, an index of mitochondrial content in the analyzed specimens.

Results

Clinical and radiological findings

Patient A

Patient A, first child of unrelated Italian parents, showed a progressive leukoencephalopathy with spinal cord calcifications, deafness, hypochromic microcytic anemia and has been already described by Orcesi et al. [13].

Patient B

The patient is a 7 year old male. The family history was unremarkable. He was born at term after an uneventful pregnancy. He showed normal psychomotor development until 6 months of age when, a few days after a febrile illness, he had seizures and psychomotor regression. He started phenobarbital treatment. In the following months he showed a slow psychomotor improvement: trunk control was recovered, he was able to walk with support at 12 months, and had been seizures free (he stopped drug at 8 months). At 18 months, after another febrile illness, he presented subacute

psychomotor regression and seizures. Valproate treatment was initiated.

He was admitted to our institute at 3 years and 10 months of age. Clinical evaluation showed stunted growth, microcephaly (<3rd percentile), marked scoliosis, nystagmus, poor eye contact and response to sounds, absence of spontaneous movements and postural control, spastic tetraparesis with extrapyramidal signs, absence of language. At last follow up, at 7 years of age, neurological conditions were stable; seizures were not reported.

Abdominal ultrasound- performed before Valproate treatment - disclosed hepatomegaly, echocardiogram was normal. Fundus oculi performed at 6 months disclosed bilateral optic atrophy; since 3 years of age, visual evoked potential showed absence of any responses; brainstem auditory evoked potential suggested profound sensorineural hypoacousia, pure tone audiometry was not performed. Serial EEG revealed poor organization of cerebral activity and multifocal abnormalities. MRI was normal at 6 months. A second MRI (1 year and 9 months) revealed diffuse signal abnormalities in deep cerebellar white matter (WM), middle cerebellar peduncles, brainstem and bi-hemispheric WM (Fig. 1a-e). A third MRI (3 years and 10 months), (Fig. 1h-j) disclosed extension of the diffuse signal abnormalities in bi-hemispheric WM, involving the U fibers (Fig. 1i, j). There was also full involvement of the posterior arm of the internal capsules, external capsules, thalami, cerebellar WM, cerebellar peduncles and brainstem

(Fig. 1f-i).T2 shine-through effect on DWI was evident in the areas of the T2 signal abnormalities. Bilateral Calcarine cortex had a malacic appearance, with a gliotic hyperintensity on T2 and focal atrophy. Diffuse cerebral atrophy was also documented (Fig. 1f-i). Spectroscopy showed reduction of NAA and lactate in the centrum semiovale.

Fig. 1

MRI in patient B. TOP, Axial T2WI. performed at 1 year and 9 months revealed diffuse hyperintensity in deep cerebellar white matter, middle cerebellar peduncles, brainstem and bi-hemispheric white matter (**a**, **b**, **c**, **d**). The signal is inhomogeneous for the presence of multiple focal marked hypointensities due to calcifications (**e**, arrows). BOTTOM, Axial T2WI. performed at 3 years and 10 months showed a dramatic extension of the diffuse signal abnormalities in both hemispheres with full involvement of the posterior arm of the internal capsules, external capsules, U fibers and thalami, with relative sparing of the putamina (**h**-**j**). The signal abnormalities extension was also evident in cerebellar white matter, cerebellar peduncles and brainstem (**f**, **g**). Bilateral symmetric hyperintensities in the bulbar pyramids and bulbar lateral regions (arrowheads in **f**), in the superior cerebellar peduncles and in the arciform fibers of their decussation (arrowheads in H) were more evident. The transverse fibers of the pons were prominent and hyperintense (insert in **g**). Both V

cranial nerves appeared swollen and hyperintense (stars in **g**), as well as the optic chiasm. Calcarine cortex showed a gliotic hyperintensity (black arrows in **c**).

A huge diffuse cerebral atrophy with ventricles and sulci dilatation associated with pronounced cortical thickness was also observed

Cranial CT showed calcifications particularly in the periventricular WM, but also evident in the cerebellar WM, pons, thalami, internal capsules and calcarine cortex (Fig. 2a-c). The last brain MRI and CT examinations (7 years) showed worsening of cerebral and cerebellar atrophy and increased cerebral calcifications.

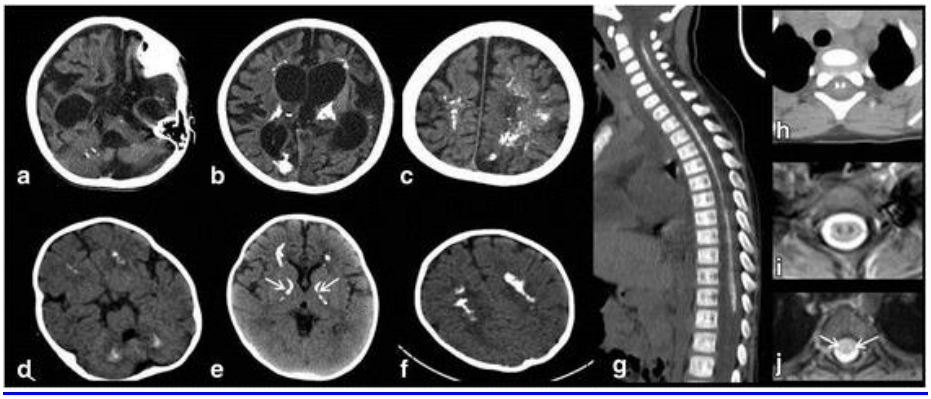

Fig. 2

Axial CT images of Patient B (**a**, **b**, **c**) and patient C (**d**, **e**, **f**) during different stages of the diseases, showing “rocks” calcifications in the cerebellar white matter (**a**, **d**), pons (**a**), periventricular white matter, thalami (**b**, **e**), and in the internal capsules, where they have a peculiar «boomerang appearance» (**e**, arrows) and centrum semiovale (**c**, **f**). Spine sagittal (**g**) and axial (**h**) CT of patient A showing extensive «track-like» calcifications along the whole spinal cord, well seen also on axial T2-fast field echo (FFE) MR images at the dorsal level and located in the region of the anterior horns

(**i**). Axial T2-FFE MR image of patient C depicts the bilateral hyperintensities on T2WI in the dorsal lateral columns (**j** arrows)

Spinal MRI disclosed on T2WIslight hyperintensity in the lateral columns of both cervical and dorsal spinal cord (Fig. 2j) and spinal CT disclosed calcifications at C6-T1 level.

Blood routine disclosed microcytic hypochromic anemia and mild elevated transaminase levels since first evaluation before valproate treatment. Galactocerebrosidase, arylsulfatases were normal. Plasma lactate and pyruvate levels were elevated: 2872–3042 μmol/l (n.v. 580–2100) and 171 μmol/l (n.v. 5–145) respectively, normal in CSF. Amino acids, creatine and guanidinoacetate were normal. Genetic screening using NGS panel for Aicardi-Goutieres syndrome was negative. A mitochondrial diseases was suspected, muscle biopsy was not possible because of marked hypotrophy. MRC complexes and pyruvate dehydrogenase (PDH) complex activities resulted normal in fibroblasts; analysis of *POLG* was negative.

Patient C

This girl was born at term after normal pregnancy and delivery from healthy unrelated parents. At 2 months of age parents started to suspect hearing impairment and at 6 months bilateral cochleopathy was diagnosed on the basis of a type A tympanogram and brainstem auditory evoked potential.

At 12 months she came to our attention. Neurological evaluation showed spastic tetraplegia and microcephaly; she was able to fixate and track a visual target, but was not able to reach an object; spontaneous movements were poor and non-finalized, postural controls absent. At last follow up, at 18 months of age, neurological conditions were stable.

Cerebral MRI (at 6, 12 and 18 months) showed progressive bilateral diffuse supra e infra-tentorial WM abnormalities with involvement of centrum semiovale, corona radiata, initially sparing U fibers; there was also involvement of the posterior arm of the internal capsules, external capsules, thalami, cerebellar and deep WM and brainstem, while putamina were relatively spared. In particular, in the brainstem we noticed bilateral symmetric hyperintensities in the bulbar pyramids and lateral regions, involvement of the superior cerebellar peduncles and in the arciform fibers of their decussation at the level of the mesencephalon. Both V cranial nerves appeared slightly hyperintense on T2WI. Progressive cerebral calcifications were also evident on CT (Fig. 2d-f), initially involving internal capsules, deep and periventricular WM (at 6 months) and since 12 months dentate nuclei.

Spinal MRI performed at 12 months documented bilateral hyperintensities on T2WI in the cervical and dorsal lateral columns (Fig. 2j) and CT showed calcifications at 12 and 18 months.

Visual evoked potentials was slightly delayed at 12 months and severely abnormal at 18, electroretinogram was normal, fundus oculi showed diffuse mild depigmentation; peripheral nerves conductions were normal; EEG showed poor organization of background activity with fronto-centro-temporal spikes at 12 months, increased at 18 months.

Biochemical exams revealed microcytic hypochromic anaemia with normal iron concentration, high level of plasma lactate

(3312 µmol/l) and pyruvate (199 µmol/l) with normal CSF concentration. MRC complexes activities resulted normal in fibroblasts.

Abdominal ultrasound revealed inhomogeneous echogenicity, with nodular aspects, liver function tests showed slight elevation of serum transaminases, with normal synthetic function and no signs of cholestasis. Liver biopsy showed mild portal sclerosis with mild distortion of venous portal vessels, without any significant inflammatory infiltrate; lobular parenchyma demonstrated focal enlarged trabeculae with compression of the peripheral hepatocytes, and preserved reticular network without fibrosis. These findings were suggestive of a vascular disturbance with nodular regenerative hyperplasia (Fig. 3).

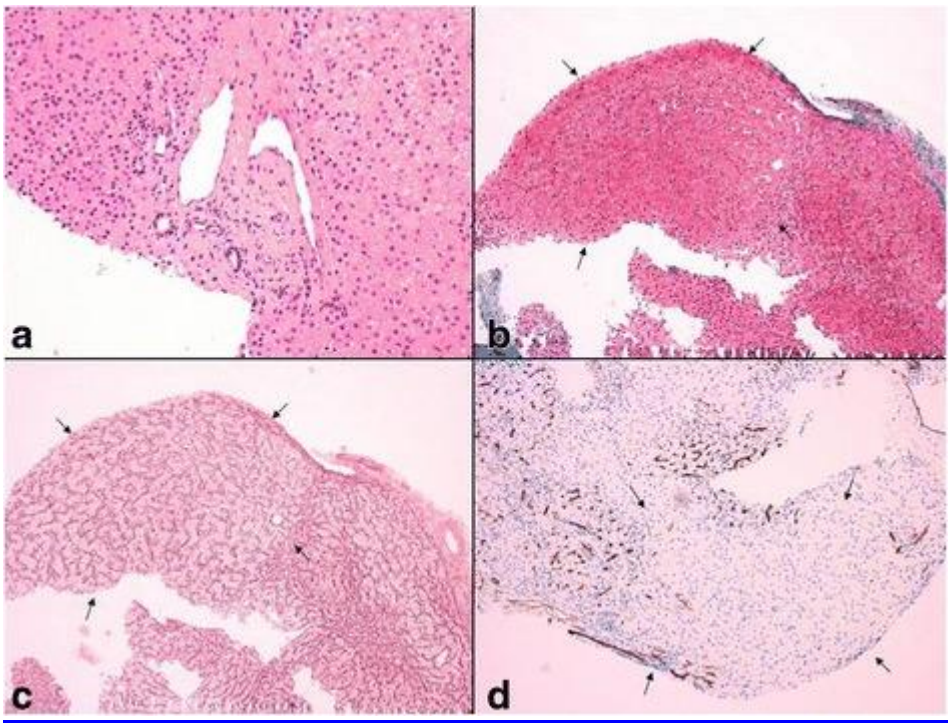

Fig. 3

Histological liver changes in patient C: mild sclerotic portal space with irregular venous vessels (**a**, hematoxylin and eosin stain, 200×); vaguely nodular lobular area with compressed peripheral trabeculae (arrows) can be highlighted by Masson's trichrome (**b**, 100×) and Reticulin (**c**, 100×) stainings, and CD34 immunohistochemistry (**d**, 100×)

Genetic studies

Whole exome sequencing was performed on patient A; following a filtering strategy that enriched for rare (MAF of < 1%) nonsynonymous/splice variants that segregated in a recessive manner, a short list of candidate genes was obtained but without any known gene associated with WM disease (Additional file 2). Independently, NGS-based screening of genes associated with mitochondrial disorders performed on patient B disclosed two heterozygous variants in *KARS* (NM_001130089.1): c.1124A > G/p.Tyr375Cys and c.381C > G/p.Phe127Leu. These variants and their segregation in the family were confirmed by Sanger sequencing.

Given the striking similarities of clinical and neuroimaging features between patient B and patient A, WES data from the latter were reconsidered and a likely causative role was assigned to the homozygous variant c.1514G > A/p.Arg505His in *KARS*. Similarly, because of her clinical presentation an NGS-based screening of *KARS* was performed on patient C, leading to the identification of two heterozygous variants: c.815 T > G/p.Phe272Cys and c.1043G > A/p.Arg348His. All the identified *KARS* variants had an extremely low frequency in public databases (< 0.01%), are predicted to be deleterious and

hit phylogenetically conserved amino acid residues, supporting their causative role (Additional file 3). Notably, the c.1514G > A/p.Arg505His found in patient A has been recently reported in compound heterozygosity with another missense change in two siblings with early-onset hearing loss and leukoencephalopathy and its pathogenicity has been experimentally proven [10].

Discussion

Mutations in different *aaRSs* have been associated with an increasing number of phenotypes [2, 3]. Encephalopathy is the most common phenotype, but other extra neurological symptoms have been reported: sideroblastic anemia (YARS2 [17, 18]), cardiomyopathy and myopathy (YARS2 [19], GARS [20], KARS [11, 12], tubulopathy (SARS2 [21]), ovarian failure (AARS2 [22], HARS2 [23], LARS2 [24]), hepatopathy (FARS2 [25], EARS2 [26]) and hearing loss (HARS2 [23], LARS2 [25], KARS [9]).

Up to now, 11 families/sporadic patients and 18 mutations in *KARS* have been reported

KARS impairment was first linked to peripheral neuropathy [8] in one patient (Pt 1) presenting with Charcot-Marie-Tooth neuropathy, developmental delay, self-abusive behavior, dysmorphic features, and vestibular Schwannoma. Compound heterozygous p.Leu133His and p.Tyr173SerfsX7 variants were identified. Functional analyses revealed that these two mutations severely affect enzyme activity.

Autosomal recessive nonsyndromic hearing loss was the second phenotype reported [9]. In affected individuals homozygosity for missense mutations (p.Asp377Asn or p.Tyr173His) in *KARS* was identified. (Pts 2–14/Fam. 2–4). Both variants were predicted to be damaging by multiple bioinformatics tools. The first case of *KARS* mutations associated with suspected mitochondrial disease was reported in 2013 [4]. The authors analyzed by exome sequencing a series of 102 patients with clinical and biochemical findings suggestive for mitochondrial disorders and identified compound heterozygous *KARS* mutations (p.Thr587Met; p.Pro228Leu) in a patient affected by psychomotor delay, hearing loss, ophthalmoplegia, dystonia and elevated CSF lactate level (Pt 15/Fam. 5). MRC activity on tissue was not investigated. No experimental proof was reported but, given the predicted severity of the mutations at highly conserved residues, the authors concluded that the observed mutations were likely the genetic cause of patient's phenotype.

A more severe phenotype was reported in two 2 siblings (Pts 16–17/Fam. 6) with early onset visual impairment, progressive microcephaly, developmental delay, seizures and very subtle deep white matter loss on MRI [5]. The patients harbored compound heterozygous mutations (p.Arg466Trp; p.Glu553Lys) within a highly conserved region of the catalytic domain. A similar clinical presentation was reported in a patient who harbored a p.Ala57Pro missense change and a 7601-base pair deletion, encompassing the first three exons of the

mitochondrial isoform of *KARS* (Pt 18/Fam. 7) [6]. Cardiac involvement associated with a deficiency of MRC complexes I and IV has been reported in two patients (Pts 19–20/Fam. 8–9), who carried novel biallelic *KARS* mutations [11, 12]. The first one presented a childhood-onset hypertrophic cardiomyopathy associated with seizures, developmental delay, in a patient harboring compound heterozygous p.Val476Asp and p.Ile346Thr mutations [11] while hypertrophic cardiomyopathy was the clinical hallmark in the second, a 14 years old patient with mild myopathic signs and cognitive disability (in spite of normal brain MRI) associated with p.Leu378His and p.Pro418Arg [12]. In both patients lactic acidosis was detected. In the first case, the mitochondrial enzyme defects were rescued by cDNA complementation with mitochondrial KARS, but not cytosolic form [11]. More recently, two mutations (p.Arg505His; p.Pro533Ser) have been reported in two siblings affected by early onset hearing loss, progressive cognitive impairment and psychiatric symptoms with onset in adulthood associated with leukoencephalopathy: brain MRI showed symmetrical confluent abnormalities in the frontal, periventricular white matter and in the corpus callosum [10]. Functional studies showed that both mutations decreased tRNA aminoacylation while p.Arg505His changed the secondary structure of KARS, leading to protein aggregation. Finally, *KARS* mutations (p.Ala526Val; p.Phe489Cys) were reported in two sisters affected by developmental delay, microcephaly, seizures, and sensorineural hearing loss;

calcifications of left occipitoparietal junction were reported in one case (Pt 23). MRC enzymes activity in muscle biopsy was normal, lactate level was not available (Pt 24) [7].

In the present manuscript we reported about a new severe phenotype associated with biallelic *KARS* mutations. Our patients presented an early onset and progressive encephalopathy characterized by acquired microcephaly, developmental delay, spastic tetraparesis, epilepsy, sensorineural hypoacusia, visual impairment, microcytic hypochromic anaemia and failure to thrive. In addition patients B and C presented liver involvement. To our knowledge, this is the first report of hepatic involvement in this disease but the exact meaning of the reported anomalies has still to be understood. Nevertheless, in patient A no evidence of liver dysfunction was reported and liver ultrasound was normal.

In patient B, the severity of the phenotype, the clinical onset related to febrile illness and the presence of lactic acidosis suggested a mitochondrial disease that was directly investigated in spite of normal MRC and PDH activities in fibroblasts.

In patient C, clinical picture and lactic acidosis claimed the idea of a mitochondrial disorder as already suggested also in patient A, supported by mild lactate elevation at spectroscopy study. In *KARS*-mutant cases reported to date, mitochondrial disease was suspected and confirmed by biochemical diagnosis only in patients with cardiomyopathy (Pt 19 and Pt 20); elevated lactate level in CSF was detected in Pt 15 but biochemical studies on

tissue were not performed. In other cases, metabolic analyses for mitochondrial disease were unremarkable or not performed. In 5 of 26 KARS patients reported to date, including our cases, both lactate level and biochemical studies (in different tissues) were performed and only in patients with cardiac involvement elevated lactate level corresponded to reduced MRC activity. Nevertheless the lack and heterogeneity of laboratory data does not permitted this phenotypic variability explanation. The MRI findings were similar in all three patients and characterized by progressive diffuse leukoencephalopathy and calcifications extending in cerebral, brainstem and cerebellar WM, with spinal cord involvement. Specifically, at the early stages of the disease the signal abnormalities were observed in the deep cerebellar WM and in the centrum semiovale. Progressively, an extensive diffuse WM involvement, including U fibers, posterior arm of the internal capsules, external capsules, thalami, cerebellar peduncles and brainstem, with selective bilateral symmetric involvement of the bulbar pyramids and lateral bulbar regions resembling the pattern of mitochondrial diseases were observed. The supratentorial WM involvement was characterized by uniform slight hyperintensity on T2WI, interrupted by marked foci of hypointensities due to calcifications. This appearance seems to be due to a demyelinating process an assumption supported also by the evidence of demyelination of the proximal intracisternal portion of the V cranial nerves (Fig. 1g).

Cerebral calcifications have a distinct pattern with initial involvement of deep cerebellar and cerebral periventricular WM and progressive extension to the thalami and internal capsules, in which a peculiar “boomerang appearance” was present. Calcifications were evident even in the initial phases of the disease and might not be a dystrophic epiphenomenon and so a secondary and aspecific event, but an intrinsic feature of the disorder. In the spine they were present in all 3 patients, even if with different severity, and were characterized by a peculiar bilateral and symmetrical distribution in the anterior horns, both extensively (Patient A) or spot-like (Patients B and C). On MRI, bilateral abnormal signal intensity in the lateral columns was also associated.

Patient B dysplayed a more severe cerebral atrophy and grey matter involvement (basal ganglia and cortex) but he underwent the first MRI later in life compared to the other two. As disease progressed, the radiological picture evolved toward a progressive cerebral atrophy in 2 patients (A and B).

WM involvement has been previously reported in few *KARS*-mutant patients but with a less severe pattern and restricted to supratentorial regions (Pt 16, Pt 17, Pt 21, Pt 22). It is interesting to note that the presence of cerebral WM and spinal cord signal abnormalities is a pretty rare association of neuroradiological features and it is typically observed in other aaRSs deficiencies, notably in *DARS* and *DARS2* related leukodystrophies [27, 28]. It is also a quite common finding in Iron-sulfur cluster related leukoencephalopathies, particularly

those caused by *GLRX5* [29], *ISCA2* [30], or *IBA57* [31] mutations. The association of cerebral WM abnormalities with spinal cord involvement should prompt to consider aaRSs-related diseases and particularly *KARS* mutations when calcifications are observed.

The extremely heterogeneous clinical presentation associated with *KARS* mutations is peculiar in the field of *aaRS*-related diseases which are usually characterized by strict genotype-phenotype associations, although a definite explanation of the molecular mechanisms underpinning this observation is still missing. Few examples of different phenotypes caused by mutations in the same *aaRS* gene have been reported (e.g. *AARS2* associated with either cardiomyopathy or leukoencephalopathy and ovarian failure [22, 32]). Differences in mode of inheritance and type of mutation cannot easily explain the variable clinical presentations since all the reported cases showed an autosomal recessive transmission of missense mutations. Only the patient described by Joshi et al. (Pt 18/Fam. 7) carried a large deletion, acting as a null allele, together with a missense mutation which disrupts the mitochondrial targeting signal, thus potentially affecting solely the mitochondrial isoform of *KARS*. All the other patients, irrespective of any evidence of mitochondrial dysfunction, harbored *KARS* variants which are predicted to strike both mitochondrial and cytosolic *KARS* isoforms. An effect of the affected functional domains was initially suggested, since the first mutations responsible for the neuropathic phenotype hit the

anticodon domain whereas hearing loss associated mutations could be in the catalytic domain. However this hypothesis was not confirmed in the following reports and in the present review of all the *KARS* mutant patients. For instance, the mutations found in our patients, with an overlapping phenotype, are scattered throughout the gene (from amino acid 127 to 505) and affect either the anticodon-binding or the catalytic domain. The few functional studies which have been performed indicated that various functions/properties of KARS (e.g. tRNA aminoacylation, secondary structure) may be affected by different mutations. Nevertheless, no genotype/phenotype correlation was evident, even considering the residual enzymatic activity of the different mutant forms. Nevertheless a mutation specific effect cannot be excluded, since all the identified *KARS* mutations were reported in single cases/families; for instance, the cardiac phenotype in *AARS2* mutant patients seems to be strictly linked to the presence of a specific amino acid change. The only *KARS* mutation presents in two unrelated families was the p.Arg505His, identified in homozygosity in patient A and in compound heterozygosity with p.Pro533Ser in Pts 21–22; all these three individuals were characterized by leukodystrophy and hearing problems but the MRI features were not identical and other clinical symptoms were different (e.g. visual impairment and spastic tetraparesis were observed in patient A but not in the two siblings). Obviously, the partially different genotype may account for the phenotype diversities.

Conclusion

With our report we define the molecular basis of the previously described Leukoencephalopathy with Brainstem and Spinal cord Calcification, that we propose to call LBSC similarly to *DARS* and *DARS2* related leukodystrophies, widening the spectrum of *KARS* related disorders, particularly in childhood onset disease suggestive for mitochondrial impairment. The review of previous cases does not suggest a strict and univocal genotype/phenotype correlation for this highly heterogeneous entity.

Moreover, our cases confirm the usefulness of search for common brain and spine MR imaging pattern and of broad genetic screening, in syndromes clinically resembling mitochondrial disorders in spite of normal biochemical assay.

References

1. Tolkunova E, Park H, Xia J, King MP, Davidson E. The human lysyl-tRNA synthetase gene encodes both the cytoplasmic and mitochondrial enzymes by means of an unusual alternative splicing of the primary transcript. J Biol Chem. 2000;275(45):35063–35069. doi: 10.1074/jbc.M006265200.

2. Diodato D, Ghezzi D, Tiranti V. The mitochondrial aminoacyl tRNA Synthetases: genes and syndromes. Int J Cell Biol. 2014;2014:787956. doi: 10.1155/2014/787956.

3. Yao P, Fox PL. Aminoacyl-tRNA synthetases in medicine and disease. EMBO Mol Med. 2013;5(3):332–343. doi: 10.1002/emmm.201100626.
4. Lieber DS, Calvo SE, Shanahan K, et al. Targeted exome sequencing of suspected mitochondrial disorders. Neurology. 2013;80(19):1762–1770. doi: 10.1212/WNL.0b013e3182918c40.
5. McMillan HJ, Humphreys P, Smith A, et al. Congenital visual impairment and progressive microcephaly due to Lysyl-transfer ribonucleic acid (RNA) Synthetase (KARS) mutations: the expanding phenotype of aminoacyl-transfer RNA Synthetase mutations in human disease. J Child Neurol. 2015;30(8):1037–1043. doi: 10.1177/0883073814553272.
6. Joshi C, Kolbe DL, Mansilla MA, Mason SO, Smith RJ, Campbell CA. Reducing the cost of the diagnostic odyssey in early onset epileptic encephalopathies. Biomed Res Int. 2016;2016:6421039. doi: 10.1155/2016/6421039.
7. Murray CR, Abel SN, McClure MB, Foster J, et al. Novel causative variants in DYRK1A, KARS, and KAT6AAssociated with intellectual disability and additional phenotypic features. J Pediatr Genet. 2017;6(2):77–83. doi: 10.1055/s-0037-1598639
8. McLaughlin HM, Sakaguchi R, Liu C, et al. Compound heterozygosity for loss-of-function lysyl-tRNA synthetase mutations in a patient with peripheral neuropathy. Am J Hum Genet. 2010;87(4):560–566. doi: 10.1016/j.ajhg.2010.09.008.
9. Santos-Cortez RL, Lee K, Azeem Z, et al. Mutations in KARS, encoding lysyl-tRNA synthetase, cause autosomal-

recessive nonsyndromic hearing impairment DFNB89. Am J Hum Genet. 2013;93(1):132–140. doi: 10.1016/j.ajhg.2013.05.018.

10. Zhou XL, He LX, Yu LJ, et al. Mutations in KARS cause early-onset hearing loss and leukoencephalopathy: potential pathogenic mechanism. Hum Mutat. 2017;38(12):1740–1750. doi: 10.1002/humu.23335.

11. Kohda M, Tokuzawa Y, Kishita Y, et al. A comprehensive genomic analysis reveals the genetic landscape of mitochondrial respiratory chain complex deficiencies. PLoS Genet. 2016;12(1):e1005679. doi: 10.1371/journal.pgen.1005679

12. Verrigni D, Diodato D, Di Nottia M, et al. Novel mutations in KARS cause hypertrophic cardiomyopathy and combined mitochondrial respiratory chain defect. Clin Genet. 2017;91(6):918–23.

13. Orcesi S, La Piana R, Uggetti C, et al. Spinal cord calcification in an early-onset progressive leukoencephalopathy. J Child Neurol. 2011;26(7):876–880. doi: 10.1177/0883073810390038.

14. Yoshimura M, Hara T, Maegaki Y, et al. A novel neurological disorder with progressive CNS calcification, deafness, renal tubular acidosis, and microcytic anemia. Dev Med Child Neurol. 1997;39:198–201. doi: 10.1111/j.1469-8749.1997.tb07410.x.

15. Legati A, Reyes A, Nasca A, Invernizzi F, Lamantea E, Tiranti V, Garavaglia B, Lamperti C, Ardissone A, Moroni I, et

al. New genes and pathomechanisms in mitochondrial disorders unraveled by NGS technologies. Biochim Biophys Acta. 2016;1857:1326–1335. doi: 10.1016/j.bbabio.2016.02.022.

16. Bugiani M, Invernizzi F, Alberio S, Briem E, Lamantea E, Carrara F, Moroni I, Farina L, Spada M, Donati MA, et al. Clinical and molecular findings in children with complex I deficiency. Biochim Biophys Acta. 2004;1659:136–147. doi: 10.1016/j.bbabio.2004.09.006.

17. Riley LG, Cooper S, Hickey P, et al. Mutation of the mitochondrial tyrosyl-tRNA synthetase gene, YARS2, causes myopathy, lactic acidosis, and sideroblastic anemia--MLASA syndrome. Am J Hum Genet. 2010;87(1):52–59. doi: 10.1016/j.ajhg.2010.06.001.

18. Ardissone A, Lamantea E, Quartararo J, et al. A novel homozygous YARS2 mutation in two italian siblings and a review of literature journal of inherited metabolic disease. JIMD Rep. 2015;20:95–101. doi: 10.1007/8904_2014_397.

19. Shahni R, Wedatilake Y, Cleary MA, Lindley KJ, Sibson KR, Rahman S. A distinct mitochondrial myopathy, lactic acidosis and sideroblastic anemia (MLASA) phenotype associates with YARS2 mutations. Am J Med Genet A. 2013;161A(9):2334–2338. doi: 10.1002/ajmg.a.36065.

20. McMillan HJ, Schwartzentruber J, Smith A, et al. Compound heterozygous mutations in glycyl-tRNA synthetase are a proposed cause of systemic mitochondrial disease. BMC Med Genet. 2014;15:36. doi: 10.1186/1471-2350-15-36.

21. Belostotsky R, Ben-Shalom E, Rinat C, et al. Mutations in the mitochondrial seryl-tRNA synthetase cause hyperuricemia, pulmonary hypertension, renal failure in infancy and alkalosis, HUPRA syndrome. Am J Hum Genet. 2011;88(2):193–200. doi: 10.1016/j.ajhg.2010.12.010.

22. Dallabona C, Diodato D, Kevelam SH, et al. Novel (ovario) leukodystrophy related to AARS2 mutations. Neurology. 2014;82(23):2063–2071. doi: 10.1212/WNL.0000000000000497.

23. Pierce SB, Chisholm KM, Lynch ED, et al. Mutations in mitochondrial histidyl tRNA synthetase HARS2 cause ovarian dysgenesis and sensorineural hearing loss of Perrault syndrome. Proc Natl Acad Sci U S A. 2011;108(16):6543–6548. doi: 10.1073/pnas.1103471108.

24. Pierce SB, Gersak K, Michaelson-Cohen R, et al. Mutations in LARS2, encoding mitochondrial leucyl-tRNA synthetase, lead to premature ovarian failure and hearing loss in Perrault syndrome. Am J Hum Genet. 2013;92(4):614–620. doi: 10.1016/j.ajhg.2013.03.007.

25. Elo JM, Yadavalli SS, Euro L, et al. Mitochondrial phenylalanyl-tRNA synthetase mutations underlie fatal infantile Alpers encephalopathy. Hum Mol Genet. 2012;21(20):4521–4529. doi: 10.1093/hmg/dds294.

26. Sellars EA, Balmakund T, Bosanko K, Nichols BL, Kahler SG, Zarate YA. Severe Metabolic Acidosis and Hepatopathy due to Leukoencephalopathy with Thalamus and Brainstem

Involvement and High Lactate. Neuropediatrics. 2017;48(2):108–10.

27. Taft RJ, Vanderver A, Leventer RJ, et al. Mutations in DARS cause hypomyelination with brain stem and spinal cord involvement and leg spasticity. Am J Hum Genet. 2013;92(5):774–780. doi: 10.1016/j.ajhg.2013.04.006.

28. Uluc K, Baskan O, Yildirim KA, et al. Leukoencephalopathy with brain stem and spinal cord involvement and high lactate: a genetically proven case with distinct MRI findings. J Neurol Sci. 2008;273(1–2):118–122. doi: 10.1016/j.jns.2008.06.002.

29. Baker PR, Friederich MW, Swanson MA, et al. Variant non ketotic hyperglycinemia is caused by mutations in LIAS, BOLA3 and the novel gene GLRX5. Brain. 2014;137(Pt 2):366–379. doi: 10.1093/brain/awt328.

30. Al-Hassnan ZN, Al-Dosary M, Alfadhel M, et al. ISCA2 mutation causes infantile neurodegenerative mitochondrial disorder. J Med Genet. 2015;52(3):186–194. doi: 10.1136/jmedgenet-2014-102592.

31. Torraco A, Ardissone A, Invernizzi F, et al. Novel mutations in IBA57 are associated with leukodystrophy and variable clinical phenotypes. J Neurol. 2017;264(1):102–11.

32. Götz A, Tyynismaa H, Euro L, et al. Exome sequencing identifies mitochondrial alanyl-tRNA synthetase mutations in infantile mitochondrial cardiomyopathy. Am J Hum Genet. 2011;88(5):635–642. doi: 10.1016/j.ajhg.2011.04.006.

Chapter 8

Clinical, biochemical and genetic spectrum of 70 patients with ACAD9 deficiency: is riboflavin supplementation effective?

Repp BM, Mastantuono E, Alston CL, Schiff M, Haad TB, Rötig A, Ardissone A, Lombès A, Catarino CB, Diodato D, S chottmann G, Poulton J, Burlina A, Jonckheere A, Munnich A, R olinski B, Ghezzi D, Rokicki D, Well esleD, Martinelli D, Wenhong D, Lamantea E, Ostergaard E, Pr onicka E, Pierre G, Smeets HJM, Wittig I, Scurr I, de Coo IFM, Moroni I, Smet J, Mayr JA, Dai L, de Meirleir L, Schuelke M, Zeviani M, Morscher RJ, McFarland R, Seneca S, Klopstock T, Meitinger T, Wieland T, Strom TM, Herberg U, Ahting U, Sperl W, Nassogne MC, Ling H, Fang F, Freisinger P, Van Coster R, Strecker V,Taylor RW, Häberle J, Vockley J, Prokisch H, Wortmann S.

Orphanet Journal of Rare Diseases 2018 Jul 13(1),120

Background

Complex I of the mammalian mitochondrial respiratory chain is a large multimeric complex composed of 44 subunits encoded by the mitochondrial and nuclear genome. Beside the structural

subunits, at least 19 complex I specific assembly factors are required to obtain fully assembled complex I [1].

One assembly factor is ACAD9. Beside its role in the proper assembly of complex I, ACAD9 exhibits acyl-CoA dehydrogenase (ACAD) activity [2, 3]. ACADs belong to a family of flavoenzymes involved in the ß-oxidation of acyl-CoA and amino acid catabolism. ACAD9 is most homologous (47% amino acid identity, 65% amino acid similarity) to very long-chain acyl-CoA dehydrogenase (VLCAD). Both ACAD9 and VLCAD function as homodimers associated with the inner mitochondrial membrane and catalyze the initial step of the fatty acid oxidation (FAO) cycle [4].

Mutations in *ACAD9* have been related to human disease [5–7]. The clinical presentation of ACAD9 deficiency is dominated by cardiomyopathy. Other features are lactic acidosis, myopathy and developmental delay. Age of onset, severity of symptoms and progression are variable. We have shown that residual ACAD9 enzyme activity, and not complex I activity, correlates with the severity of clinical symptoms in ACAD9 deficient patients [3].

In anecdotal reports of patients with a predominance of myopathic features, alleviation of symptoms under riboflavin treatment has been reported [5, 7, 8]. Riboflavin is the precursor of flavin adenine dinucleotide (FAD) and flavin mononucleotide (FMN), which are cofactors for complex I and numerous dehydrogenases involved in FAO. The mode of action is unclear, previous studies suggested that riboflavin

increases the mitochondrial FAD concentration thereby supporting FAD binding and consecutively improving ACAD9 folding and stability, thus promoting complex I assembly [9].

Bezafibrate, a peroxisome proliferator-activated receptor (PPAR)-alpha activator that controls the expression of many FAO genes, has been reported as a potential treatment for FAO disorders, with beneficial response in six patients [10]. Recently, this was weakened by a double-blind randomized crossover study of bezafibrate in five individuals with acyl-CoA dehydrogenase very long chain (ACADVL) deficiencies in whom no improvement could be detected [11].

In this study, we provide a comprehensive overview of the clinical, biochemical and genetic spectrum of 70 ACAD9 deficient individuals, of whom 29 are unpublished. We further evaluate the effect of riboflavin in patients and the effect of riboflavin and bezafibrate supplementation in patient-derived fibroblast cell lines.

Methods

Individuals

All procedures followed were in accordance with the ethical standards of the responsible committee on human experimentation (institutional and national) and with the Helsinki Declaration of 1975, as revised in 2000. Written informed consent was obtained from all individuals or caregivers. The clinical data were collected via an online survey completed by the respective physician. The online survey included 93 questions regarding age at presentation, current age or age at

death, signs and symptoms during the fetal and neonatal period, at the beginning and during the course of disease, circumstances of death etc.. A special emphasis lay on the cardiac and neurological phenotype, daily life activities and the use of cardiac medication as well as vitmains and co-factors (e.g. riboflavin).

Kaplan Meier curves were created using the R project for statistical computing (survival package, https://www.r-project.org/).

Molecular genetic investigations

Exome sequencing, panel sequencing and Sanger sequencing was performed as described previously [7, 12–22].

Cell culture

Human fibroblast cells were grown in Dulbecco's modified Eagle medium-high glucose supplemented with 10% fetal bovine serum, 1% penicillin-streptomycin (Invitrogen) and 200 µM uridine (Sigma-Aldrich) at 37 °C in an atmosphere containing 5% CO_2.

Riboflavin and bezafibrate treatment

The fibroblast cell lines were treated with 400 µM bezafibrate, 530 nM riboflavin or vehicle (DMSO) for 72 h as previously described [23, 24]. On the second day the cells were seeded at 20,000 cells/well in 80 µl DMEM in 96 well cell culture microplate and incubated overnight at 37 °C and 5% CO_2. On the third day of the experiment the medium was changed to 180 µl unbuffered DMEM and incubated for at least 30 min at 37 °C without CO_2.

Oxygen consumption measurement

Oxygen consumption rate (OCR) was measured using an XF96 extracellular flux analyzer (Seahorse Biosciences, North Billeric, MA, USA) as previously described [25, 26] under basal conditions, in the presence of oligomycin (1 µM, ATP synthase inhibitor), FCCP (0.4 µM, mitochondrial oxidative phosphorlyation system (OXPHOS) uncoupler) antimycin A (2.5 µM, complex III inhibitor) and/or rotenone (0.5 µM, complex-I inhibitor). Antimycin and/or rotenone blocked all mitochondrial respiration and were subtracted from all values. Data was normalized to DNA content with CyQuant (Invitrogen).

Western blot and BN-PAGE analysis

Western Blot analyses of different proteins were performed according to standard protocols [5, 27] ACAD9, VLCAD, MCAD, subunits of the respiratory chain complex I (NDUFS1, NDUFA9) and complex II (SDHA) were investigated and ß-actin was used as a loading control (Abcam, Sigma-Aldrich, MitoSciences 1:1000). [28, 29].

Results

Individuals

Seventy individuals (41 females) from 50 families were recruited, of which 29 were previously unreported (Additional file 2: Table S1 [30–32] and Additional file 3: Table S2). Individuals were numbered I1-I70, their respective fibroblast cell lines (if available) accordingly F1-F70. In the majority of patients investigated ($n = 55$) a complex I deficiency

was found in sceletal ($n = 44$) or heart muscle ($n = 7$) and/or fibroblast cell line ($n = 26$).

Molecular genetic investigations

.

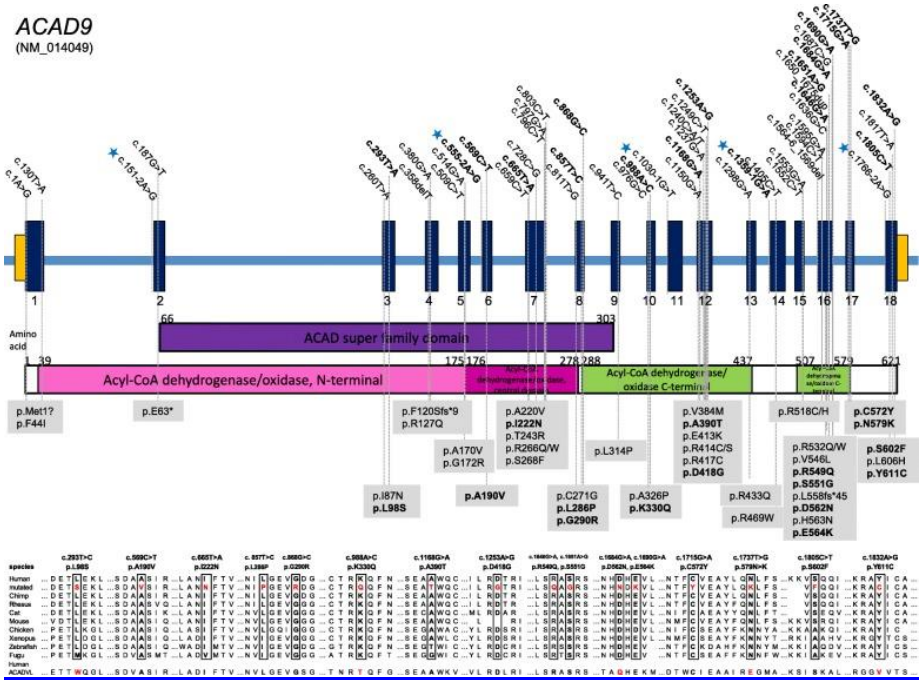

Fig. 1

ACAD9 mutation status, gene structure and conservation of affected amino acid residues. Gene structure of ACAD9 with localization of mutations in 70 patients. Blue asterisks indicate splice site mutations. Newly identified mutations are shown in bold. Conservation of amino acid residues affected by missense variants

Based on the prevalence of deleterious *ACAD9* alleles in the normal population (GnomAD, www.gnomad.broadinstitute.org, [33]) we estimated that approximately 59 children with ACAD9 deficiency will be born each year in Europe

Clinical spectrum

Not all data were available for all patients, the denominator indicates the number of patients for which data were available. Currently 37 individuals are alive at a median age of 14 years (range 24 days – 44 years), the median age of patients deceased was 3 months (range 1 day – 44 years). Patients with a presentation in the first year of life ($n = 50$) show a significantly worse survival when compared to patients presenting later ($n = 20$, Fig. 2a). One individual (I18) was reported with fetal cardiomegaly, two were reported with fetal rhythm abnormalities, all passed away early, on day 1 (I18), 2 (I42) and 280 (I55), respectively.

Cardiomyopathy and treatment

I20 presented with hypertrophic cardiomyopathy in the first year of life. Due to rapid deterioration, she received heart transplantation at 2 years. She died of cardiac failure 4 years later. I21 presented with hypertrophic cardiomyopathy at 18 months and subsequently developed neurological symptoms (ataxia and epilepsy), which were non-progressive and mild. She was successfully heart transplanted at the age of 9 years and is currently 15 years old. I22, currently 35 years old, presented with a progressive biventricular hypertrophic cardiomyopathy in childhood and was transplanted at the age of 18 years. After a follow up of six and 17 years, respectively, their cardiac function remained satisfactory. I30 showed tachycardia in the first days of life birth and signs of heart failure at 1 month. Despite undergoing cardioverter-defibrillator

implantation and subsequent heart transplantation, he died at 3 months of age.

Regarding drug treatment, a positive effect on heart failure was reported for beta-blocking agents (14/44 = 32%), ACE inhibitors (6/40 = 15%), calcium-channel blockers (1/37 = 3%) and diuretics (3/39 = 8%). No patient received digitoxin or digoxin. A worsening effect was only reported for one patient on beta blockers.

Riboflavin and other oral vitamin treatment

Of the entire cohort of 67 patients, 20 patients were reported as not treated; data about treatment and/or effect were unavailable for 15 patients. Data on the general clinical effect of riboflavin as reported by the responsible physician were available for 31 patients. For 20 patients (20/31 = 65%) physicians reported a beneficial effect, for 11 (35%) no effect. No clinical deterioration or side effects were reported. Detailed data on onset of riboflavin treatment, dosage, duration and clinical effect were only available for a minority of patients and have not been investigated.

To analyze the effect of riboflavin treatment, we focused on the patients presenting during the first year of life as these was the biggest subgroup and the group with the shortest survival suggesting the most severe course. For 39 of these 50 patients, data on riboflavin treatment were available ($n = 17$ untreated, $n = 22$ treated). Figure 2b shows the Kaplan-Meier curve for both groups of patients and indicates a significantly better survival rate for patients with oral riboflavin treatment

(deceased *n* = 7/22) in contrast to untreated patients (deceased *n* = 16/17).

Regarding other food supplements, several patients were reported as taking coenzyme Q10, biotin and L-carnitine with anecdotal positive effects.

Cell culture experiments

Effect of different ACAD9 mutations on ACAD9 protein level and respiratory chain complex I activity

ACAD9 levels were significantly reduced in all but two of 14 examined patient fibroblast cell lines; both exceptional cell lines (F9, F43) carried a homozygous p.(Arg518His) variant and showed normal ACAD9 levels (Fig. 3a).

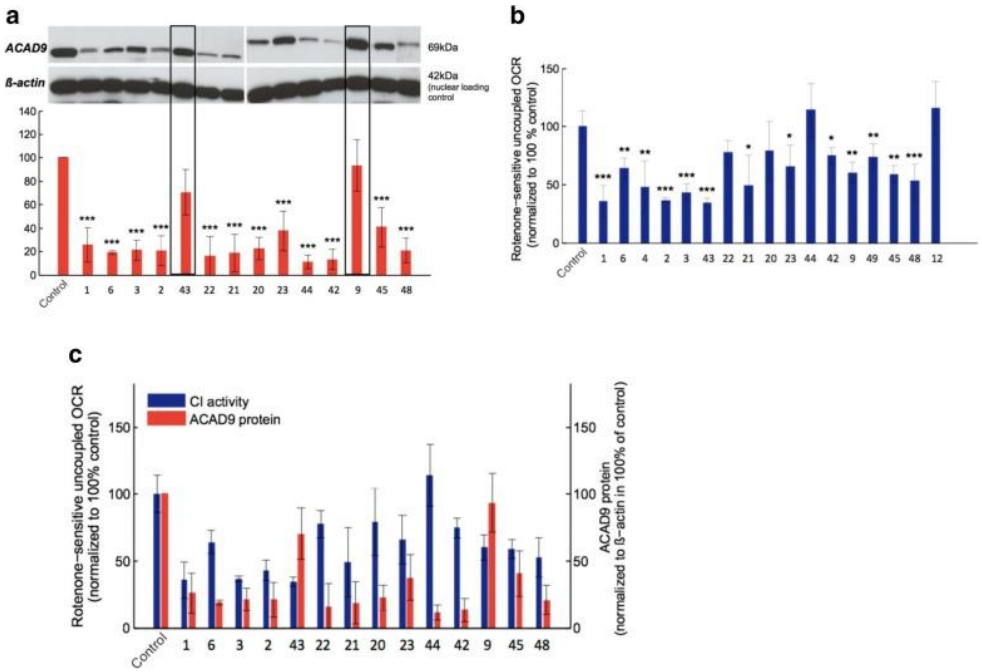

Fig. 3

Measurements of ACAD9 protein level and complex I activity in patient derived fibroblasts. **a** Western blot and quantification of ACAD9 protein levels in patient derived fibroblasts and control. **b** Complex I activity in patient derived fibroblasts and control. **c** Comparison between remaining ACAD9 protein (red) and Complex I activity (blue). Data expressed as average of three independent western blots and average of > 10 technical replicates (oxygen consumption rate ± SD)

Complex I-dependent respiration was found to be significantly decreased in 13 of 17 evaluated patient cell lines. The cell lines F44 (homozygous p.[Leu98Ser]) and F12 (homozygous p.[Arg532Trp]) showed no complex I deficiency; F22 (p.[splice];[Arg433Gln]) and F20 (p.[Phe120Serfs*9];[Arg532Trp] showed only mildly reduced levels (Fig. 3b).

There was no correlation between complex I activity and residual ACAD9 protein levels. Interestingly, nearly normal complex I activity was recorded in the cell line of F42 (p.[Glu564Lys];[Tyr611Cys]) despite very low steady-state ACAD9 protein levels, indicating that the remaining ACAD9 chaperone activity might be high enough to correct assembly of complex I (Fig. 3c).

Respiratory chain complex I activity after bezafibrate and riboflavin supplementation

After 72 h of bezafibrate treatment, the complex I activity increased in the control and in all but three patients cell lines. The increase was significant in 12 out of 17 patient cell lines. Five patient cell lines reached almost normal levels (Fig. 4a). The already normal complex I activity of two cell lines (**F44 and F12**) remained unchanged.

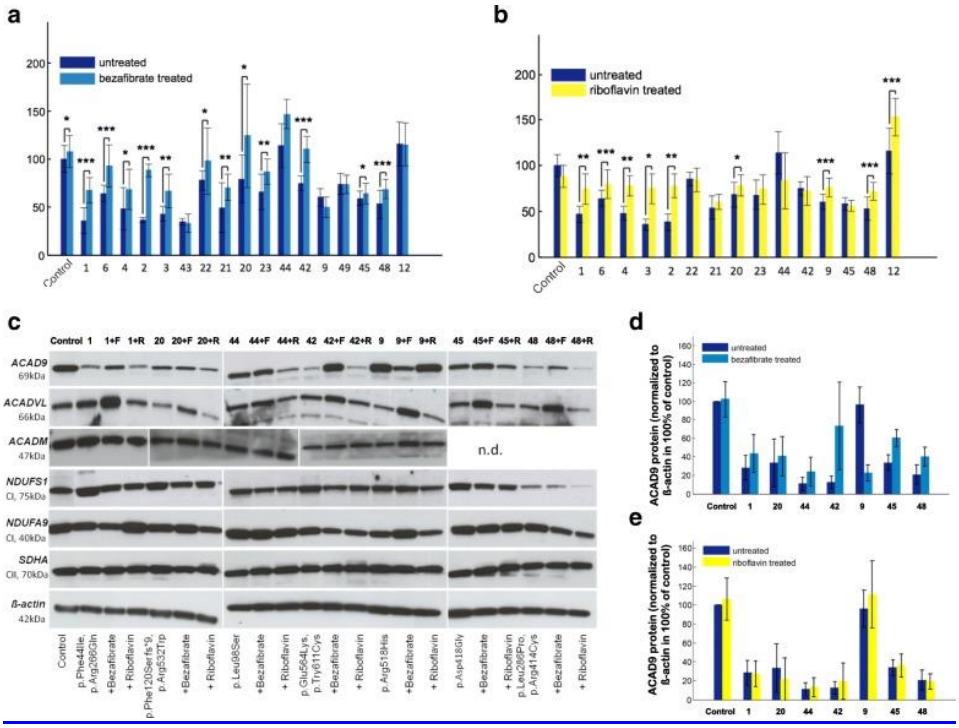

Fig. 4

Effect of bezafibrate and riboflavin supplementation on respiratory chain activities in fibroblast cell lines. Maximal oxygen consumption rate (OCR) was measured in pmol/(s*Mill) of *ACAD9* patient and control fibroblasts with and without (**a**) bezafibrate (400 µM for 72 h) and (**b**) riboflavin (530 nM for 72 h) treatment. Data are expressed as the average of > 10 technical replicates and normalized to control. ± SD. ***$P < 0.001$, **$P < 0.01$, *$P < 0.05$. (**c**) Whole cell lysate of control and different *ACAD9* deficient fibroblasts +/− bezafibrate/riboflavin visualized with antibodies against ACAD9, ACADVL, ACADM, SDHA, ß-actin (loading control), NDUFS1 and NDUFA9 (**d**, **e**) Quantification of ACAD9 and ACADVL protein levels

Riboflavin supplementation led to a significant improvement of complex I activity in nine out of 15 patient cell lines and had no effect in the remaining six cell lines. The increase ranged from 14 to 109% (Fig. (Fig.4b4b).

Supercomplex formation after bezafibrate treatment

All investigated cell lines had a clear reduction of assembled supercomplexes, however, there was no correlation between the amount of ACAD9 protein and the extent of supercomplex formation, (e.g. F23 with almost normal amount of ACAD9 presented a complete loss of supercomplexes whereas F44 with nearly absent ACAD9 protein presented a high amount of assembled supercomplexes). This indicates that small quantities of productive ACAD9 can fulfill assembly function. An increase in the assembly of supercomplexes was found in four out of five cell lines treated with bezafibrate

Findings in cell culture versus clinical effect in patients supplemented with riboflavin

The same mutation as in I12/F12 has previously been reported in I6/F6 (P2 in [7]). I6 was reported to benefit from oral riboflavin. Both cell lines, F6 and F12, consequently showed improving complex I activity under riboflavin treatment (Fig. (Fig.3b).3b). Data for treatment of paired cells and patients were only available for eight patients. In seven pairs the effect was concordant in cells and patients. Six pairs (I/F2, 3, 4, 6, 9, 12) showed positive effects both in cell culture and clinical, one pair (I/F44) did not show any response. I48 did clinically not respond to treatment, whereas his cells did.

Discussion

Complex I deficiency is the most common biochemical signature of mitochondrial disorders. Given the number of ACAD9 deficient patients described here for a disorder

genetically defined only in 2010, and based on the frequency of deleterious alleles described to date, ACAD9 is likely to be one of the more common causes of mitochondrial respiratory chain deficiency, with a conservative estimate of 59 new patients born every year in Europe, and 689 world-wide (Additional file 3 Table S2).

The mutations of the 70 patients from 50 families with ACAD9 deficiency were located across the coding sequence of the gene, with no founder mutations identified. However, no individual harbored two clear loss of function alleles, suggesting that a complete loss of ACAD9 function might be incompatible with life. This is also supported by the fact that the homozygous knock out mouse was found to be embryonic lethal (Schiff, Vockley, *personal communication*). No genotype-phenotype correlation for mutations could be identified based on specific regions of the gene or functional domains of the protein.

The vast majority of patients presented with hypertrophic cardiomyopathy, lactic acidosis, muscle weakness, and exercise intolerance. However, patients without cardiomyopathy also were identified our study. Although both ACAD9 and VLCAD deficiency can present with cardiomyopathy, the clinical phenotype is otherwise distinct, with hypoglycemia, rhabdomyolysis and liver failure, typically seen in VLCAD. These symptoms were infrequently seen in our ACAD9 deficient cohort.

Our data suggest, that there are two subgroups of ACAD9 deficient patients. Patients who presented in the first year of life

often died early and, if surviving, did more poorly than those who presented later. In contrast to many other mitochondrial disorders, severe intellectual disability and developmental delay, as well as other neurological features, were seen in only a minority of (surviving) patients. Indeed, all patients with severe developmental delay ($n = 4$) or intellectual delay ($n = 1$) had early disease onset. Furthermore, most patients currently alive were able to perform routine activities of daily living.

This observation, is not only very important for providing anticipatory guidance, but might also influence a decision regarding heart transplantation. Four patients of our cohort underwent heart transplantation. Unfortunately, the two patients who presented within the first year died despite all efforts. In contrast, the two patients presenting after the age of 1 year developed normally and are currently aged 15 and 35 years, respectively. Additional longitudinal studies are warranted to better identify which patients with ACAD9 deficiency are appropriate heart transplant candidates.

Supplementation with riboflavin showed improvement in complex I activity in the vast majority of patient fibroblasts, and most patients similarly were reported to have clinical benefit with treatment. Most notably, patients presenting within the first year of life show a significant better survival when treated with riboflavin. One limitation of this observation could be that most of the deaths occurred at the end of the first year of life. This might indicate that our analysis is prone to survivor treatment selection bias. Detailed data about the starting point of

riboflavin treatment, the dosage etc. in more patients are needed.

This observation supports anecdotal reports in the literature. In our cohort, families 1 and 33 are particularly instructive. In both families the first child (I1, I45) died within the first 2 years of life without riboflavin supplementation, whereas the younger affected siblings (I2, I45 and I46), in whom supplementation was begun immediately upon diagnosis, are currently still alive (aged 10, 1.5 and 11 years, retrospectively). Cases I5 and I6 were first reported with riboflavin responsive complex I deficiency before their molecular defect was known [7, 34]. Paired data on fibroblasts and patient riboflavin treatment were available for eight patients, six of which showed parallel beneficial effects and one no effect. Further cellular studies are necessary to define the mode of action of riboflavin in ACAD9 deficiency.

The PPAR promotor activator bezafibrate has been reported to be of benefit in other FAODs. In all cell lines examined in this study, bezafibrate improved the formation of respiratory chain super complexes, likely explaining the improved respiration of the patient cell lines as measured by whole cell oximetry. While only a limited number of cell lines were tested, these results suggest a potential role for bezafibrate or other PPAR activators in the treatment of ACAD9. However, similar effects for bezafibrate have been reported in cell models of other fatty acid oxidation defects, but were not proven in humans.

Our retrospective data provides additional description of the clinical and genetic spectrum of ACAD9 deficiency, and provides valuable insight for the development of future clinical trials of riboflavin, bezafibrate, or other therapies. While the current study was not designed to be a clinical trial, the anecdotal improvement of many ACAD9 deficient patients to riboflavin justifies a trial of riboflavin (20 mg/kg/day, maximum 200 mg/day) in every patient with this diagnosis. Given the high frequency of ACAD9 deficiency, we propose that it would be reasonable to consider riboflavin administration for phenotypically-consistent patients whilst their genetic investigations are underway [35]. This also underlines that in patients with suspicion of a mitochondrial disorder next generation sequencing techniques should be initiated promptly, in selected cases accompanied by studies in affected tissues. For these patients, early diagnosis and therapeutic intervention could be the difference between life and death.

Conclusions

ACAD9 typically presents with cardiomyopathy, exercise intolerance and muscular weakness and the clinical course might respond to riboflavin

References

1. Sánchez-Caballero L, Guerrero-Castillo S, Nijtmans L. Unraveling the complexity of mitochondrial complex I assembly: a dynamic process. BBA - Bioenerg. 1857;2016:980–990.

2. Ensenauer R, He M, Willard J-M, Goetzman ES, Corydon TJ, Vandahl BB, et al. Human acyl-CoA Dehydrogenase-9 plays a novel role in the mitochondrial β-oxidation of unsaturated fatty acids. J Biol Chem. 2005;280:32309–32316. doi: 10.1074/jbc.M504460200.

3. Schiff M, Haberberger B, Xia C, Mohsen A-W, Goetzman ES, Wang Y, et al. Complex I assembly function and fatty acid oxidation enzyme activity of ACAD9 both contribute to disease severity in ACAD9 deficiency. Hum Mol Genet. 2015;24:3238–3247. doi: 10.1093/hmg/ddv074.

4. Zhang J, Zhang W, Zou D, Chen G, Wan T, Zhang M, et al. Cloning and functional characterization of ACAD-9, a novel member of human acyl-CoA dehydrogenase family. Biochem Biophys Res Commun. 2002;297:1033–1042. doi: 10.1016/S0006-291X(02)02336-7.

5. Haack TB, Danhauser K, Haberberger B, Hoser J, Strecker V, Boehm D, et al. Exome sequencing identifies ACAD9 mutations as a cause of complex I deficiency. Nat Genet. 2010;42:1131–1134. doi: 10.1038/ng.706.

6. Nouws J, Nijtmans L, Houten SM, van den Brand M, Huynen M, Venselaar H, et al. Acyl-CoA dehydrogenase 9 is required for the biogenesis of oxidative phosphorylation complex I. Cell Metab. 2010;12:283–294. doi: 10.1016/j.cmet.2010.08.002.

7. Gerards M, van den Bosch BJC, Danhauser K, Serre V, van Weeghel M, Wanders RJA, et al. Riboflavin-responsive oxidative phosphorylation complex I deficiency caused by defective ACAD9: new function for an old gene. Brain. 2011;134:210–219. doi: 10.1093/brain/awq273

8. Aintablian HK, Narayanan V, Belnap N, Ramsey K, Grebe TA. An atypical presentation of ACAD9 deficiency: diagnosis by whole exome sequencing broadens the phenotypic spectrum and alters treatment approach. Mol Genet Metab rep. 2017;10:38–44. doi: 10.1016/j.ymgmr.2016.12.005

9. Lucas TG, Henriques BJ, Rodrigues JV, Bross P, Gregersen N, Gomes CM. Cofactors and metabolites as potential stabilizers of mitochondrial acyl-CoA dehydrogenases. Biochim Biophys Acta - Mol Basis Dis. 1812;2011:1658–1663.

10. Bonnefont JP, Bastin J, Laforêt P, Aubey F, Mogenet A, Romano S, et al. Long-term follow-up of Bezafibrate treatment in patients with the Myopathic form of carnitine Palmitoyltransferase 2 deficiency. Clin Pharmacol Ther. 2010;88:101–108. doi: 10.1038/clpt.2010.55.

11. Orngreen MC, Madsen KL, Preisler N, Andersen G, Vissing J, Laforet P. Bezafibrate in skeletal muscle fatty acid oxidation disorders: a randomized clinical trial. Neurology. 2014;82:607–613. doi: 10.1212/WNL.0000000000000118.

12. Haack TB, Haberberger B, Frisch E-M, Wieland T, Iuso A, Gorza M, et al. Molecular diagnosis in mitochondrial complex I deficiency using exome sequencing. J Med

Genet. 2012;49:277–283. doi: 10.1136/jmedgenet-2012-100846.
13. Garone C, Donati MA, Sacchini M, Garcia-Diaz B, Bruno C, Calvo S, et al. Mitochondrial encephalomyopathy due to a novel mutation in ACAD9. JAMA Neurol. 2013;70:1177–1179. doi: 10.1001/jamaneurol.2013.3197.
14. Nouws J, te Brinke H, Nijtmans LG, Houten SM. ACAD9, a complex I assembly factor with a moonlighting function in fatty acid oxidation deficiencies. Hum Mol Genet. 2014;23:1311–1319. doi: 10.1093/hmg/ddt521.
15. Lagoutte-Renosi J, Ségalas-Milazzo I, Crahes M, Renosi F, Menu-Bouaouiche L, Torre S, et al. Lethal neonatal progression of fetal cardiomegaly associated to ACAD9 deficiency. JIMD Rep. 2015;28:1. doi: 10.1007/8904_2015_499
16. Wortmann SB, Koolen DA, Smeitink JA, van den Heuvel L, Rodenburg RJ. Whole exome sequencing of suspected mitochondrial patients in clinical practice. J Inherit Metab Dis. 2015;38:437–443. doi: 10.1007/s10545-015-9823-y.
17. Alston CL, Howard C, Oláhová M, Hardy SA, He L, Murray PG, et al. A recurrent mitochondrial p.Trp22Arg *NDUFB3* variant causes a distinctive facial appearance, short stature and a mild biochemical and clinical phenotype. J Med Genet. 2016;53:634–641. doi: 10.1136/jmedgenet-2015-103576.
18. Collet M, Assouline Z, Bonnet D, Rio M, Iserin F, Sidi D, et al. High incidence and variable clinical outcome of cardiac

hypertrophy due to ACAD9 mutations in childhood. Eur J Hum Genet. 2016;24:1112–1116. doi: 10.1038/ejhg.2015.264.

19. Kohda M, Tokuzawa Y, Kishita Y, Nyuzuki H, Moriyama Y, Mizuno Y, et al. A comprehensive genomic analysis reveals the genetic landscape of mitochondrial respiratory chain complex deficiencies. PLoS Genet. 2016;12:e1005679. doi: 10.1371/journal.pgen.1005679.

20. Legati A, Reyes A, Nasca A, Invernizzi F, Lamantea E, Tiranti V, et al. New genes and pathomechanisms in mitochondrial disorders unraveled by NGS technologies. Biochim Biophys Acta Bioenerg. 1857;2016:1326–1335.

21. Leslie N, Wang X, Peng Y, Valencia CA, Khuchua Z, Hata J, et al. Neonatal multiorgan failure due to ACAD9 mutation and complex I deficiency with mitochondrial hyperplasia in liver, cardiac myocytes, skeletal muscle, and renal tubules. Hum Pathol. 2016;49:27–32. doi: 10.1016/j.humpath.2015.09.039.

22. Pronicka E, Piekutowska-Abramczuk D, Ciara E, Trubicka J, Rokicki D, Karkucińska-Więckowska A, et al. New perspective in diagnostics of mitochondrial disorders: two years' experience with whole-exome sequencing at a national paediatric Centre. J Transl Med. 2016;14:174. doi: 10.1186/s12967-016-0930-9.

23. Bastin J, Aubey F, Rötig A, Munnich A, Djouadi F. Activation of peroxisome proliferator-activated receptor pathway stimulates the mitochondrial respiratory chain and can correct deficiencies in patients' cells lacking its components. J Clin

Endocrinol Metab. 2008;93:1433–1441. doi: 10.1210/jc.2007-1701.

24. Cornelius N, Byron C, Hargreaves I, Fernandez Guerra P, Furdek AK, Land J, et al. Secondary coenzyme Q10 deficiency and oxidative stress in cultured fibroblasts from patients with riboflavin responsive multiple acyl-CoA dehydrogenation deficiency. Hum Mol Genet. 2013;22:3819–3827. doi: 10.1093/hmg/ddt232.

25. Invernizzi F, D'Amato I, Jensen PB, Ravaglia S, Zeviani M, Tiranti V. Microscale oxygraphy reveals OXPHOS impairment in MRC mutant cells. Mitochondrion. 2012;12:328–335. doi: 10.1016/j.mito.2012.01.001

26. Kremer LS, Prokisch H. Identification of disease-causing mutations by functional complementation of patient-derived fibroblast cell lines. New York: Humana Press; 2017. pp. 391–406.

27. Haack TB, Gorza M, Danhauser K, Mayr JA, Haberberger B, Wieland T, et al. Phenotypic spectrum of eleven patients and five novel MTFMT mutations identified by exome sequencing and candidate gene screening. Mol Genet Metab. 2014;111:342–352. doi: 10.1016/j.ymgme.2013.12.010.

28. Schägger H. Tricine–SDS-PAGE. Nat Protoc. 2006;1:16–22. doi: 10.1038/nprot.2006.4.

29. Wittig I, Braun H-P, Schägger H. Blue native PAGE. Nat Protoc. 2006;1:418–428. doi: 10.1038/nprot.2006.62.

30. Calvo SE, Compton AG, Hershman SG, Lim SC, Lieber DS, Tucker EJ, et al. Molecular diagnosis of infantile mitochondrial

disease with targeted next-generation sequencing. Sci Transl Med. 2012;4:118ra10. doi: 10.1126/scitranslmed.3003310.

31. Nouws J, Wibrand F, Van Den Brand M, Hanka V, Duno M, et al. A patient with complex I deficiency caused by a novel ACAD9 mutation not responding to riboflavin treatment. JIMD Rep. 2014;12:37–45. doi: 10.1007/8904_2013_242.

32. Fragaki K, Chaussenot A, Boutron A, Bannwarth S, Cochaud C, Richelme C, et al. Severe defect in mitochondrial complex I assembly with mitochondrial DNA deletions in *ACAD9* -deficient mild myopathy. Muscle Nerve. 2017;55:919–922. doi: 10.1002/mus.25262

33. Lek M, Karczewski KJ, Minikel EV, Samocha KE, Banks E, Fennell T, et al. Analysis of protein-coding genetic variation in 60,706 humans. Nature. 2016;536:285–291. doi: 10.1038/nature19057.

34. Scholte HR, Busch HFM, Bakker HD, Bogaard JM, Luyt-Houwen IEM, Kuyt LP. Riboflavin-responsive complex I deficiency. Biochim Biophys Acta. 1995;1271:75–83. doi: 10.1016/0925-4439(95)00013-T.

35. Distelmaier F, Haack TB, Wortmann SB, Mayr JA, Prokisch H. Treatable mitochondrial diseases: cofactor metabolism and beyond. Brain. 2017;140:e11. doi: 10.1093/brain/aww303

Chapter 9

Clinical-genetic features and peculiar muscle histopathology in infantile DNM1L-related mitochondrial epileptic encephalopathy.

Verrigni D, Di Nottia M, Ardissone A (co-first author), Baruffini E, Nasca A, Legati A, Bellacchio E, Fagiolari G, Martinelli D, Fusco L, Battaglia D, Trani G, Versienti G, Marchet S, Torraco A, Rizza T, Verardo M, D'Amico A, Diodato D, Moroni I, Lamperti C, Petrini S, Moggio M, Goffrini P, Ghezzi D, Carrozzo R, Bertini E.

Hum Mutat. 2019 May;40(5):601-618

INTRODUCTION

The *DNM1L* (dynamin-1 like) gene encodes for the DRP1 protein, an evolutionary conserved member of the dynamin family, responsible for fission of mitochondria, a process required for normal mitochondrial dynamics and distribution. When activated, DRP1 translocates from a cytosolic pool to the outer mitochondrial membrane, where it oligomerizes, hydrolyzes guanosine triphosphate (GTP), and assembles into spiral filaments around mitochondrial tubules, allowing the organelles division. After the completion of this process, DRP1

spirals likely disassemble from mitochondria for future rounds of mitochondrial fission (Youle & van der Bliek, 2012).

DRP1 has an important role in the maintenance of mitochondrial (Otsuga et al., 1998) and peroxisomal morphology (Pitts, McNiven & Yoon, 2004; Schrader, Costello, Godinho, Azadi, & Islinger, 2016), mediating organelle membrane remodeling during a variety of cellular processes. Mitochondria exist as a dynamic tubular network with projections that move, break, and reseal in response to local environmental changes; the size and morphologic arrangement of mitochondria are due to a dynamic balance between mitofusins-dependent mitochondrial fusion and DRP1-dependent mitochondrial fission (Santel & Fuller, 2001).

Defects in mitochondrial dynamics, including the inhibition of mitochondrial fission and fusion, are responsible for many human diseases (Alexiou et al., 2018; Kim, Lee, Oh, Kim, & Han, 2017; Lenaers et al., 2012; Pozo Devoto & Falzone, 2017; Stuppia et al., 2015). Besides mutations in *DNM1L* (Waterham et al., 2007), dysfunctions in mitochondrial fission have been also associated with mutations in genes codifying for adaptors of DRP1, such as MFF and MID49/MIEF2 (Bartsakoulia et al., 2018; Koch et al., 2016; Shamseldin et al., 2012).

DRP1 impairment is implicated in several neurological disorders associated with either de novo dominant or compound heterozygous *DNM1L* mutations (MIM #603850). Encephalopathy due to defective mitochondrial and peroxisomal fission-1 is characterized by early onset with

psychomotor delay and hypotonia, progressive course, and death in childhood. Many patients develop refractory seizures, consistent with an epileptic encephalopathy, and thereafter show a neurological decline. Age at onset, symptoms, and severity are variable, and some patients may not have clinical/biochemical evidence of mitochondrial or peroxisomal dysfunction (Fahrner, Liu, Perry, Klein, & Chan, 2016; Nasca et al., 2016).

Better known clinical conditions that occur more frequently are related to defects in factors that are conversely implicated in mitochondrial membrane fusion such as Charcot–Marie–Tooth disease type 2A caused by dominant or recessive mutations in *MFN2* (mitofusin 2; MIM #608507), and optic atrophy or Leigh-like infantile encephalopathies caused by dominant or recessive mutations in *OPA1* (MIM #605290). Additional rare neurological phenotypes of “optic atrophy plus” syndrome and 3-methylglutaconic aciduria or cataracts are related to recessive or dominant mutations in *OPA3* (MIM #606580), a factor involved in mitochondrial shaping; a mild Charcot–Marie–Tooth disease type 2K is caused by biallelic recessive mutations in *GDAP1* (MIM #606598), that encodes for a mitochondrial protein involved in mitochondrial dynamics; and finally mitochondrial myopathy and ataxia have been recently reported to be due to dominant or recessive mutations in *MSTO1* (MIM #617619), encoding a cytoplasmic promitochondrial fusion protein (Nasca, Scotton et al., 2017).

Cultured fibroblasts from patients with these genetic conditions usually show either mitochondrial fragmentation, corresponding to genetic defects of factors implicated in mitochondrial membrane fusion (MFN2, OPA1; Zanna et al., 2008), or abnormally elongated mitochondria and aberrant peroxisomes in cases with mutations in *MFF* (Koch et al., 2016) and *DNM1L* (Nasca et al., 2016).

Histochemical and ultrastructure characterization of skeletal muscle biopsies of subjects harboring *OPA1* mutations showed the presence of cytochrome c oxidase (COX)-deficient fibers associated with multiple mitochondrial DNA deletions in the majority of patients, either affected by dominant optic atrophy plus variants or with isolated optic nerve involvement (Yu-Wai-Man et al., 2010). On the other hand, few papers have reported studies on muscle biopsy of patients with mutations in additional genes regulating mitochondrial morphology, and no abnormalities have been found (Fahrner et al., 2016; Koch et al., 2016; Nasca et al., 2016; Waterham et al., 2007; Yoon et al., 2016), although Chao et al. (2016) reported mitochondrial shape abnormalities at electron microscopy (EM).

Here we describe on a series of five sporadic patients affected by severe epileptic encephalopathy associated with heterozygous mutations in *DMN1L* showing peculiar mitochondrial distribution changes in the muscle biopsy. So far, these abnormalities of mitochondrial distribution in muscle seem to be specific for the *DMN1L*-related epileptic encephalopathy.

2 METHODS

2.1 Histological, ultrastructural, and biochemical analyses in muscle

Cryostatic cross-sections of quadriceps muscle biopsies were processed according to standard histochemical and immunohistochemical procedures. Immunohistochemical studies were performed with the rabbit polyclonal TOMM20 antibody (in green; Santa Cruz Biotechnology, Dallas, TX) and with a monoclonal antibody against merosin (in red; Chemicon, Burlington, MA). Confocal microscopy was performed on a Leica TCS-SP8X laser-scanning confocal microscope (Leica Microsystems, Mannheim, Germany) equipped with a white light laser source, 405 nm diode laser, three internal spectral detector channels (PMT) and two internal spectral detector channels GaAsP. Sequential confocal images were acquired using a 63×-oil immersion objective (1.42 numerical aperture; Leica Microsystems) with a 1024 × 1024 format, and scan speed 400 Hz. Z-reconstructions (30 stacks) were obtained with a z-step size of 0.3 μm. To improve contrast and resolution of mitochondrial distribution, confocal raw images were deconvolved by the Hyvolution 2 software (Leica Microsystems) before 3D reconstruction. Then deconvolved z-stacks were imported into the LASX 3D Analysis (Leica Microsystems) software to obtain their three-dimensional surface rendering. Each group of image was processed and analyzed using the same settings (i.e. laser power and detector amplification). For ultrastructural studies, muscle specimens were fixed in 2.5%

glutaraldehyde in 0.1 M cacodylate buffer (pH 7.4) at 4°C. Samples were postfixed with 2% OsO_4 in 0.1 M cacodylate buffer (pH 7.4) for 1 hr. Specimens were dehydrated in a graded series of ethanol and embedded in epon resin. Thin sections were evaluated with a transmission electron microscope (EM 109 Zeiss; Fattori et al., 2018).

Respiratory chain complexes (RCCs) activities were assayed in muscle homogenate and normalized to citrate synthase activity, using a previously reported spectrophotometric method (Bugiani et al., 2004).

2.2 Mutational analysis

Genomic DNA was isolated from blood and cultured skin fibroblasts using the QIAamp DNA Mini Kit (Qiagen, Valencia, CA). DNA from patient 1 (Pt.1), Pt.2, and Pt.3 underwent high-throughput sequencing by TruSight One panel (Illumina, San Diego, CA) comprehensive of greater than 4.800 clinically relevant genes. The enrichment was achieved following manufacturer instruction and the sequencing analysis was performed on the MiSeq System. The Variant-Studio software was applied for analysis, classification, and reporting of genomic variants. After excluding previously annotated single nucleotide changes occurring with high frequency in populations (>1%), we prioritized variants predicted to have a functional impact (i.e. nonsynonymous variants and changes affecting splice sites). Pt.4 and Pt.5 were analyzed using a custom gene panel for the screening of 224 genes associated with mitochondrial diseases (Ardissone et al., 2018). Sanger

sequencing was used to validate all the annotated functionally relevant variants, as well as to check variant segregation in the families. Bioinformatics tools based on heuristic methods, SIFT (http://sift.jcvi.org), PolyPhen-2 (http://genetics.bwh.harvard.edu/pph2), and Mutation Taster (http://www.mutationtaster.org/) were used for the pathogenicity prediction of variants.

For the identification of multiple deletions, we performed Long Range PCR using TaKara LA Taq DNA Polymerase (Takara Biotechnology Co., Ltd., Dalian, China) amplifying a 11242 bp mitochondrial DNA (mtDNA) fragment with forward-4800 (5′-TTCACTTCTGAGTCCCAGA-3′) and backward-16042 primers (5′-CTGCTTCCCCATGAAAGAGAACAGAGAA-3′).

2.3 Western blotting analysis and antibodies

For sodium dodecyl sulfate-polyacrylamide gel electrophoresis, 40 µg of fibroblasts homogenate was loaded in a 12% denaturating gel. Western blot (WB) was achieved by transferring proteins onto polyvinylidene difluoride membrane and probed with specific antibodies. Specific bands were detected using Lite Ablot Extend Long Lasting Chemiluminescent Substrate (Euroclone, Pero, MI, Italy). Densitometry analysis was performed using the Quantity One software (BioRad, Hercules, CA).

RCC subunits were detected using the following monoclonal antibodies purchased from MitoScience (Eugene, OR): Complex I: NDUFA9; Complex II: SDHB; Complex IV: COXII; Complex V: ATP5B; porin (voltage-dependent anion channels).

Polyclonal rabbit GAPDH (Sigma-Aldrich, St. Louis, MI) and monoclonal antibody OPA1 (BD Biosciences, San Jose, CA), and DRP1 (Abcam, Cambridge, UK) were also used.

2.4 Biochemical analysis, immunostaining, and imaging in fibroblasts

Human fibroblasts were obtained from a diagnostic skin biopsy and grown in Dulbecco's modified Eagle medium supplemented with 10% fetal bovine serum, 4.5 g/L glucose, and 50 µg/mL uridine. Complex V activity (in the direction of ATP synthesis) was measured in fibroblast mitochondria, using reported spectrophotometric methods (Rizza et al., 2009). Mitochondrial respiration was measured using a SeaHorse XF96 apparatus (Agilent Technologies, Santa Clara, CA), as previously described (Invernizzi et al., 2012).

To display the mitochondrial network arrangement, fibroblasts from Pt.1, Pt.2, and Pt.3 were fixed and permeabilized using methanol:acetone (2:1) for 10 min at room temperature, then a blocking solution containing 5% bovine serum albumin in phosphate-buffered saline was used. The polyclonal rabbit TOMM20 antibody (Santa Cruz Biotechnology) was applied overnight and visualized using the Alexa Fluor 647 secondary antibody (Jackson ImmunoResearch, Cambridgeshire Business Park, UK), both antibodies were used at the dilution of 1:500. Images were acquired with a fluorescence-inverted microscope (Leica DMi8). An average of eight image planes was obtained along the *z*-axis at 0.2 µm increments using the LASX 3.0.4 (Leica) software. For Pt.4 and Pt.5 the mitochondrial network

was visualized in living cells using the mitochondrial fluorescent dye MitoTracker Red-CMXRos (Invitrogen, Carlsbad, CA) at final concentrations of 50 nM for 30 min; then images were acquired with a confocal microscope (Leica TSC-SP8).

For peroxisomal immunostaining, we used the polyclonal rabbit PMP70 antibody (Sigma-Aldrich) applied overnight at the concentration of 1:200, followed by an Alexa Fluor 488 secondary antibody (1:500). The peroxisomal staining was visualized using the same parameters used above. Analysis of peroxisomal morphology was conducted using the image processing package ImageJ (Fiji). Images were then binarized, thresholded, and subjected to particle analysis to acquire form factor ("circularity": 4π*area/perimeter^2).

2.5 Functional studies in yeast

2.5.1 Yeast strains and media

The yeast strains used in this work were the haploid strain W303-1B (*MATa leu2–3, trp1-1, can1–100, ura3-1, ade2-1, his3–11*) and its isogenic strain *dnm1*::KanR, and the hemizygous diploid strain W303 *dnm1Δ* (*MATa*/*MATa leu2–3/leu2–3, trp1-1/trp1-1, can1–100/can1–100, ura3-1/ura3-1, ade2-1/ade2-1, his3–11/his3–11 DNM1/dnm1*::KanR). All experiments were performed in Synthetic Complete Medium (SC; 6.9 g/L yeast nitrogen base without amino acids [ForMedium, Norfolk, UK], 1 g/L drop-out mix without amino acids or bases necessary to keep plasmids; Kaiser, Michaelis, & Mitchell, 1994). Media were supplemented with carbon sources (Carlo Erba Reagents, Barcelona, Spain) as indicated

in the text in liquid phase or after solidification with 20 g/L agar (ForMedium).

2.5.2 Construction of *dnm1* mutant strains

Dnm1 mutant alleles and *dnm1* mutant strains were constructed as previously reported (Nasca et al., 2016). Briefly, *dnm1* mutant alleles were constructed using mutagenic overlap PCR with the oligonucleotides reported in Table S1, digested with *Bam*HI and *Xba*I or *Xba*I and *Sal*I, and subcloned in pFL38DNM1. In order to obtain haploid wild-type or mutant strains, all plasmids were introduced by transformation in the W303-1B *dnm1Δ* haploid strain and in the W303 *dnm1Δ* hemizygous diploid strain using the "LiAc/SS carrier DNA/PEG quick method" as previously reported (Gietz & Woods, 2002).

2.5.3 Yeast analyses

Spot assay was performed by spotting 5×10^4, 5×10^3, 5×10^2, and 5×10^1 cells on SC supplemented with different carbon sources. *Petite* frequency was measured as previously reported (Baruffini, Ferrero, & Foury, 2010) in six to eight independent clones for each strain. The oxygen consumption rate was measured in SC medium as previously described (Goffrini et al., 2009) on five independent clones, after growth in conditions, which minimized the *petite* frequency, which was lower than 5%. (Nolli et al., 2015). All experiments were performed at 37°C, except for the measurement of the *petite* frequency in the diploid strains, which was performed at 28°C.

2.6 Statistical analysis

For each experiment, data obtained were calculated as the mean of replicates ± standard deviation (*SD*). For analysis on peroxisomal morphology data were analyzed using unpaired two-tailed Student's *t* tests; for yeast experiments, data were compared with one-way analysis of variance followed by the Bonferroni's test.

2.7 Structural analysis

The residues affected by the missense mutations described in this work (p.Gly223Val, p.Gly362Asp, p.Phe370Cys, and p.Arg403Cys) were mapped on crystal structures of homologues proteins. The crystal structure of a dimeric human dynamin-1-like protein (Protein Data Bank [PDB], 3W6O) was used for the p.Gly223Val mutation. The crystal structure of the dynamin-3 tetramer (PDB 5A3F) was used for the p.Gly362Asp, p.Phe370Cys, and p.Arg403Cys mutations. The cryoelectron microscopy structure of human dynamin-1 coassembled with MID49 (PDB 5WP9) was used to obtain a detailed view of the site of the p.Phe370Cys mutation. Molecular structures were rendered with the PyMOL (http://www.pymol.org).

2.8 Ethical approval

The study was approved by the Ethical Committees of the Bambino Gesù Children's Hospital, Rome, Italy, and the Carlo Besta Neurological Institute, Milan, Italy, in agreement with the Declaration of Helsinki.

3 RESULTS

3.1 Clinical features and brain magnetic resonance imaging findings

Patient 1 is a girl single-born from unrelated healthy young parents. At birth, there was no breathing distress, no jaundice, and weight was 2.850 kg. She had normal motor milestones in the first year of life and was able to walk without any support at age 17 months. She pronounced her first words around 1 year of age, and later at age 4 years she started in kindergarten and had good attendance and integration. At age 2 years and a half, the child manifested generalized clonic seizures while falling asleep, and then displayed an ataxic syndrome with a prominent intentional and postural tremor that persisted for 2 weeks. About 7 to 8 weeks later, a cluster of myoclonic seizures of face and left side limbs with vomiting and drooling appeared together with relapsing of ataxia. She was admitted at a local hospital where the brain magnetic resonance imaging (MRI) showed T2 hyperintensities in the posterior white matter regions and some T2 hyperintensities in the cortical areas. More recently, an MRI performed at age 6 years showed moderate global cerebral and cerebellar atrophy (Figure 1a,b,e,f). Serial MRIs taken in the same month at different days showed that the cortical dynamic time warping (DTW) restriction hyperintensity in the right precentral gyrus and in the pallidum and thalamus of the right hemisphere (Figure 1C) spontaneously vanished 20 days later when a serial brain MRI was performed (Figure 1d). She was admitted at our hospital for a Super refractory Status Epilepticus (SRSE) which began one month before and was unresponsive to multiple doses of thiopentone. SRSE was treated with propofol and with a high dose of topiramate and

perampanel and was characterized by repetitive to continuous focal myoclonic seizures clinically lateralized to the right side, especially involving the face and the right arm. The polymyographic video/electroencephalography (EEG) recordings showed high amplitude theta–delta activity, lateralized to the left side. Ictal EEG confirmed the cortical nature of the seizures as it was characterized by low amplitude rhythmic fast discharge lateralized to the left side evolving into a focal spike-and-wave complex, corresponding to the clinical focal contralateral myoclonus. Intercritical EEG confirmed the interhemispheric asymmetry with persistent slow activity over the left central regions. SRSE lasted for 50 days and was the only status epilepticus she had so far.

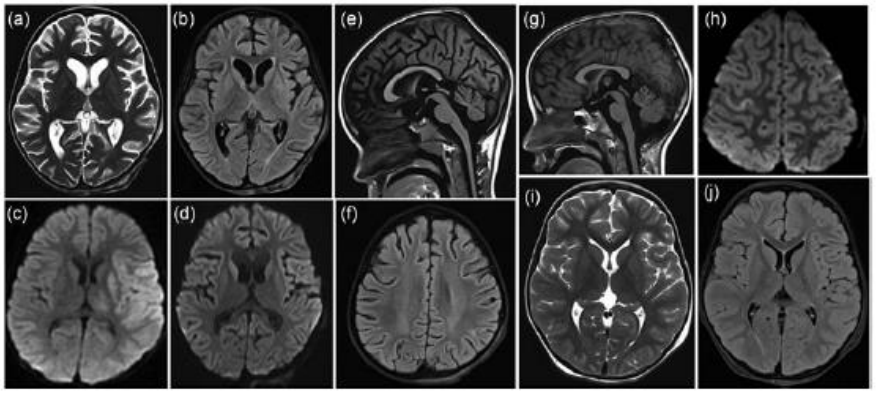

Figure 1

MRI pattern of Pt.1 (a–f) obtained at age 6 years and Pt.2 (g–j) obtained at age 7 years. (a) T2 weighted axial image. (b) FLAIR weighted axial image. (c,d) Serial DTI images obtained serially in two different days of the same month. In Pt1 the MRI shows signs of global cerebral and cerebellar atrophy, with moderate enlargement of the ventricles. Two serial brains axial DTI weighted MRIs were performed in the same month with a distance of 20 days; the first MRI showed a cortical DTW restriction hyperintensity in the right precentral gyrus, and abnormal DTI restriction hyperintensities corresponding to the pallidum and thalamus of the right hemisphere

(c). These abnormalities vanished spontaneously 20 days later when a serial brain MRI was performed (d). In Pt.2 the T1 weighted sagittal image (g) and axial T2 weighted (i) and corresponding axial FLAIR-weighted images were consistent with a slight global cerebral atrophy, while a cortical DTW restriction hyperintensity was observed only once in the right precentral gyrus (g–j) of three MRI scans performed within 3 months of time. DTI: diffusion tensor imaging; DTW: dynamic time warping; FLAIR: fluid-attenuated inversion recovery; MRI: magnetic resonance imaging

Patient 2 is a boy born as a preterm infant from computed tomography (CT) scheduled at 36 weeks of gestational age because prenatal ultrasound monitoring indicated a fetal growth restriction appearing in the last trimester. At birth weight was 2.020 kg, Apgar 9–10. The neonatal period was uneventful, and developmental milestones were regular because he started to walk without support at the age 15 months, although he showed a delay in attaining language and failure to thrive (weight always around 3rd centile) from the first months of life. Preliminary genetic investigations (karyotype, MLPA 22q12.2, telomeres, fragile X) yielded no abnormalities. Moreover, gastroenterological and endocrinological investigations (FT4, TSH, IgA, EMA, Anti TG, AGA) carried out during hospitalization showed increased glutamic oxaloacetic transaminase (GOT) (84.9 IU/L), central hypothyroidism (TSH levels 1.27 mU/ml, Ft3 2.4 pg/ml with NV of 2.4–4.2, and Ft4 7.6 pg/ml with NV of 8.5–16.5) and low levels of adrenocorticotropic hormone (18 pg/ml with NV of 0–46 pg/ml). During the follow-up, increased serum lactate was detected (4.71 mmol/l, NV 0.6–2.3 mmol/L). The child was treated with thyroid hormone and started therapy with hydrocortisone. Around age 3 years the boy started with a prolonged repetitive

left hemiclonic SRSE and additional single episodes relapsed during the follow-up with a frequency of at least twice a month although he was taking antiepileptic polytherapy with phenobarbital, topiramate, and clonazepam. At age 7 years serial brain MRIs performed three times in a timeframe of 3 months, showed only a slight global cerebral atrophy, and a cortical DTW restriction hyperintensity was observed only once in the right precentral gyrus (Figure 1g–j). MR spectroscopy did not detect any lactate peek. Polymyographic video/EEG recordings during one episode of SRSE with subsequent left focal myoclonic seizures, showed, only as a counterpart of the seizures, a pattern of RHADs (Rhythmic High Amplitude Delta superimposed by fast activity) over the contralateral central regions. Focal RHADs were also present during sedation. Later on, during the SRSE, which was treated with topiramate, propofol, and ketamine, RHADs were no longer recorded and were replaced by persistent focal slow activity. SRSE lasted 17 days together with epilepsia partialis that was noticed over the left side of the body.

Patient 3. The girl is the second child from unrelated parents; the eldest sister aged 12 years was healthy. She was born by a planned TC delivery, at term, and weight was 2.950 kg at 40 weeks of gestation. The child had a normal development from the newborn period to the age of 5 years, although a mild hearing loss was suspected. Around the age of 5 years, she was admitted to the intensive care for the abrupt manifestation of a myoclonic status epilepticus during an intercurrent febrile

episode. The patient needed a prolonged hospital admission because she manifested repeated severe myoclonic or right prolonged hemiclonic SRSE that was associated with a psychomotor deterioration. During the follow-up, the child presented with very frequent and long duration seizures of generalized or hemiclonic SRSE and persistent interictal myoclonus at upper and lower limbs. One previous brain MRI performed at age 3 years was considered normal, while the last brain MRI performed at age 7 years (Figure 2a–d) showed global cortical atrophy that was prominent in both the right hemisphere and the homolateral cerebral peduncle. There was also abnormal T2 high-intensity signal (long TR images) of the deep white substance at the semioval white matter and in the paratrigonal site bilaterally with the involvement of the subcortical spaces in the temporo-insular areas bilaterally (data not shown). The DWI study did not show any signs of recent cerebral and cerebellar parenchymal abnormalities. The ventricular system was moderately enlarged. Polygraphic video/EEG recordings performed during the chronic phase of the disease showed poorly organized cerebral activity, both in wakefulness and sleep, with theta activity superimposed by fast rhythms. Polymyographic recording confirmed right side high-frequency myoclonus, predominantly at the right hand and right face, rhythmic in nature, persistent during sleep, without a clear-cut correlation with the EEG transients.

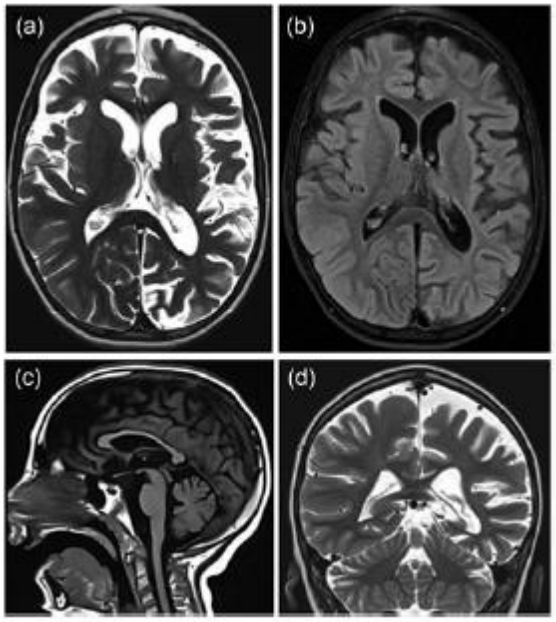

Figure 2

MRI pattern of Pt3. Brain MRI performed at age 7 years. (a) T2 weighted axial image. (b) The corresponding FLAIR weighted axial image. (c) Sagittal T1 weighted. (d) Coronal T2 weighted image, showing global severe cortical atrophy that was prominent in both the right hemisphere and the homolateral cerebral peduncle (a,b). FLAIR: fluid-attenuated inversion recovery; MRI: magnetic resonance imaging

Patient 4 is the only child from unrelated parents. A half-brother from previously mother's marriage presented with severe psychomotor delay, refractory epilepsy, and myoclonic status epilepticus at 2 years of age; he died for an unknown reason at 3 years. This boy was born at term after an uncomplicated pregnancy and delivery. The psychomotor delay was reported since the first months of life: he achieved sitting position at 12 months, autonomous gait and first words at 3 years of age. First neurological evaluation performed at 4 years showed psychomotor delay and pyramidal signs at lower limbs; instrumental exams including brain MRI and EEG were

reportedly normal. At 5 years and 5 months of age, a few days after a viral illness, he presented partial motor status epilepticus. In the after months, refractory epilepsy and psychomotor regression were reported. He manifested motor partial, tonic, myoclonic seizures and spasms, and experienced two episodes of myoclonic status epilepticus resembling SRSE, refractory to midazolam, thiopentone, vitamin B6, and propofol. EEGs were not available; brain MRI performed one month after first status epilepticus disclosed T2 hyperintensities in thalami and in right hemisphere temporo-parieto-occipital cortex that appeared reduced 40 days later when a serial brain MRI was performed (Figure S1 A–E). He was admitted to our hospital at 5 years and 9 months manifesting spastic tetraparesis, no postural control, hyperkinesis but poor voluntary movements, and severe cognitive impairment. Seizures frequency was daily. Polymyographic video/EEG disclosed epilepsia partialis continua at the right arm intermingled with asymmetric tonic seizures mainly involving left side arm and related with generalized low voltage fast rhythms with parieto-occipital prevalence, EEG background activity, and sleep pattern were not organized. Brain MRI showed global cerebral atrophy (Figure S1 F–J). Visual and sensory evoked potential showed central conduction abnormalities, motor and sensory nerve conduction velocities disclosed sensitive and motor axonal neuropathy. Fundus oculi and brainstem auditory evoked were normal. Blood routine exams, pyruvate, amino acids plasmatic levels, very long chain fatty acid (VLCFA), phytanic acid, and

urinary organic acids were normal. Mild elevated lactate level in serum was detected (2.3 mmol/L NV 0.8–2.1). RCCs activity was normal in muscle. The patient died for respiratory failure at 6 years of age.

Patient 5 is the only child from unrelated parents. Family history was unremarkable. She was born at term after an uneventful pregnancy. At birth weight was 3.050 kg, Apgar 9–9. After birth, she presented respiratory distress that required intensive care and oxygen supplementation for 20 days. During the first months, psychomotor development was reportedly normal (head control at 2 months of age). Between 4 and 6 months of age development delay and failure to thrive became evident; from 7 to 8 months to 1 year of age she suffered from self-inflicted finger and mouth ulcers and pain insensitivity were reported (i.e. receiving vaccine injections). In the second year of life she presented prolonged clonic seizures at left face. At 3 years of age she was first evaluated in our institute: she presented with short stature (weight and length <3rd percentile), microcephaly (<3rd percentile), dysphagia, tetraparesis with extrapyramidal signs, dystonic postures involving both upper and lower limbs, dyskinesias and athetoid movements, absence of postural control, absence of language. Epileptic seizures were not noticed from parents but polymyographic video/EEG recorded tonic seizures at upper limbs related to multifocal generalized epileptiform abnormalities and showed poorly organized cerebral activity, both in wakefulness and sleep. Treatment with levetiracetam was started but EEG pattern

remained unchanged. From the age of 4 years, dyskinesias and dystonia worsened. Serial brain MRI (7 months, 2 years and 1 month, 4 years and 4 months) showed thin corpus callosum together with signs of increased cortical subarachnoid spaces suggesting cortical involvement, and progressive cerebellar atrophy (Figure S2); no cortex involvement was noticed. Brainstem auditory evoked and visual evoked potential showed central conduction abnormalities, motor, and sensory nerve conduction velocities disclosed sensitive and motor axonal neuropathy. Fundus oculi were normal. Blood routine exams, plasmatic uric acid, lactate and pyruvate in plasma and CFS, plasmatic amino acids levels, VLCFA were normal. Molecular analysis of *PLA2G6*, *POLG1*, and NARP/MILS mutations was negative. Muscle biopsy was not performed. At last follow-up, at 5 years, clinical conditions were stable.

3.2 Histological and biochemical analyses

Histochemistry of the muscle sample of Pt.1, Pt.2, and Pt.3 showed scattered fibers with a patchy reduction of COX and succinate dehydrogenase (SDH) stain with aspects of the polymorphic core like areas (Figure 3, left and central panels). Similarly, areas of reduced immunoreactivity were observed using the TOMM20 antibody confirming impairment of the mitochondrial network distribution (Figure 3, right panel). Muscle histochemistry in Pt.4 also showed multiple areas of patchy reduction of COX (Figure S3 A), while EM showed enlarged mitochondria; sometimes two mitochondria were

coupled and appeared to be in close relationship to each other (Figure S3 B–C). Occasionally, the sarcomeric organization appeared to be normal, though the Z line was often absent (Figure S3 D). In addition, in some areas mitochondria were quite absent (Fig S3 E–F), whereas in others they were present in large collections (Fig S3 G–H). Histochemical serial sections of the muscle biopsy in Pt. 3 showed that fibers devoid of mitochondria were type 1 fibers (Figure S4). Furthermore, confocal microscopy of the muscle biopsy (Figures S5 and S6) showed an altered and irregular array of Z bands, while patchy areas devoid of mitochondria were clearly observed with TOM20 staining. In spite of the irregular aspect of the Z bands in confocal microscopy, no major alterations such as streaming of the Z bands were observed at the EM level (Figure S3).

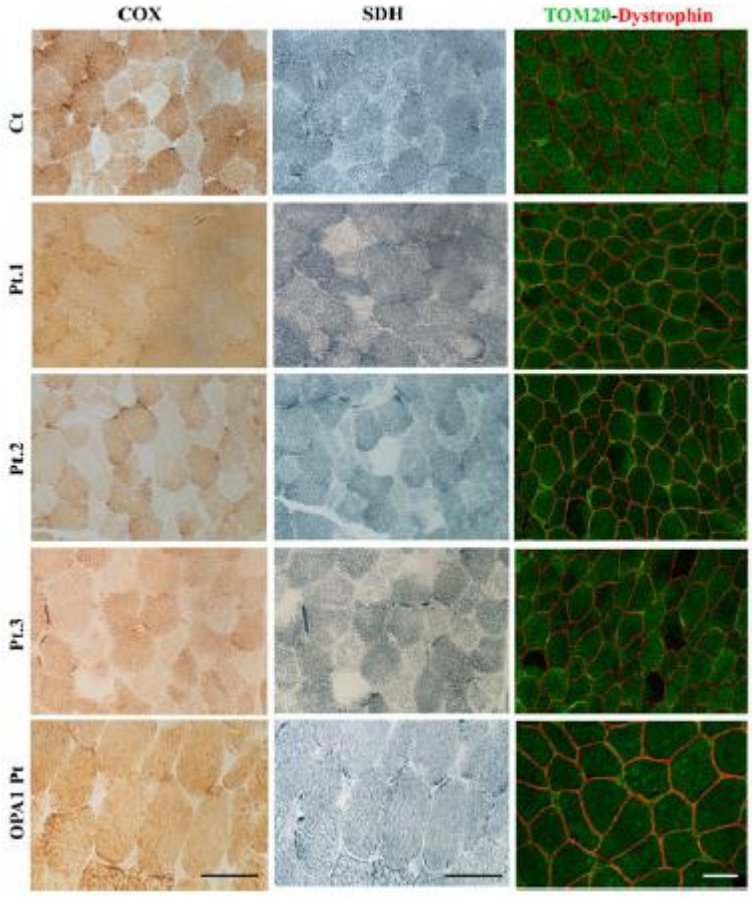

Figure 3

Panel showing the histochemistry of quadriceps muscle samples of Pt.1, Pt.2, Pt.3, and control. The muscle histochemistry of serial sections of three patients with heterozygous dominant mutations in *DNM1L* and stained with cytochrome *c* oxidase (COX) and succinate dehydrogenase (SDH) showed scattered fibers with a patchy reduction of both COX and corresponding SDH staining, with aspects of polymorphic core like areas (left and central panel). Similarly, areas of reduced immunoreactivity were observed using the TOMM20 antibody confirming impairment of the mitochondrial network distribution (right panel). These abnormalities were not detected in the muscle biopsy of a patient with biallelic mutations in *OPA1* (last bottom row) already described (Nasca, Rizza et al., 2017). The plasma membrane is stained in red fluorescence with an antibody against dystrophin [Color figure can be viewed at wileyonlinelibrary.com]

Histochemistry of the muscle sample of a patient harboring compound heterozygous mutations in *OPA1* (Nasca, Rizza et al., 2017) was studied and compared with those of *DNM1L* patients and showed no patchy staining abnormalities (Figure 3 lowest panel). In addition, by Long Range PCR we also searched comparatively for multiple deletions in muscle samples and found multiple deletions only in the *OPA1* mutated patient and not in the *DNM1L* patients (data not shown).

Muscle biopsy was not performed in Pt.5.

RCCs biochemical analysis in muscle homogenate was normal in all patients (data not shown). Accordingly, the activity of Complex V (in the direction of synthesis of ATP) measured in Pt.1 fibroblast mitochondria, as well the oxygen consumption in Pt.4 and Pt.5 fibroblasts were normal (data not shown).

3.3 Mutational analysis

Bioinformatics analysis carried out on the TruSight One panel, performed in Pt.1, Pt.2, and Pt.3, led to the identification of a single gene entry, *DNM1L* (NM_012062, NP_036192). In Pt.1 we identified the heterozygous, previously unreported variant c.668G>T (p.Gly223Val; Figure 4a); in Pt.2 we identified the heterozygous variant c.1207C>T (p.Arg403Cys), already reported (Fahrner et al., 2016; Figure 4b); in Pt.3 we identified the heterozygous unreported variant c.1109T>G (p.Phe370Cys; Figure 4c). Segregation for the three mutations in the corresponding families was negative, and then they can be considered as de novo mutations. Similar filtering analysis was

applied to the panel, containing approximately 230 genes associated with mitochondrial disease, used for Pt.4 and Pt.5. In Pt.4 we identified two heterozygous *DNM1L* variants: c.1085G>A (p.Gly362Asp) and c.1535T>C (p.Ile512Thr; Figure 4d–d'). The first nucleotide change corresponded to rs148686457, with a frequency of 0.008% in the ExAC database, whereas the second was not reported in any public database. Given that *DNM1L* mutations may present as recessive or dominant traits, we evaluated the segregation in the healthy parents of Pt.4 by Sanger sequencing: we found that the c.1535T>C (p.Ile512Thr) was inherited from the mother (Figure 4d') while the c.1085G>A (p.Gly362Asp) was not present in any of the two parents and may represent a de novo event (Figure 4d). Indeed, the same change has been recently reported as a de novo mutation (Vanstone et al., 2016). An in-depth evaluation of the familial history revealed that the mother had a son with epileptic encephalopathy from another man. This child died at 3 years of age: no material was available for genetic studies. By subcloning PCR products obtained from Pt.4′s cDNA, we were able to assess that the two *DNM1L* variants were on the same allele (i.e., the maternal allele, harboring the c.1535T>C variant identified in the mother). Moreover, a further analysis of *DNM1L* genomic region using a next-generation sequencing (NGS) approach revealed that the c.1085G>A was present in the mother's blood DNA, although at a very low level (~5%). These findings suggested maternal germline mosaicism for the dominant mutation c.1085G>A

(p.Gly362Asp), that may even explain the affected status of the Pt.4's half-brother (Figure S7). In Pt.5 we identified a heterozygous variant c.1084G>A (p.Gly362Ser); the variant was not detected in the parents' DNA by Sanger or NGS analyses (Figure 4e). The variant was absent in public SNP databases; nevertheless, it was reported as a de novo mutation in a patient with refractory epilepsy (Sheffer et al., 2016).

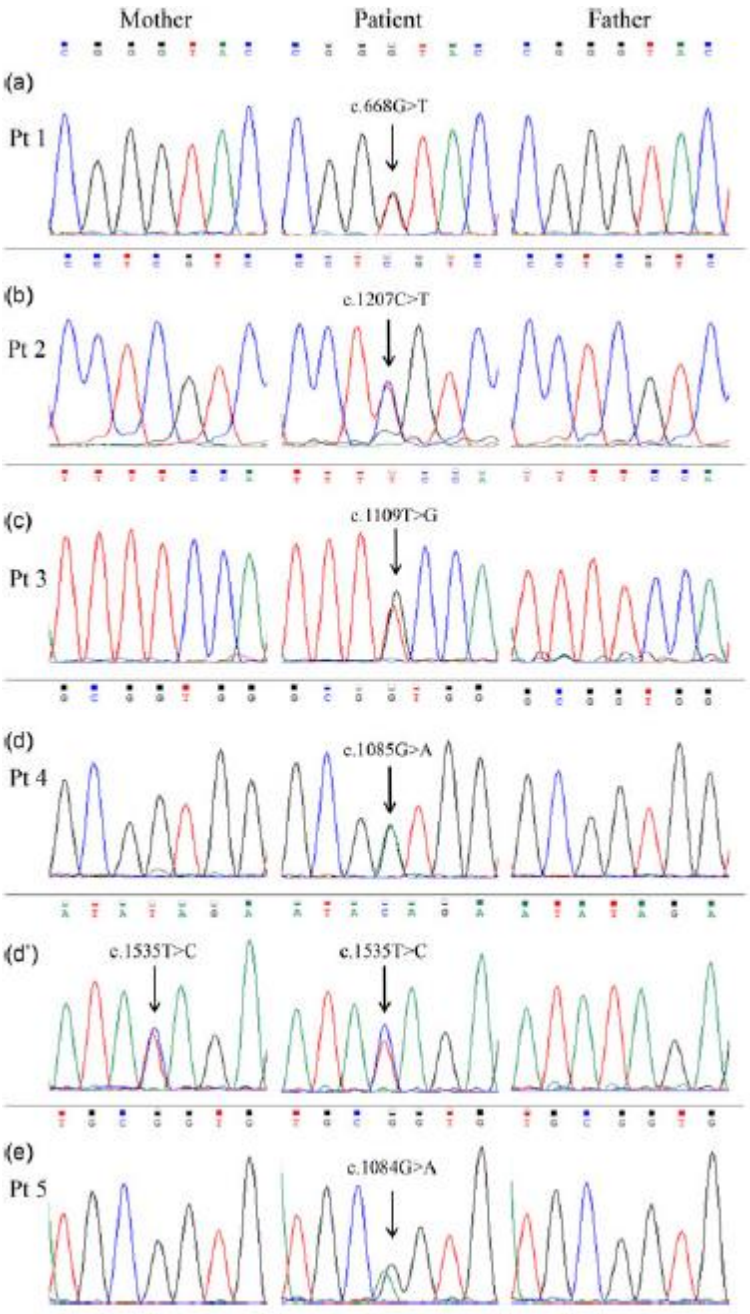

Figure 4

Electropherograms. The variants identified by NGS in *DNM1L* (a–e) have been confirmed by Sanger sequencing in all patients and their parents. In (d') the second

variant identified in Pt.4 (c.1535T>C), inherited from the mother. NGS: next-generation sequencing [Color figure can be viewed at wileyonlinelibrary.com]

All new mutations herein reported were pathogenetic while tested in silico (Table S2), and were not reported in public (dbSNP142, ExAC, 1000 Genomes, HGMD, gnomAD) and in-house databases.

3.4 WB analysis

To evaluate the impact of the mutations on DRP1 stability, we performed WB analysis on fibroblasts. We observed a significantly increased (in Pt.3) or normal (in Pt.1, Pt.2, Pt.4, and Pt.5) level of the protein when normalized to GAPDH (Figure 5a,b), in contrast with the strong reduction present in *DNM1L*-recessive cases (Nasca et al., 2016). The expression level of OPA1 and of different subunits of the RCCs showed no differences compared to controls (data not shown).

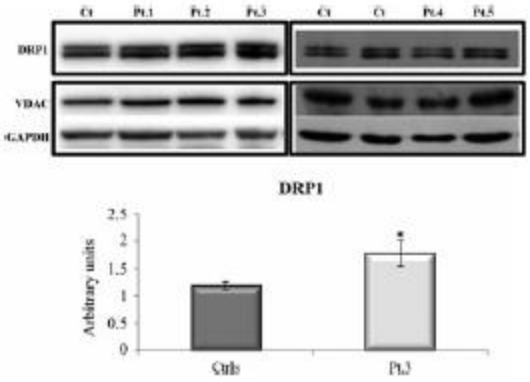

Figure 5

Western blotting analysis. Immunoblot analysis of total lysates from controls (Ct) and patients (Pt) fibroblasts using DRP1, VDAC, and GAPDH antibodies. The latter was used as loading control. The steady-state level of DRP1 protein is significantly increased in Pt.3 fibroblasts. Values in the graph are given as the mean ± *SD* ($n = 4$–5); *$p < 0.05$. SD: standard deviation; VDAC: voltage-dependent anion channels

3.5 Immunostaining and imaging in cultured fibroblasts

Because of the pivotal role of DRP1 on dynamics of mitochondria and peroxisomes, we performed morphological studies on patients' fibroblasts. We used the antibody TOMM20 in fixed cells (for Pt.1, Pt.2, and Pt.3) or Mitotracker red in living cells (for Pt.4 and Pt.5), both specific for mitochondrial staining. In normal glucose medium, we observed an increased filamentous network in mutant fibroblasts of all patients (Figure S8, left panels), although Pt.1 displayed a mixed population in which hyperfused mitochondria are associated with swollen and rod-shaped mitochondria and Pt.5 showed dot-shaped mitochondria (Figure 6, left panel). In galactose-supplemented medium, a condition that forces cells to use the oxidative phosphorylation for ATP production and usually causes elongation of mitochondrial network in control cells, the mitochondrial network of *DNM1L*-mutant fibroblasts showed a lower tendency to fuse associated with a more disorganized network and an altered mitochondria morphology, with swollen, dots, rings, and "chain-like" structures (Figure 6, right panels; Figure S8 right panels).

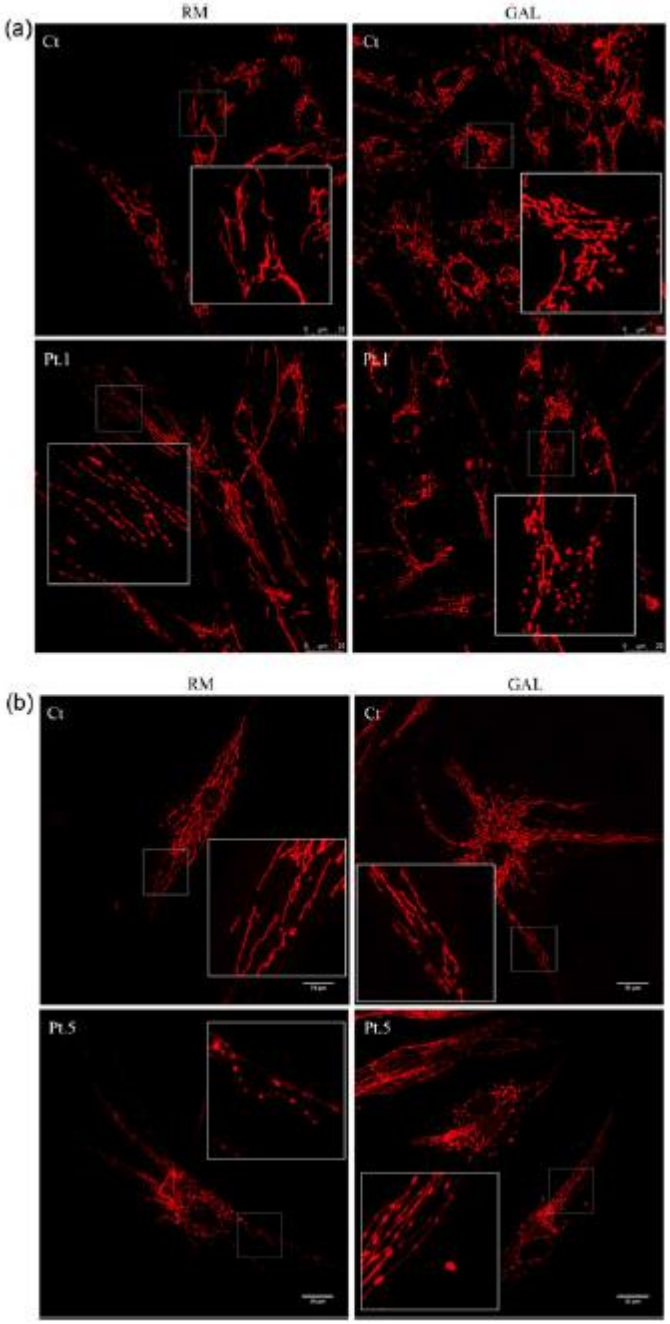

Figure 6

Characterization of the mitochondrial network: analysis by fluorescence microscopy. (a,b) Representative images of mitochondrial morphology in fibroblasts from Pt.1,

Pt.5, and Ct, grown either in glucose or galactose medium. In glucose medium (left panel) patients' fibroblasts are characterized by a mixed population with hyperfused swollen and rod-shaped mitochondria; in galactose medium (right panel) the mitochondrial network of patients' fibroblasts showed a lower tendency to fuse associated with a more disorganized network and an altered mitochondria morphology, with swollen, dots, rings, and "chain-like" structures. (Scale bar = 25 μm). Ct: controls [Color figure can be viewed at wileyonlinelibrary.com]

For the immunovisualization of peroxisomes, we used an antibody against a peroxisomal protein, PMP70. In contrast with the highly diffused punctuated staining present in control cells, in Pt.4 and Pt.5 cytoplasm (Figure 7) we observed organelles longer, larger, and less uniformly distributed into the cytoplasm; although in a minor extent, peroxisomal alterations were present also in Pt.1, Pt.2 and Pt.3 (Figure S9). Accordingly, the morphometric analysis showed decreased form factors for circularity in the patient's cells compared with controls, with a significant reduction for Pt.4 and Pt.5 (Figure 7; Figure S9).

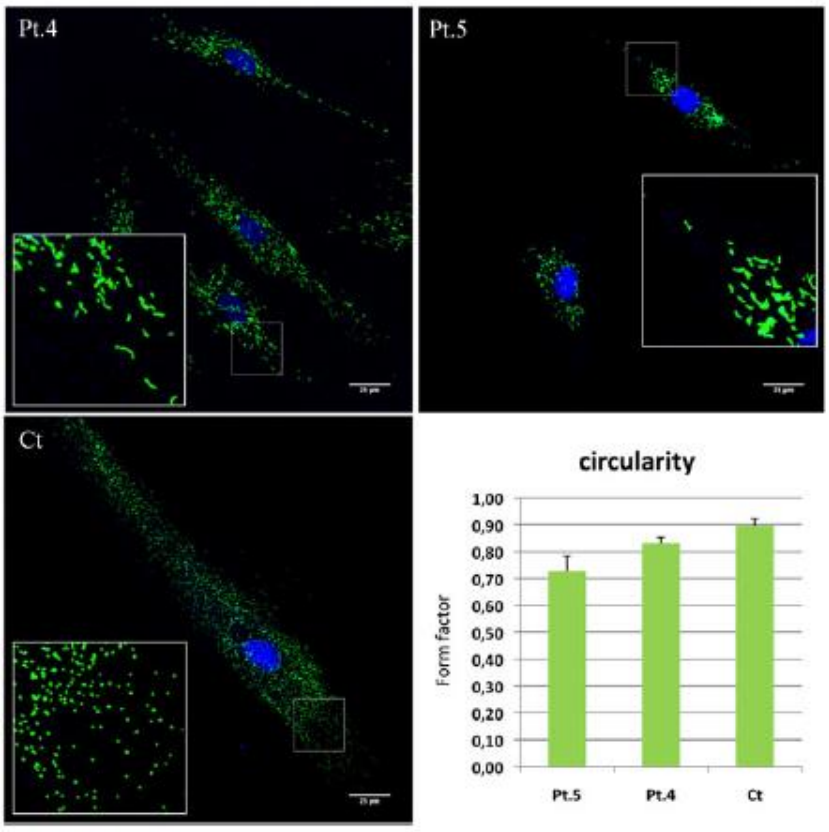

Figure 7

Characterization of the peroxisomal network: analysis by fluorescence microscopy. Immunofluorescence staining with the anti-PMP70 antibody of fibroblasts from Ct, Pt.4, and Pt.5. Patients' fibroblasts displayed organelles longer, larger, and less uniformly distributed into cytoplasm compared with control (Scale bar = 25 μm). A form factor ("circularity") value of 1.0 indicates a perfect circle; values approaching to 0.0 indicate increasingly elongated shapes. Ct: controls [Color figure can be viewed at wileyonlinelibrary.com]

3.6 Functional studies in yeast

The deleterious effect of the p.Arg403Cys substitution was already experimentally demonstrated (Fahrner et al., 2016). To assess the pathogenic role of the other identified *DNM1L* variants as well as to compare the effects of different substitutions on the same amino acid (p.Gly362), we

performed complementation studies in a *Saccharomyces cerevisiae* strain lacking *DNM1*, hereafter referred to as *Δdnm1. DNM1* is the yeast orthologue of human *DNM1L;* the amino acid residues corresponding to p.Gly223Val, p.Gly362Asp, p.Gly362Ser, and p.Ile512Thr variants are conserved between the two species, being in yeast p.Gly252, p.Gly397, p.Ile543, whereas human p.Phe370 is not conserved, being p.Tyr405 in yeast. The *dnm1*Δ strain was transformed either with the wt *DNM1*, the $dnm1^{G252V}$, $dnm1^{G397D}$, $dnm1^{G397S}$, or $dnm1^{I543T}$ mutant alleles, under the endogenous *DNM1* promoter, as well as with the empty plasmid. To test the possible effects on mitochondrial function, we first evaluated the oxidative growth by spot assay analysis on medium supplemented with either glucose or ethanol or glycerol. The oxidative growth of the $dnm1^{G397D}$ and the $dnm1^{G397S}$ mutant strains was partially affected compared with the *DNM1* wild-type strain, especially on ethanol, whereas the growth of the $dnm1^{G252V}$ was similar to the strain *dnm1Δ*; on the contrary, the growth of the $dnmI^{I543T}$ mutant was unaffected (Figure 8a). To further investigate the OXPHOS defect, the oxygen consumption was measured and according to the growth phenotype, the oxygen consumption rate of the $dnm1^{G397D}$ and of the $dnm1^{G397S}$ mutants was respectively 30% and 20% lower than that of the wild-type strain, whereas the oxygen consumption rate of $dnm1^{G252V}$ and of the *dnm1* null strain was decreased by 60%; also the $dnmI^{I543T}$ mutant showed a slight though significant reduction of respiratory

activity (Figure 8b). In yeast, mutations in several nuclear genes encoding for proteins involved in mitochondrial dynamics, such as *MGM1* (the homologous gene of human *OPA1*; Nolli et al., 2015; Sesaki, Southard, Yaffe, & Jensen, 2003), *FZO1* (h*MFN1*; Rapaport, Brunner, Neupert, & Westermann, 1998), and *DNM1* itself (Bernhardt, M¨uller, Reichert, & Osiewacz, 2015), affect mtDNA stability. Although the patients reported in this study did not show any mtDNA defects, we measured the frequency of *petite*, that is clones that are unable to grow on an oxidative carbon source due to large deletions or lack of mtDNA, in order to further highlight the defect of mutant Dnm1 proteins. Deletion of *DNM1* as well as the expression of $dnm1^{G252V}$ resulted in a significant increase of *petite* frequency (~50%) compared with the wild-type strain, whereas expression of $dnm1^{G397D}$ or $dnm1^{G397S}$ partially decreased mtDNA stability (~40% and ~25%, respectively), which is, however, lower than the *DNM1* wild-type strain or the $dnm1^{I543T}$ (~8% and ~15%, respectively; Figure 8c).

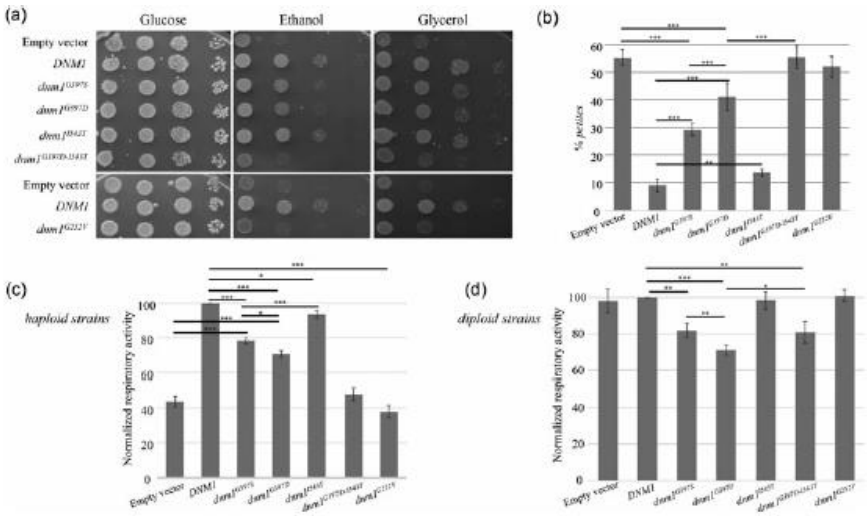

Figure 8

Functional studies in yeast. (a) Phenotypic analysis of haploid strains through the spot assay. Serial cell dilutions (5×10^4, 5×10^3, 5×10^2, and 5×10^1 cells/spot) of *dnm1Δ* haploid strain transformed with *DNM1* wild-type (wt) or mutant alleles were spotted on SC medium supplemented with either 2% glucose or 2% glycerol. Pictures were taken after a 3-day incubation at 37°C. (b) *Petite* frequency of *dnm1Δ* haploid strain transformed with *DNM1* wt or mutant alleles. Values are means of six to eight independent clones ± *SD*. $^{**}p < 0.01$ and $^{***}p < 0.001$ in an ANOVA test followed by the Bonferroni's test. (c) Respiratory activity of *dnm1Δ* haploid strain transformed with *DNM1* wt or mutant alleles. Values are means ± *SD* of experiments on five clones and have been normalized to the respiratory activity of the *DNM1* wt strain. $^{*}p < 0.05$ and $^{***}p < 0.001$ using ANOVA with post-hoc Bonferroni's test. (d) Respiratory activity of *DNM1*/*dnm1Δ* diploid strain transformed with *DNM1* wt or mutant alleles. Values are means ± *SD* of experiments on five clones and have been normalized to the respiratory activity of the *DNM1* wt strain. $^{*}p < 0.05$ and $^{***}p < 0.001$ using ANOVA with post-hoc Bonferroni's test. ANOVA: analysis of variance; SC: synthetic complete; SD: standard deviation

Altogether these results validated the pathogenicity of the mutations Gly252Val, Gly397Asp, and Gly397Ser, showing also that substitution of Gly397 with aspartate is more deleterious than substitution with serine. The amino acid change Ile543Thr slightly affects the activity of the protein as well, being the respiratory activity and the *petite* frequency slightly altered compared with *DNM1* wild type. Since the variant Ile512Thr was present in the patient in *cis* with the Gly362Asp, we also constructed a yeast mutant allele carrying both the corresponding variants. Interestingly, the *dnm1*$^{G397D\,I543T}$ strain showed a more severe phenotype than the strain carrying the sole mutation Gly397Asp; in fact, the oxidative growth, the respiratory activity, and the mtDNA mutability become similar to

that of the null mutant suggesting that Ile543Thr is a phenotypic modifier (Figure 8a–c).

Finally, we tested whether the mutations have a dominant or recessive effect by measuring the oxygen consumption rate of the diploid hemizygous *DNM1*/*dnm1Δ* strain transformed with the plasmid having mutant alleles or with the empty vector. The respiratory activity of the heteroallelic strains *DNM1*/*dnm1*^{G397D}, *DNM1* /*dnm1*^{G397S}, and *DNM1*/*dnm1*$^{G397D\,J543T}$, but not that of *DNM1*/*dnm1*^{G252V} and *DNM1*/*dnm1*^{I543T}, was lower compared with the hemizygous strain *DNM1*/*dnm1Δ*. This indicates that Gly397Asp and Gly397Ser have a partial dominant-negative effect, whereas Ile543Thr and, quite unexpectedly, Gly252Val act as recessive mutations (Figure 8d), at best concerning the effect on oxygen consumption. To better deepen this point, we investigated in the heteroallelic strain *DNM1*/*dnm1*^{G252V} another phenotype, that is the *petite* frequency, based on the observation that the mutation Lys41Ala, generally recognized as dominant (Frank et al., 2001), increased the *petite* frequency in a heteroallelic diploid mutant strain (Nasca et al., 2016). The significant increase (3.3-fold ± 0.6; $p < 0.001$) of the *petite* frequency observed, compared with the hemizygous strain, suggests that also the Gly252Val mutation behaves as partially dominant, at least for this specific phenotype.

3.7 Structural analysis

All the identified missense mutations affect sites, which are totally or highly conserved sites among species (Figure 9a) and

imply replacements with residues presenting physicochemical properties that differ significantly from those of the wild-type amino acids. The p.Gly223Val mutation causes the substitution of the tiny and flexible glycine with a hydrophobic valine, which is expected to induce structural changes in the GTPase domain near residues 215 to 221 important for the binding of GTP (Figure 9b). The p.Gly362Asp and p.Gly362Ser mutations replace the tiny glycine with the anionic aspartic acid or with the hydrophilic serine, respectively, modifying the N-terminus of an α-helix also exploited in dynamin tetramerization (Figure 9c), as inferred by homology of dynamin-1 like with dynamin-3, another member of the dynamin family. The p.Phe370Cys mutation affects the large and hydrophobic phenylalanine that is important for the stability of monomers and for the tetramer formation (Figure 9d). In fact, Phe370 is involved in several intramolecular hydrophobic interactions, which are disrupted by the replacement with the small cysteine and the latter might also become engaged in disulfide bond formation with other cysteines located nearby (Figure S10). The p.Arg403Cys mutation implies the change of the cationic arginine into the tiny and neutral cysteine at sites that contribute to the core of tetrameric dynamin assembly (Figure 9e), as previously reported (Fahrner et al., 2016).

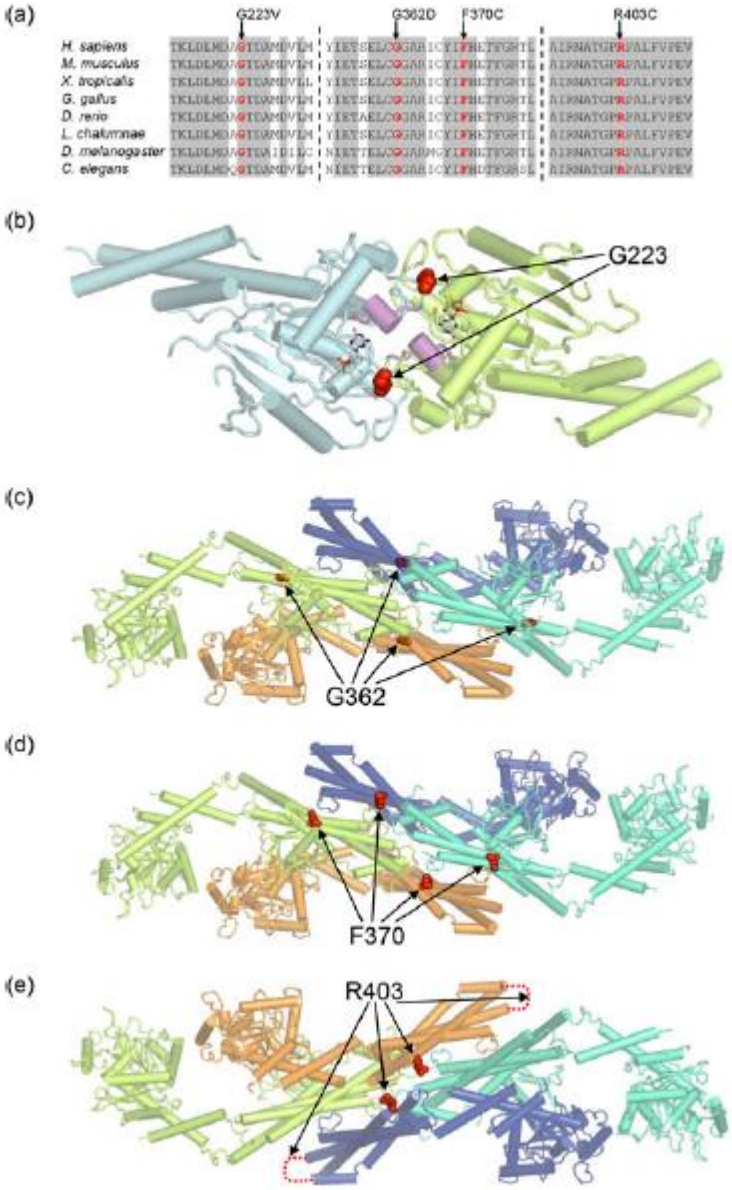

Figure 9

Conservation and structural mapping of residues affected by the missense mutations G223V, G362D, F370C, and R403C. (a) multiple sequence alignment among species (invariant columns are grayed). (b) mapping of G223 on the crystal structure of a dimeric human dynamin-1-like protein (PDB 3W6O; residues 215–221, colored in magenta, are important for GTP binding; the cocrystallized nucleotide analog is

shown as sticks). Mapping of G362 (c), F370 (d), and R403 (e) on dynamin tetramer (PDB 5A3F). The red dotted lines indicate the disordered regions in which R403 is hosted in two of the four dynamin monomers. The different dynamic chains are in distinct colors. Amino acid numbering is made according to the isoform 1 of dynamin-1-like protein (NP_036192.2). GTP: guanosine triphosphate; PDB: Protein Data Bank [Color figure can be viewed at wileyonlinelibrary.com]

4 DISCUSSION

Here we described five patients with epileptic encephalopathy and de novo dominant missense mutations in *DNM1L*. We identified two novel variants in Pt.1 and Pt.3, whereas in Pt.2 and Pt.5 we found two variants that were reported so far (Fahrner et al., 2016; Sheffer et al., 2015). Pt.4 showed two variants on the same allele; the first was inherited from the mother and the second, recently described as a de novo mutation (Vanstone et al., 2016), was present in the mother's blood DNA at a low level (~5%), suggesting maternal mosaicism. We observed a quite strict genotype–phenotype correlation, with overlapping clinical presentations between Pt. 2, Pt. 4, Pt. 5 and the previously described patients harboring the same mutation (reported by Fahrner et al., 2016; Vanstone et al., 2016; and Sheffer et al., 2015 respectively).

After the first description of Waterham et al. (2007), there have been increasing reports in the last 2 years on patients, frequently sporadic, with de novo dominant-negative *DNM1L* mutations who are affected by early onset encephalopathy with microcephaly and drug-resistant seizures, progressive brain atrophy or abnormal brain development, optic atrophy, and occasionally persistent lactic acidemia. The degree of severity was broad, ranging from neonatal death to

prolonged survival (Chao et al., 2016; Fahrner et al., 2016; Sheffer et al., 2016; Vanstone et al., 2016; Zaha et al., 2016). A similar spectrum of clinical presentations has been also reported for *DNM1L*-recessive mutations (Nasca et al., 2016; Yoon et al., 2016). More recently, dominant mutations in *DNM1L* have been also related to isolated optic atrophy in three large families (Gerber et al., 2017).

The patients described here presented clinical manifestations quite similar to previously reported *DNM1L* cases manifesting early onset encephalopathy and characterized by development delay, together with episodes of SRSE, progressive cerebral atrophy, and transitory abnormal T2 hyperintensities and DTI restriction areas at MRI. In addition, elevated lactate level in serum was detected in Pt.2 and Pt.4, whereas lactate was normal in other patients. There are no clues about a peroxisomal dysfunction: when available (Pts. 4 and 5), plasma phytanic and pristanic acids concentrations, typically increased in patients with peroxisomal disorders (ten Brink, et al., 1992), were normal. Excluding the 16 patients with mild nonsyndromic optic atrophy, 6 patients of the 12 reported in literature showing similar clinical manifestations died in early-childhood (Chao et al., 2016; Waterham et al., 2007; Yoon et al., 2016; Zaha et al., 2016), and in four cases death occurred in the first year of age (Chao et al., 2016; Waterham et al., 2007; Yoon et al., 2016). It is not clear why some mutations give rise to premature death. The cause of the early-childhood death cannot be attributed to the mode of transmission, since early

death occurred both in patients with a dominant de novo mutation and in patients with recessive mutations (Chao et al., 2016; Waterham et al., 2007; Yoon et al., 2016; Zaha et al., 2016), neither to the residual amount of DRP1, given that fibroblasts from a patient with long survival showed a strong reduction of the total amount of the protein (Nasca et al., 2016). In the cohort of our patients, only the Pt.4 died at 6 years of age, differently from the one already described with the same p.Gly362Asp mutation who showed prolonged survival (Vanstone et al., 2016). However, Pt.4 carried also a second, maternally inherited heterozygous *DNM1L* variant (p.Ile512Thr), which may explain the different degree of severity in these two cases; indeed, the yeast studies suggested that the p.Ile512Thr change can be a modifier, able to worsen the phenotype associated with the p.Gly362Asp mutation.

Clinical signs of a severe epileptic encephalopathy with frequent episodes of SRSE and EEG abnormalities do not seem to be peculiar signs of this condition. Noteworthy, MRI abnormalities, and particularly the detection of transitory abnormal T2 hyperintensities and DTI restriction areas in the basal ganglia or the cortical areas are quite characteristic for *DNM1L* encephalopathy, although may rarely occur in other conditions such as MELAS or may represent an unspecific sign due to status epilepticus.

Probably the most peculiar finding in the cohort of our patients is the muscle histology/histochemistry showing core like areas using oxidative enzyme staining for COX and SDH, which

suggest an abnormal distribution of mitochondria in the muscle tissue. We found this pattern in all the examined muscle biopsies. Notably, reduced mitochondrial numbers and size and a paucity of mitochondria between sarcomeres in muscle have been noticed in transgenic Drosophila models expressing *DNM1L* variants identified in patients (Chao et al., 2016). Areas devoted of mitochondria have not been found in muscle biopsies of *OPA1* mutated patients that can sometimes show ragged red-COX negative fibers correlated with mitochondrial DNA instability (Amati-Bonneau et al., 2008). In the investigated patient with recessive OPA1 defect, although COX-negative fibers were not detected, we confirmed multiple deletions. Contrariwise, in muscle samples of *DNM1L* patients, the impairment of the mitochondrial network distribution was not associated with mitochondrial DNA instability.

The primary sequence of DRP1 consists of four conserved regions: the GTPase domain, the middle, the variable, and the GTPase effector domain (GED). Revising all the cases published, we noted that mutations that fall into the GTPase domain are typically associated with a recessive trait (except for the cases not associated with early encephalopathy, reported by Gerber et al., 2017), while mutations that fall into the middle domain are expressed as dominant-negative. Here, we report on four mutations falling in the middle domain, which we suggest having a dominant-negative effect on oligomers stability. In fact, we likely exclude DRP1 haploinsufficiency, as we observed a normal or significant increase of protein level by

WB analysis. Moreover, we excluded a gain of function effect on the physiological activity of DRP1 because we did not observe an increase in mitochondrial fission; on the contrary patient' fibroblasts showed hyperfused mitochondria. In only one of our patients (Pt.1) we identified a mutation (p.Gly223Val) which falls into the GTPase domain, even if the nucleotide change is located at the boundary between the GTPase and the central domain. The yeast model indicated that it acts with a dominant-negative effect but probably through a mechanism different from the other mutations located in the middle domain. It is possible that the same mechanism may explain also the cases with isolated optic atrophy, harboring dominant mutations in the GTPase domain (Gerber et al., 2017); nevertheless, a gain of function effect has been postulated as well (Wangler et al., 2018).

In the cytosol, DRP1 exists as a mixture of dimers and tetramers (Macdonald et al., 2014) and, when recruited to mitochondria via receptors anchored to the mitochondrial outer membrane (Losón, Song, Chen, & Chan, 2013), hydrolysis of GTP triggers conformational changes in DRP1 oligomers that generate the mechanical force to promote mitochondrial membrane scission (Francy, Alvarez, Zhou, Ramachandran, & Mears, 2015). The middle and GED domains promote DRP1 self-assembly, required for mitochondrial fission (Chang et al., 2010), while the variable domain seems to act as a negative regulator of DRP1 self-assembly (Francy et al., 2015).

Structural analysis revealed hypothetical mechanisms of protein impairment and malfunctioning for all the missense mutations presented in this study. Specifically, p.Gly223Val substitution seems to hamper the binding of GTP, hence the GTPase activity, the p.Gly362Asp mutation impairs the tetramer formation, as previously described by the two-hybrid experiment of Fahrner et al. (2016). Finally, also the p.Phe370Cys could influence protein oligomerization. In the patient fibroblasts with this mutation we observed a significant increase of DRP1 level probably due to its altered degradation, in fact, this amino acid change might cause disulfide-mediated abnormal multimerization. As matter of fact, in the protein structure the p.Phe370Cys mutation is located close to the mouse p.Cys452Phe substitution (p.Cys446Phe in the human protein), which has been demonstrated to cause an increase in higher-ordered assembly with supranormal GTPase function and failure of oligomer disassembly (Cahill et al., 2016).

At the cellular level we found the presence of hyperfused, swollen, and rod-shaped mitochondria in fibroblasts from all our patients, as reported for others *DNM1L* mutations (Fahrner et al., 2016; Gerber et al., 2017; Ladds et al., 2018; Nasca et al., 2016; Ryan et al., 2018; Sheffer et al., 2016; Vanstone et al., 2016; Waterham et al., 2007; Zaha et al., 2016). The morphological anomalies were not associated with overt OXPHOS dysfunctions, in fact, we did not observe the reduction of OXPHOS subunits levels and cellular respiration was unaffected. Likewise, the activities of the medical research

council (MRC) complexes in muscle were normal in the four patients of our cohort for whom muscle biopsy was obtained. The same findings have been reported in most of the *DNM1L*-mutant cases; in only a few patients slightly decreased activity of Complex IV, altered ATP production or impaired oxygen consumption were observed in fibroblasts (Nasca et al., 2016; Sheffer et al., 2016), or in muscle (Ladds et al., 2018). Surprisingly, histochemistry of Pt.1, Pt.2, Pt.3, and Pt.4 showed scattered fibers with a partial reduction of COX and SDH stainings, and with aspects of the polymorphic core like areas. Moreover, we also identified areas with reduced immunoreactivity to mitochondrial signal, suggesting an abnormal distribution of organelles. Accordingly, the EM examination showed a few fields, mainly located at the center of the fibers, devoid of mitochondria. In these areas, the sarcomeric organization was quite normal, though the Z lines were often absent (Figure S3) as reported in selenoprotein-related diseases (Cagliani et al., 2011), or somewhat irregular (Figures S5 and S6). Interestingly, at EM the areas devoid of mitochondria did not show any major misalignment such as streaming of the Z bands, that is well known to occur in the cores which are typically devoid of oxidative stains in RYR1 related myopathies (Monnier et al., 2000). This is a new finding and can be considered as a key aspect suggesting mutations in *DNM1L*. In fact, no peculiar histochemical alterations have been reported so far in the muscle biopsies of *DNM1L* patients. The histological features of muscle biopsies associated with the

de novo dominant mutation p.Arg403Cys, very recently reported (Ladds et al., 2018), are often found in other mitochondrial diseases and cannot be considered specific for DRP1 impairment.

In addition to mitochondrial fission, DRP1 is also implicated in the division of peroxisomes (Schrader et al., 2016); to this purpose we investigated peroxisomal morphology and in fibroblasts from Pt. 4 and Pt. 5 we observed organelles significantly longer, larger, and less uniformly distributed into cytoplasm, in contrast with the highly diffused punctuated staining present in control cells; the same condition has been described for other patients with mutations in *DNM1L* (Nasca et al., 2016; Waterham et al., 2007; Zaha et al., 2016) and in transgenic Drosophila model expressing a mutant form of *DNM1L* (Chao et al., 2016).

It is not clear why defects of mitochondrial and peroxisomal fission affect predominantly the nervous system. It was demonstrated that DRP1 is required for embryonic and brain development in mice (Ishihara et al., 2009; Wakabayashi et al., 2009). Particularly, DRP1 knockout (KO) caused alteration of mitochondrial morphology and proliferation of embryonic Purkinje cells, suggesting that their development depends highly on mitochondrial division (Wakabayashi et al., 2009). Subsequently, it has been demonstrated that loss of DRP1 led to the accumulation of oxidative damage, decreased respiratory function, and neurodegeneration also in postmitotic Purkinje cells, while DRP1 KO Mouse Embryonic Fibroblasts (MEFs)

maintain normal respiration and ATP levels (Kageyama et al., 2012). Given that postmitotic neurons contain high reactive oxygen species levels and do not proliferate, the mitochondrial quality control mechanism is essential, while in MEFs, which actively proliferate, mitochondria are produced continuously during cell proliferation and therefore the effect of any oxidative damage may be diluted by the newly formed mitochondria. Moreover, a previous study has shown that the delivery of mitochondria into dendritic protrusions in response to synaptic stimulation is strictly dependent on an efficient mitochondrial transport, that requires DRP1-dependent division (Li, Okamoto, Hayashi, & Sheng, 2004); altered mitochondrial distribution likely affects the function and formation of synapses as well as the survival of neurons (Sheng & Cai, 2012; Sheng, 2017). Therefore, the retained DRP1 activity is likely sufficient for organs with limited mitochondrial remodeling, while impaired DRP1 activity could strongly affect the nervous system, thus explaining the involvement of DRP1 in many neurodegenerative disorders.

References

- Alexiou, A., Nizami, B., Khan, F. I., Soursou, G., Vairaktarakis, C., Chatzichronis, S., … Ashraf, G. M. (2018). Mitochondrial dynamics and proteins related to neurodegenerative diseases. *Current Protein & Peptide Science*, **19**, 850– 857.

- Amati-Bonneau, P., Valentino, M. L., Reynier, P., Gallardo, M. E., Bornstein, B., Boissière, A., … Carelli, V. (2008). OPA1 mutations induce mitochondrial DNA instability and optic atrophy 'plus' phenotypes. *Brain: A Journal of Neurology*, **131**, 338– 351.
- Ardissone, A., Tonduti, D., Legati, A., Lamantea, E., Barone, R., Dorboz, I., … Ghezzi, D. (2018). KARS-related diseases: progressive leukoencephalopathy with brainstem and spinal cord calcifications as new phenotype and a review of literature. *Orphanet Journal of Rare Diseases*, **13**, 45.
- Bartsakoulia, M, Pyle, A, Troncoso-Chandía, D, Vial-Brizzi, J, Paz-Fiblas, MV, Duff, J, … Horvath, R (2018). A novel mechanism causing imbalance of mitochondrial fusion and fission in human myopathies. *Human Molecular Genetics*, **27**, 1186– 1195.
- Baruffini, E., Ferrero, I., & Foury, F. (2010). In vivo analysis of mtDNA replication defects in yeast. *Methods*, **51**, 426– 436.
- Bernhardt, D., Müller, M., Reichert, A. S., & Osiewacz, H. D. (2015). Simultaneous impairment of mitochondrial fission and fusion reduces mitophagy and shortens replicative lifespan. *Scientific Reports*, **5**, 7885.
- ten Brink, H. J., Schor, D. S., Kok, R. M., Poll-The, B. T., Wanders, R. J., & Jakobs, C. (1992). Phytanic acid alpha-oxidation: Accumulation of 2-hydroxyphytanic acid

and absence of 2-oxophytanic acid in plasma from patients with peroxisomal disorders. *Journal of Lipid Research*, **33**, 1449– 1457.

- Bugiani, M., Invernizzi, F., Alberio, S., Briem, E., Lamantea, E., Carrara, F., … Zeviani, M. (2004). Clinical and molecular findings in children with complex I deficiency. *Biochimica et Biophysica Acta/General Subjects*, **1659**, 136– 147.
- Cagliani, R., Fruguglietti, M. E., Berardinelli, A., D'Angelo, M. G., Prelle, A., Riva, S., … Comi, G. P. (2011). New molecular findings in congenital myopathies due to selenoprotein N gene mutations. *Journal of the Neurological Sciences*, **300**, 107– 113.
- Cahill, T. J., Leo, V., Kelly, M., Stockenhuber, A., Kennedy, N. W., Bao, L., … Ashrafian, H. (2016). Resistance of dynamin-related protein 1 oligomers to disassembly impairs mitophagy, resulting in myocardial inflammation and heart failure. *Journal of Biological Chemistry*, **291**, 25762.
- Chang, C. R., Manlandro, C. M., Arnoult, D., Stadler, J., Posey, A. E., Hill, R. B., & Blackstone, C. (2010). A lethal de novo mutation in the middle domain of the dynamin-related GTPase Drp1 impairs higher order assembly and mitochondrial division. *Journal of Biological Chemistry*, **285**, 32494– 32503.
- Chao, Y. H., Robak, L. A., Xia, F., Koenig, M. K., Adesina, A., Bacino, C. A., … Wangler, M. F. (2016). Missense

variants in the middle domain of DNM1L in cases of infantile encephalopathy alter peroxisomes and mitochondria when assayed in Drosophila. *Human Molecular Genetics*, **25**, 1846– 1856.

- Fahrner, J. A., Liu, R., Perry, M. S., Klein, J., & Chan, D. C. (2016). A novel de novo dominant negative mutation in DNM1L impairs mitochondrial fission and presents as childhood epileptic encephalopathy. *American journal of medical genetics. Part A*, **170**, 2002– 2011.
- Fattori, F., Fiorillo, C., Rodolico, C., Tasca, G., Verardo, M., Bellacchio, E., … D'Amico, A. (2018). Expanding the histopathological spectrum of CFL2-related myopathies. *Clinical Genetics*, **93**, 1234– 1239.
- Francy, C. A., Alvarez, F. J., Zhou, L., Ramachandran, R., & Mears, J. A. (2015). The mechanoenzymatic core of dynamin-related protein 1 comprises the minimal machinery required for membrane constriction. *Journal of Biological Chemistry*, **290**, 11692– 11703.
- Frank, S., Gaume, B., Bergmann-Leitner, E. S., LeitnerWW, Robert, E. G., Catez, F., … Youle, R. J. (2001). The role of dynamin-related protein 1, amediator ofmitochondrial fission, in apoptosis. *Developmental Cell*, **1**, 515– 525.
- Gerber, S., Charif, M., Chevrollier, A., Chaumette, T., Angebault, C., Kane, M. S., … Lenaers, G. (2017). Mutations in DNM1L, as in OPA1, result in dominant optic atrophy despite opposite effectson

mitochondrial fusion and fission. *Brain: A Journal of Neurology*, **140**, 2586– 2596.

- Gietz, R. D., & Woods, R. A. (2002). Transformation of yeast by the LiAc/SS carrier DNA/Peg method. *Methods in Enzymology*, **350**, 87– 96.
- Goffrini, P., Ercolino, T., Panizza, E., Giachè, V., Cavone, L., Chiarugi, A., … Mannelli, M. (2009). Functional study in a yeast model of a novel succinate dehydrogenase subunit B gene germline missense mutation (C191Y) diagnosed in a patient affected by a glomus tumor. *Human Molecular Genetics*, **18**, 1860– 1868.
- Invernizzi, F., D'Amato, I., Jensen, P. B., Ravaglia, S., Zeviani, M., & Tiranti, V. (2012). Microscale oxygraphy reveals OXPHOS impairment in MRC mutant cells. *Mitochondrion*, **12**, 328– 335.
- Ishihara, N., Nomura, M., Jofuku, A., Kato, H., Suzuki, S. O., Masuda, K., … Mihara, K. (2009). Mitochondrial fission factor Drp1 is essential for embryonic development and synapse formation in mice. *Nature Cell Biology*, **11**, 958– 966.
- Kageyama, Y., Zhang, Z., Roda, R., Fukaya, M., Wakabayashi, J., Wakabayashi, N., … Sesaki, H. (2012). Mitochondrial division ensures the survival of postmitotic neurons by suppressing oxidative damage. *Journal of Cell Biology*, **197**, 535– 551.
- Kaiser, C., Michaelis, S., & Mitchell, A. (1994). *Methods in yeast genetics : A cold spring harbor laboratory course*

manual, Cold Spring Harbor, NY: Cold Spring Harbor Laboratory Press.

- Kim, D. I., Lee, K. H., Oh, J. Y., Kim, J. S., & Han, H. J. (2017). Relationship between β-Amyloid and mitochondrial dynamics. *Cellular and Molecular Neurobiology*, **37**, 955– 968.
- Koch, J., Feichtinger, R. G., Freisinger, P., Pies, M., Schr¨odl, F., Iuso, A., … Haack, T. B. (2016). Disturbed mitochondrial and peroxisomal dynamics due to loss of MFF causes Leigh-like encephalopathy, optic atrophy and peripheral neuropathy. *Journal of Medical Genetics*, **53**, 270– 278.
- Ladds, E., Whitney, A., Dombi, E., Hofer, M., Anand, G., Harrison, V., … Poulton, J. (2018). De novo DNM1L mutation associated with mitochondrial epilepsy syndrome with fever sensitivity. *Neurology: Genetics*, **4**, e258.
- Lenaers, G., Hamel, C., Delettre, C., Amati-Bonneau, P., Procaccio, V., Bonneau, D., … Milea, D. (2012). Dominant optic atrophy. *Orphanet Journal of Rare Diseases*, **7**, 46.
- Li, Z., Okamoto, K., Hayashi, Y., & Sheng, M. (2004). The importance of dendritic mitochondria in the morphogenesis and plasticity of spines and synapses. *Cell*, **119**, 873– 887.
- Losón, O. C., Song, Z., Chen, H., & Chan, D. C. (2013). Fis1, Mff, MiD49, and MiD51 mediate Drp1

recruitment in mitochondrial fission. *Molecular Biology of the Cell*, **24**, 659– 667.

- Macdonald, P. J., Stepanyants, N., Mehrotra, N., Mears, J. A., Qi, X., Sesaki, H., & Ramachandran, R. (2014). A dimeric equilibrium intermediate nucleates Drp1 reassembly on mitochondrial membranes for fission. *Molecular Biology of the Cell*, **25**, 1905– 1915.
- Monnier, N., Romero, N. B., Lerale, J., Nivoche, Y., Qi, D., MacLennan, D. H., … Lunardi, J. (2000). An autosomal dominant congenital myopathy with cores and rods is associated with a neomutation in the RYR1 gene encoding the skeletal muscle ryanodine receptor. *Human Molecular Genetics*, **9**, 2599– 2608.
- Nasca, A., Legati, A., Baruffini, E., Nolli, C., Moroni, I., Ardissone, A., … Ghezzi, D. (2016). Biallelic mutations in DNM1L are associated with a slowly progressive infantile encephalopathy. *Human Mutation*, **37**, 898– 903.
- Nasca, A., Rizza, T., Doimo, M., Legati, A., Ciolfi, A., Diodato, D., … Niceta, M. (2017). Not only dominant, not only optic atrophy: Expanding the clinical spectrum associated with OPA1 mutations. *Orphanet Journal of Rare Diseases*, **12**(1), 89– 98.
- Nasca, A., Scotton, C., Zaharieva, I., Neri, M., Selvatici, R., Magnusson, O. T., … Phadke, R. (2017). Recessive mutations in MSTO1 cause mitochondrial dynamics

impairment, leading to myopathy and ataxia. *Human Mutation*, **38**(8), 970– 977.

- Nolli, C., Goffrini, P., Lazzaretti, M., Zanna, C., Vitale, R., Lodi, T., & Baruffini, E. (2015). Validation of a MGM1/OPA1 chimeric gene for functional analysis in yeast of mutations associated with dominant optic atrophy. *Mitochondrion*, **25**, 38– 48.
- Otsuga, D., Keegan, B. R., Brisch, E., Thatcher, J. W., Hermann, G. J., Bleazard, W., & Shaw, J. M. (1998). The dynamin-related GTPase, Dnm1p, controls mitochondrial morphology in yeast. *Journal of Cell Biology*, **143**, 333– 349.
- Pitts, K. R., McNiven, M. A., & Yoon, Y. (2004). Mitochondria-specific function of the dynamin family protein DLP1 is mediated by its C-terminal domains. *Journal of Biological Chemistry*, **279**, 50286– 50294.
- Pozo Devoto, V. M., & Falzone, T. L. (2017). Mitochondrial dynamics in Parkinson's disease: Role for α-synuclein? *Disease Models & Mechanisms*, **10**, 1075– 1087.
- Rapaport, D., Brunner, M., Neupert, W., & Westermann, B. (1998). Fzo1p is a mitochondrial outer membrane protein essential for the biogenesis of functional mitochondria in Saccharomyces cerevisiae. *Journal of Biological Chemistry*, **273**, 20150– 20155.

- Rizza, T., Vazquez-Memije, M. E., Meschini, M. C., Bianchi, M., Tozzi, G., Nesti, C., … Carrozzo, R. (2009). Assaying ATP synthesis in cultured cells: A valuable tool for the diagnosis of patients with mitochondrial disorders. *Biochemical and Biophysical Research Communications*, **383**, 58– 62.
- Ryan, C. S., Fine, A. L., Cohen, A. L., Schiltz, B. M., Renaud, D. L., Wirrell, E. C., … Payne, E. T. (2018). De novo DNM1L variant in a teenager with progressive paroxysmal dystonia and lethal super-refractory myoclonic status epilepticus. *Journal of Child Neurology*, **33**, 651– 658.
- Santel, A., & Fuller, M. T. (2001). Control of mitochondrial morphology by a human mitofusin. *Journal of Cell Science*, **114**, 867– 874.
- Schrader, M., Costello, J. L., Godinho, L. F., Azadi, A. S., & Islinger, M. (2016). Proliferation and fission of peroxisomes—An update. *Biochimica et Biophysica Acta/General Subjects*, **1863**, 971– 983.
- Sesaki, H., Southard, S. M., Yaffe, M. P., & Jensen, R. E. (2003). Mgm1p, a dynamin-related GTPase, is essential for fusionof themitochondrial outermembrane. *Molecular Biology of the Cell*, **14**, 2342– 2356.
- Shamseldin, H. E., Alshammari, M., Al-Sheddi, T., Salih, M. A., Alkhalidi, H., Kentab, A., … Alkuraya, F. S. (2012). Genomic analysis of mitochondrial diseases in

a consanguineous population reveals novel candidate disease genes. *Journal of Medical Genetics*, **49**, 234– 241.

- Sheffer, R., Douiev, L., Edvardson, S., Shaag, A., Tamimi, K., Soiferman, D., … Saada, A. (2016). Postnatal microcephaly and pain insensitivity due to a de novo heterozygous DNM1L mutation causing impaired mitochondrial fission and function. *American Journal of Medical Genetics Part A*, **170**, 1603– 1607.
- Sheng, Z. H. (2017). The interplay of axonal energy homeostasis and mitochondrial trafficking and anchoring. *Trends in Cell Biology*, **27**, 403– 416.
- Sheng, Z. H., & Cai, Q. (2012). Mitochondrial transport in neurons: Impact on synaptic homeostasis and neurodegeneration. *Nature Reviews Neuroscience*, **13**, 77– 93.
- Stuppia, G., Rizzo, F., Riboldi, G., Del Bo, R., Nizzardo, M., Simone, C., … Corti, S. (2015). MFN2-related neuropathies: Clinical features, molecular pathogenesis and therapeutic perspectives. *Journal of the Neurological Sciences*, **356**, 7– 18.
- Vanstone, J. R., Smith, A. M., McBride, S., Naas, T., Holcik, M., Antoun, G., & Lines, M. A. (2016). DNM1L-related mitochondrial fission defect presenting as refractory epilepsy. *European Journal of Human Genetics: EJHG*, **24**, 1084– 1088.

- Wakabayashi, J., Zhang, Z., Wakabayashi, N., Tamura, Y., Fukaya, M., Kensler, T. W., … Sesaki, H. (2009). The dynamin-related GTPase Drp1 is required for embryonic and brain development in mice. *Journal of Cell Biology*, **186**, 805– 816.
- Wangler, M. F., Assia Batzir, N., Robak, L. A., Koenig, M. K., Bacino, C. A., Scaglia, F., & Bellen, H. J. (2018). The expanding neurological phenotype of DNM1L-related disorders. *Brain: A Journal of Neurology*, **141**, e28.
- Waterham, H. R., Koster, J., van Roermund, C. W., Mooyer, P. A., Wanders, R. J., & Leonard, J. V. (2007). A lethal defect of mitochondrial and peroxisomal fission. *New England Journal of Medicine*, **356**, 1736– 1741.
- Yoon, G., Malam, Z., Paton, T., Marshall, C. R., Hyatt, E., Ivakine, Z., & Cohn, R. D. (2016). Lethal disorder of mitochondrial fission caused by mutations in DNM1L. *Journal of Pediatrics*, **171**, 313– 316.
- Youle, R. J., & van der Bliek, A. M. (2012). Mitochondrial fission, fusion, and stress. *Science*, **337**, 1062– 1065.
- Yu-Wai-Man, P., Griffiths, P. G., Gorman, G. S., Lourenco, C. M., Wright, A. F., Auer-Grumbach, M., & Chinnery, P. F. (2010). Multi-system neurological disease is common in patients with OPA1 mutations. *Brain: A Journal of Neurology*, **133**, 771– 786.
- Zaha, K., Matsumoto, H., Itoh, M., Saitsu, H., Kato, K., Kato, M., & Nonoyama, S. (2016). DNM1L-related

encephalopathy in infancy with Leigh syndrome-like phenotype and suppression-burst. *Clinical Genetics*, **90**, 472– 474.

- Zanna, C., Ghelli, A., Porcelli, A. M., Karbowski, M., Youle, R. J., Schimpf, S., & Carelli, V. (2008). OPA1mutations associated with dominant optic atrophy impair oxidative phosphorylation and mitochondrial fusion. *Brain: A Journal of Neurology*, **131**, 352– 367.

Chapter 10

Mitochondrial diseases related to mtDNA in childhood: novel mutation in mtCO3 associated to familiar mitochondrial leukoencephalopathy espanding repertoire of mtDNA mutations in human diseases

The results of this study have been presented in the 10th International Meeting on Mitochondrial Pathology (Euromit) 2017 in Cologne (poster presentation).
The paper to submitt to peer review journal is in progress.

Introduction

Cytochrome c oxidase subunit III (COIII or MTCO3) is 1 of 3 mitochondrial DNA (mtDNA) encoded subunits of respiratory Complex IV. To date MTCO3 mutations have been associated to Leber optic atrophy (Johns et al 1993) myopathy with exercise intolerance (Keightley et al 1996, Horvath et al 2002) or infantile encephalopathy Leigh like (Tiranti et al 2000). Cerebral white matter involvement has been reported to mtDNA-related diseases with later onset as MELAS, MERRF and KSS; to date only few cases case have been reported in childhood (Hung et al 2007,Biancheri et al 2010). Infantile mitochondrial leukoencepahlopathy (ML) are related to nDNA

genes mutations and isolated complex deficiency . Recently, cavitated pattern has been reported in an increased number of nDNA genes associated to MMDS and Aars.

Case report

We report a 4 years-old boy, only child of unrelated parents of Italian origin. The mother suffered from unspecified lower limbs pain. Gestational hypertension was referred in last months of pregnancy, delivery was uneventful. In first day of life he presented metabolic acidosis associated to hyperlactetemia and hypoglycemia. Mild psychomotor and speech development delay was referred since firsts months: head control 4 months, sitting 7 months, autonomous gait 15-17 months, firsts word at 18 months.

Two brain MRI performed at 1 month and 10 months of age were reported normal. Elevated lactate levels in plasma and CSF were detected: 3,2 mmol/l (reference range <2.2 mmol/L) and 4,9 mmol/l(reference range <1.9) respectively.

He was admitted to our Institute at 2 ys 8 months.Neurological examination showed psychomotor and language delay, hypotonia . He underwent to instrumental exams. Retinopathy and sensorineural hypoacusia were disclosed by electroretinogram and auditory-evoked potential respectively. EEG revealed poor organization of cerebral activity, no abnormalities; fundus oculi and visual evoked potential were normal. Brain MRI disclosed sovratentorial cavited leukoencephalopathy (fig 1).

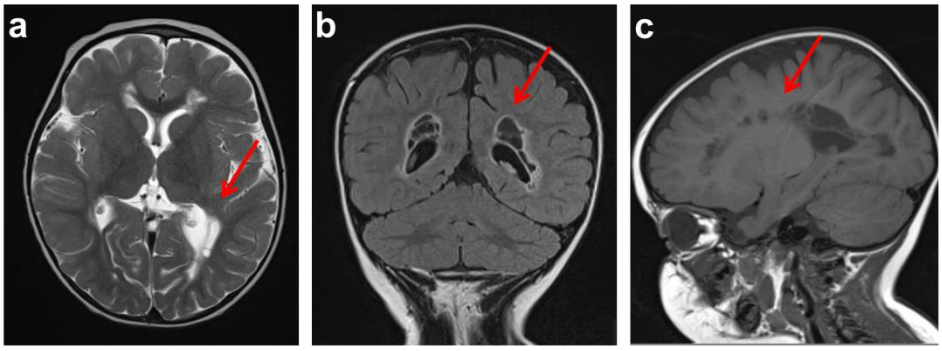

Fig. 1: Axial T2-wi (a), coronal FLAIR (b), sagittal T1-wi (c) images.Caviting leucoencephalopathy involving deep white matter (a, b) and corpus callosum (c)

Metabolic screening confirmed elevated plasmatic lactate levels 2231-2571 µmol/l (n.v. 580-2100) and pyruvate 145-171 µmol/l (n.v. 5-145); +lasmatic aminoacids level and Urinary organic acids were normal.

Mother's proband suffered from unspecified lower limbs pain. After son's evaluation, she underwent medical evaluation that disclosed hypomimia, rhinolalia, hypotonia and reduced deep tendon reflexes, peripheral sensory neuropathy and focal gliosis area at brain MRI (Fig 2), multievoked potential and plasmatic lactate were normal.

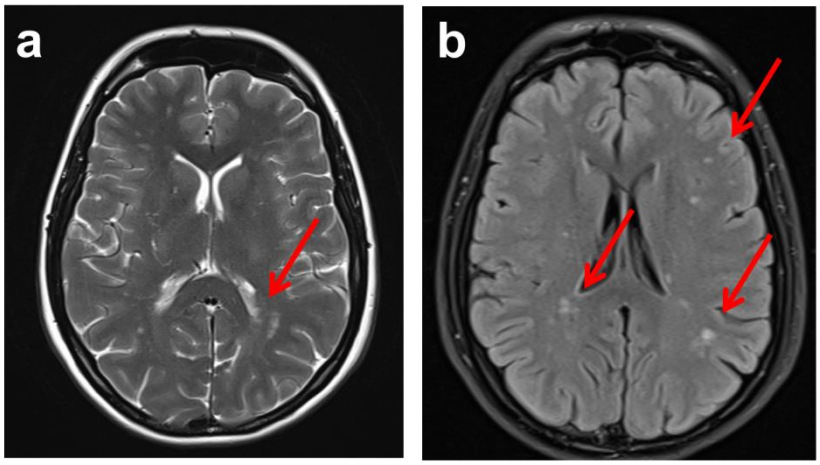

Fig. 2: Axial T2-wi (a) and axial FLAIR (b) images.
Focal gliosis area in sovratentorial white matter is present.

In the suspect of mitochondrial disease, muscle biopsy was performed in the proband. No histological or histoenzymatic alterations were found, however biochemical assays showed the isolated CIV deficiency (Fig. 3a). The same reduction was observed in fibroblasts cultured (Fig. 3b).

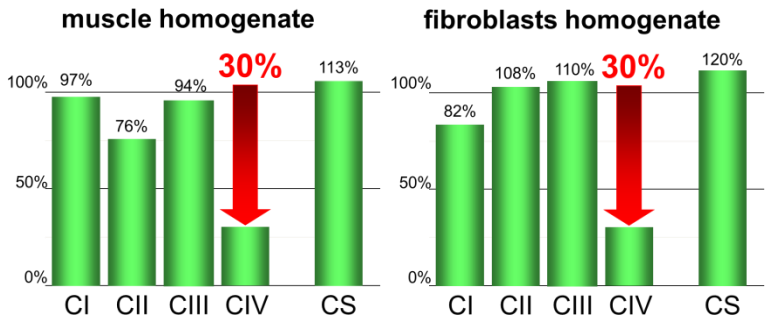

Fig. 3: Respiratory chain complexes analysis in muscle homogenate (a) and in fibroblasts homogenate (b). Isolated significant reduction of CIV activity was found in both tissues.

Screening of a panel of nuclear genes related to ML and defect of CIV performed by Next Generation Sequencing, using MiSeq

Illumina platform, were negative. Conversely, mtDNA sequence identified a novel alleged homoplasmic mutation in MTCO3 gene (Fig. 4a) m.9907G>A that causes the substitution of a Glycine in position 234 with an Aspartic acid (p.Gly121Asp) in the COIII protein. The mutation has never been reported, the p.Gly234Asp change scored very highly for likelihood to be deleterious according to ad-hoc softwares for pathogenicity prediction (Polyphen2, MutPred, SIFT and SNP&Go) and the amino-acid involved is highly conserved in the phylogenies (Fig 4b).

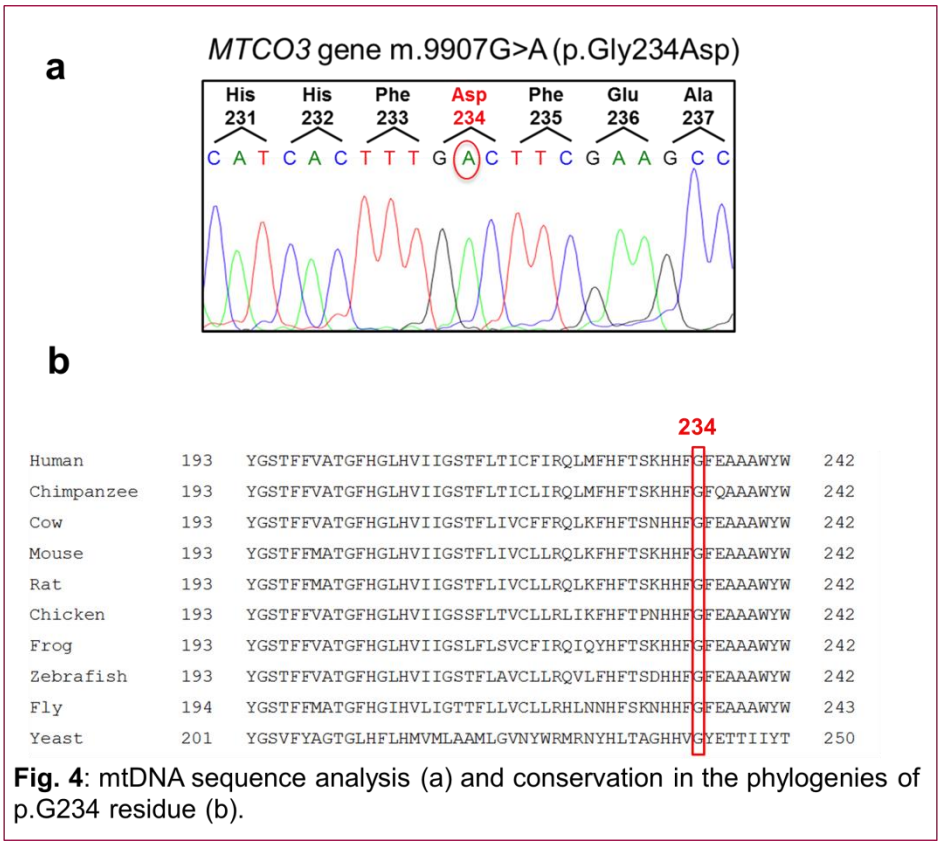

Fig. 4: mtDNA sequence analysis (a) and conservation in the phylogenies of p.G234 residue (b).

The mutation was quantified with MiSeq Illumina by Nextera XT protocol and resulted present nearly 100% of mtDNA molecules in muscle, urinary sediment, blood and fibroblast of patient 1 , while was was present in 69% of urinary sediment and 2% of peripheral leukocytes of his mother.

Blue-Native PAGE, Western Blot and immunodetection of CIV in three different cybrid clones (Cl. 1, 5 and 11) carrying the homoplasmic MTCO3 mutation from the patient were performed (fig 5).

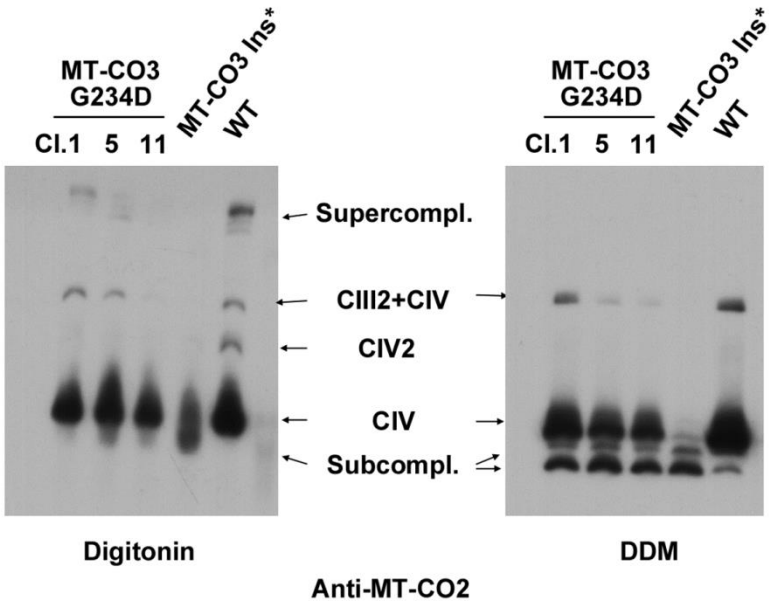

* Tiranti et al. (2000) Hum Mol Genet 9, 2733-2742.

Fig 5: Blue-Native PAGE, Western Blot and immunodetection of CIV in three different cybrid clones (Cl. 1, 5 and 11) carrying the homoplasmic MTCO3 mutation from the patient. The left panel shows the samples solubilised with the detergent digitonin and the right panel corresponds to the same cell lines solubilised with n-dodecyl ß-maltoside (DDM).

The amounts of fully assembled CIV are reduced and there is an accumulation of CIV assembly intermediates in the mutated cybrids. However, this defect is not as drastic as the one displayed by those carrying the m.9536_9537insC (p.Gln111Profs*113) mutation described in Tiranti et al. 2000

Discussion and conclusion

Here we described a novel mutation in mtCO3 associated to a caviting leukoencephaliopathy.

To date mtCO3 has been described in childhood only in a report associated to Leigh pattern: Tiranti el al described homoplasmic frameshift mutation in the CO3 gene, due to the insertion of an extra C at nucleotide position 9537 of mtDNA associated to infantile encephalopathy Leigh like. Since 4 years of age, the patient developed a progressive spastic paraparesis associated with ophthalmoparesis and moderate mental retardation. Instrumental exams disclosed severe lactic acidosis and Leigh-like lesions of putamina at MRI, In muscle and cultured finroblast a profound, isolated defect of COX (15% residual activity) was found.

Infantile mitochondrial leukoencepahlopathy (ML) are related to nDNA genes mutations and isolated complex deficiency (Melchionda L et al 2014, Dallabona et al 2017)

Recently, cavitated pattern has been reported in an increased number of nDNA genes associated to MMDS (invernizzi et al 2014, Torraco et al 2017).

This is the first report of caviting leukodistrophy associated to mtDNA. Our report expands phenotype related to CO3 mutations, lends further evidence to the expanding repertoire of mtDNA mutations in human diseases and suggests to look for variants in the mitochondrial genome when dealing with otherwise undetermined leukodystrophies of childhood.

References

- Johns, D. R., Neufeld, M. J.Cytochrome c oxidase mutations in Leber hereditary optic neuropathy.Biochem. Biophys. Res. Commun. 196: 810-815, 1993
- Keightley, J. A., Hoffbuhr, K. C., Burton, M. D., Salas, V. M., Johnston, W. S. W., Penn, A. M. W., Buist, N. R. M., Kennaway, N. G. A microdeletion in cytochrome c oxidase (COX) subunit III associated with COX deficiency and recurrent myoglobinuria. Nature Genet. 12: 410-416, 1996
- Horvath, R., Scharfe, C., Hoeltzenbein, M., Do, B. H., Schroder, C., Warzok, R., Vogelgesang, S., Lochmuller, H., Muller-Hocker, J., Gerbitz, K. D., Oefner, P. J., Jaksch, M. Childhood onset mitochondrial myopathy and lactic acidosis caused by a stop mutation in the mitochondrial cytochrome c oxidase III gene. J. Med. Genet. 39: 812-816, 2002
- Tiranti, V., Corona, P., Greco, M., Taanman, J.-W., Carrara, F., Lamantea, E., Nijtmans, L., Uziel, G., Zeviani, M. A

novel frameshift mutation of the mtDNA COIII gene leads to impaired assembly of cytochrome c oxidase in a patient affected by Leigh-like syndrome. Hum. Molec. Genet. 9: 2733-2742, 2000

- Hung PC, Wang HS. A previously undescribed leukodystrophy in Leigh syndrome associated with T9176C mutation of the mitochondrial ATPase 6 gene. Dev Med Child Neurol. 2007 Jan;49(1):65-7

- Melchionda L, Haack TB, Hardy S, Abbink TE, Fernandez-Vizarra E, Lamantea E, Marchet S, Morandi L, Moggio M, Carrozzo R, Torraco A, Diodato D, Strom TM, Meitinger T, Tekturk P, Yapici Z, Al-Murshedi F, Stevens R, Rodenburg RJ, Lamperti C, Ardissone A, Moroni I, Uziel G, Prokisch H, Taylor RW, Bertini E, van der Knaap MS, Ghezzi D, Zeviani M. Mutations in APOPT1, encoding a mitochondrial protein, cause cavitating leukoencephalopathy with cytochrome c oxidase deficiencyAmerican Journal of Human Genetics, 2014 Sep 4; 95(3):315-25

- C.Dallabona, E.M. Abbink, R.Carrozzo, A.Torraco, A.Legati,C.G.M. van Berkel, M.Niceta, T.Langella, D.Verrigni, T.Rizza, D.Diodato, F.Piemonte, E.Lamantea, M.Fang, J.Zhang, D.Martinelli, E.Bevivino, C.Dionisi-Vici, A.Vanderver, S.G. Philip, M.Kurian, C. Verma, S.Bijarnia-Mahay, S.Jacinto, F.Furtado, P.Accorsi, A.Ardissone, I.Moroni, I.Ferrero, M.Tartaglia, P.Goffrini, D.Ghezzi, M.S. van der Knaap, E. Bertini

- LYRM7 mutations cause a multifocal cavitating leukoencephalopathy with a distinct magnetic resonance imaging Brain. 2016 Mar;139(Pt 3):782-94
- -Invernizzi F, Ardissone A, Lamantea E, Garavaglia B, Zeviani M, Farina L, Ghezzi D and Moroni I,Cavitating leukoencephalopathy with multiple mitochondrial dysfunction syndrome and NFU1 mutations Frontiers genetics, 2014 Nov 20;5:412

Chapter 11

Leigh Syndrome: a study from the large cohort of 103 patients

The results of this study have been presented in the 8tth National Congress on Mitochondrial disease of Mitocon Onlus Association –Rome, May 2018 (oral communication).
The paper to submitt to peer review journal is in progress.

Introduction

Leigh syndrome (LS) , also known as subacute necrotizing encephalopathy, is a progressive neurodegenerative disorder associated with primary or secondary dysfunction of mitochondrial oxidative phosphorylation. Clinical manifestations include psychomotor regression or retardation and signs of brainstem dysfunction, such as respiratory disturbance, nystagmus, ophthalmoplegia, or dysphagia (Thorburn and Rahman 1993). Symptoms often start in infancy, and many patients do not survive into childhood (Sofou et al. 2014). LS was originally defined neuropathologically by bilateral necrotic lesions in the basal ganglia and/or brainstem that were found at autopsy (Leigh 1951). Such lesions can now be observed in vivo with brain magnetic resonance imaging (MRI) (Gropman 2013). LS is clinically diagnosed based on typical manifestations and neuroimaging, accompanied by an elevated lactate in the blood or cerebrospinal fluid (CSF). The clinical

diagnosis is followed by enzyme assays and genetic analysis to confirm the biochemical and molecular background (Baertling et al. 2014).

Numerous reports on the biochemical and molecular profiles of LS have been published, but there are limited studies on clinically genotype-phenotype correlation in cases series (Chae JH et 2008, Lee et al 2016, Bonfant et al 2016, Ogawa et al 2017, Sofou et al 2018), particularly referred to different clinical finding in cases relatedo to mtDNA or nDNA genoma.

Aim of the study is analyze a series of 103 patients, described clinical and molecular finding and to identify phenotypic features that may differentiate between mtDNA and nuclear DNA (nDNA) associated Leigh syndrome.

Patients and methods

We reviewed the data of all of the 103 clinically, biochemically and/or molecularly LS defined patients present in our “Nation-wide Italian Collaborative Network of Mitochondrial Diseases” database and followed up by the involved paediatric 5 centers.

The database establishment (and its use for scientific purposes) was permitted by the local Ethical Committees of the single centers, which obtained written informed consent from all patients or their tutors, and has been performed in accordance with the ethical standards laid down in the 1964 Declaration of Helsinki. This project has been supported by a Telethon grant (GUP09004).

This is a retrospective study; all the involved centers have specific expertise in mitochondrial disorders. The clinical section of our web-based database includes “yes or no” dichotomic items agreed by all centers in a preliminary consensus phase. The consensus phase was specifically designed to include the clinical features known to be relevant in mitochondrial medicine . Clinical and MRI findings, metabolic results and biochemical profile in muscle homogenate and in cultured fibroblasts have been analyzed to define genotype-phenotype correlations, and highlight differences in phenotypes related to nDNA genes versus mt-DNA genome.

Results

We studied 103 patients (59 male; 44 female) with Leigh pattern at MRI and diagnosed as “Leigh syndrome”

Family history was referred positive in 28 pts, follow up was available in 89, clinical and radiological data was available in all the pts. Biochemical diagnosis performed in 93 and molecular defined in 91.

The median age of onset was 3 months (range: from intrauterine to 6.6 years).

Clinical onset in 79 pts (78%) was before 12 months of age, in 12 pts (12%) from 1 -2 years, in 5 pts (5%) from 2-3 years, in 4 pts (4%) from 3-6 years, only one patient presented clinical onset after 6 years of age.

Most common symptoms at onset were psychomotor delay (45/103 pts), hypotonia (33/103 pts), faiure to thrive (24/103

pts). In 40% of cases , clinical onset was referred associate to trigger factors (e.g. infection, fever). At diagnosis time the most common features were hypotonia and psychomotor delay (83/103), followed by hypertonia and/ or spasticity (60/103), failure to thrive (40/103) and dystonia 39/103). Ataxia and ocular involvement were less common (37/103). Myopathy, epilepsy , peripheral neuropathy were seen in one third of pts (35/103). Only 3 patients suffered from cardiopathy and 2 from hepatopathy (figure 1)

Follow up was available in 89 pts, range from 6 months to 18 years (mean time 6.6 years): outcome was worsened in 55 pts (62%) and stable in 27 pts (30%). Onset after 2 yeasr of age was associate to better outcome.

No significant differences were seen in terms of age of onset, clinical symptoms and signs between these two major groups.

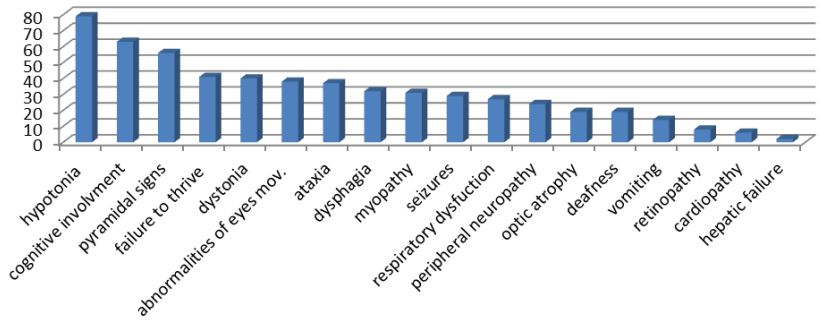

figure 1: clinical findins

Lactate levels were available in 94 pts in plasma and in 30 pts in CSF: was elevated in 61/94 pts in plasma and in 31/40 in CSF. In 8 pts lactate levels were normal.

MRI pattern was divided in 3 subgroups on the basis of different CNS regions involved, related to different functions and signs: 1.sovratentorial (basal ganglia, thalami, subthalami) 2. Sovra and subtentorial (Basal ganglia, Thalami, subthalami, brainstem, dentate nuclei) and 3. Subtentorial (brainstem, dentate nuclei).

MRI lesions were both in sovratentorial and subtentorial grey matter in 68 pts (66%), only sovratentorial in 30 pts (29%), 5 patients presented alteration only in dentate nuclei and/or midbrain grey matter. MRI findings are similar in both nDNA and mtDNA related cases (figure 2a-b)

figure 2a: MRI lesions

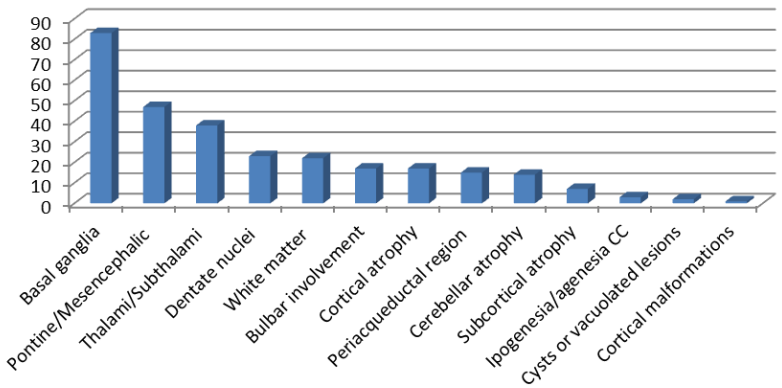

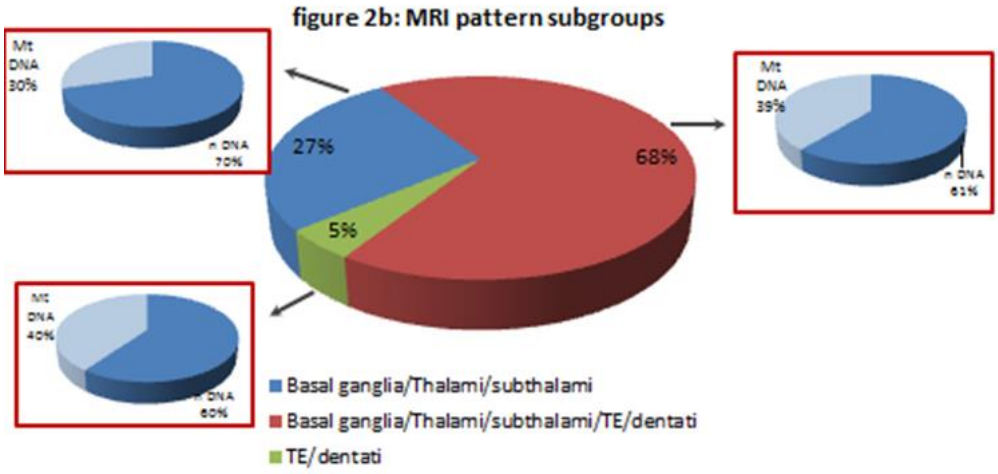

MRI pattern of both sovratentorial (basal ganglia , thalami) and subtentorial (midbrain and nuclei dentate) was observed in 32 pts with diagnosis of complex IV deficit, in 94% of cases associated to nDNA (most common gene involved SURF1, figure 3), in 23 pts with diagnosis of complex I deficit in 73% related to mtDNA (figure 4) , and in 14 pts with mutation MILS/NARP.

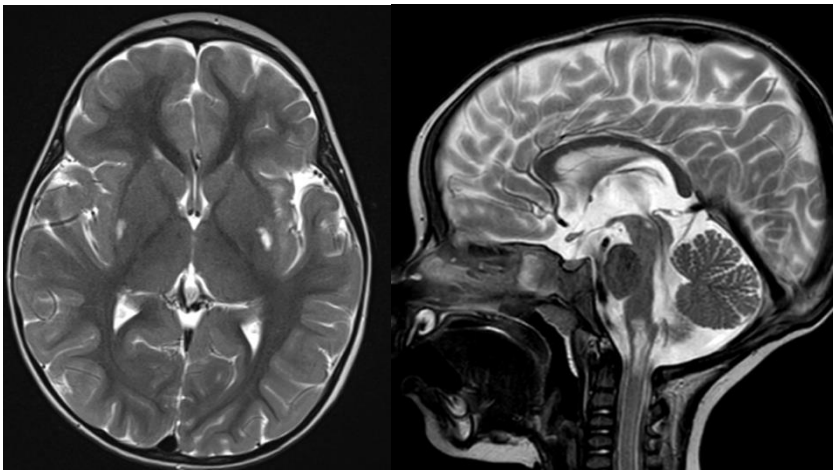

(a) (b)

Fig 3 MRI, axial (a) and sagittal (b) T2 sequence: iperintensity in putamen(a) and midbrain grey matter (b), in SURF1 case

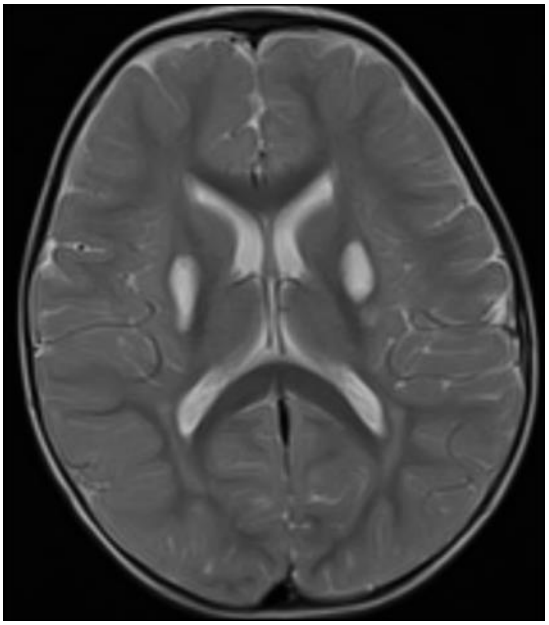

Fig. 4 MRI, axial T2 sequence: iperintensity in putamen, in mtND3 case

Only basal ganglia involvement was observed only in nDNA associated cases (e.g. SUCLA2, SUCGL1, AIFM1, SERAC1, GFM1). MRI was not associate to differences in outcome.

Disease outcome was more sfavorable in SURF1 cases and midbrain involvement at MRI.

Biochemical diagnosis was available in 93 pts; the most common was deficit of complex IV (30/93), followed by complex I (23/93).

Molecular diagnosis was confirmed in 91 pts, in 58 pts (63%) was related to nDNA , in 33 (37%) to mtDNA (table 1).

Nuclear gene more involved was SURF1 (in 21 pts); MILS/NARP mutation was identified in 13 pts , mtDNA gene encoding or complex I (ND1, ND3, ND5, ND6) were disclosed in 15 pts.

Biochemical defect	Molecular diagnosis	Number
	n DNA	**58**
complex I	NDUFA10	1
	NDUFAF6	2
	NDUFS4	3
complex III	TTC19	1
	BCS1L	1
complex IV	SURF1	30
	COX15	1
Complexes I-III-IV	SUCLA2	4
	SUCLG1	1
PDH	PDHA1	7
n.d.	EARS2	1
complexes III-IV	AIFM1	2
complexes I-IV	GFM1	1
complexes I-II-IV	SERAC1	1
none	ECHS1	2
	mt DNA	**33**
complex I	ND1	2
	ND3	5
	ND5	7
	ND6	1
	MTTL1	2
complex IV	COIII	1
nd	MILS/NARP	13
complexes I-III-IV	mtDNA deletion	2

Table 1 : biochemical and molecular diagnosis

Conclusion

Our study included 103 patients with diagnosis of Leigh syndrome diagnosed and followed in five centers in Italy. This is, to our knowledge, the largest phenotype-genotype correlation study in Leigh syndrome to be performed on systematically evaluated patients.

We observed clinical onset before one year of age in 80% of cases. Most common symptoms are hypotonia and psychomotor dealy, in 40% of cases onset is associated to trigger factor.

Lactate level is elevated in the majority of cases, but normality don't exclude diagnosis.

Biochemical diagnosis more common is deficit of complex IV related to nDNA gene SURF1, complex I associated to mtDNA genes and MILS/NARP mutation.

No significant differences were seen in terms of age of onset, clinical symptoms and signs and outcome between mtDNA and nDNA-associated Leigh syndrome groups.

References

- Thorburn DR, Rahman S, Pagon RA, Adam MP, Ardinger HH, etal (1993) Mitochondrial DNA-associated Leigh syndrome and NARP. In: GeneReviews

- Sofou K, De Coo IF, Isohanni P, etal (2014) A multicenter study on Leigh syndrome: disease course and predictors of survival. Orphanet J Rare Dis, 9: 52, 4021638
- Leigh D (1951) Subacute necrotizing encephalomyelopathy in an infant. J Neurol Neurosurg Psychiatry, 1 (14): 216– 221,
- Gropman AL (2013) Neuroimaging in mitochondrial disorders. Neurotherapeutics, 10 (2): 273– 285
- Baertling F, Rodenburg RJ, Schaper J, etal (2014) A guide to diagnosis and treatment of Leigh syndrome. J Neurol Neurosurg Psychiatry, 85 (3): 257– 265,
- Chae JH, Lee JS, Kim KJ, Hwang YS, Hirano M. Biochemical and genetic analysis of Leigh syndrome patients in Korea. Brain Dev. 2008 Jun;30(6):387-90
- Lee JS, Kim H, Lim BC, Hwang H, Choi J, Kim KJ, Hwang YS, Chae JH. Leigh Syndrome in Childhood: Neurologic Progression and Functional Outcome. J Clin Neurol. 2016 Apr;12(2):181-7
- Bonfante E, Koenig MK, Adejumo RB, et al The neuroimaging of Leigh syndrome: case series and review of the literature.Pediatr Radiol. 2016 Apr;46(4):443-51.
- Ogawa E, Shimura M, Fushimi T, et al Clinical validity of biochemical and molecular analysis in diagnosing Leigh syndrome: a study of 106 Japanese patients. J Inherit Metab Dis. 2017 Sep;40(5):685-693
- Sofou K, de Coo IFM, Ostergaard E, et al Phenotype-genotype correlations in Leigh syndrome: new insights from a

multicentre study of 96 patients. J Med Genet. 2018 Jan;55(1):21-27.

Chapter 12

Summary

The aim of my project was to identify the underlying molecular defects in patients clinically and biochemically suspected of MD, using a NGS strategy for mitochondrial diseases diagnosis studing both nDNA and mtDNA and define phenotype-genotype correlation.

We define novel phenotype associated to nuclear gene: leukodystrophy related to mutation in COA7, IBA57, KARS and syndromic optic neuropathy associated to OPA1 and RTN4IP1. The careful clinical evaluation and phenotypic diagnosis required to evaluate on molecular study disclosing intronic variant unrevealed by exome sequencing, sparing the lack of diagnosis. In collaboration with other centers, we define clinical features of a riboflavin responvise MD related to ACAD9, potentially fatal.

The most common phenotype of mitochondrial disease in childhood is Leigh Syndrome. The systematic evaluation and genotype-pheotype correlation defined clinical findings in a cohort of 103 patients and revealed no significant differences in terms of age of onset, clinical symptoms and signs and outcome between mtDNA and nDNA-associated Leigh syndrome groups.

Application of NGS in mtDNA analysis disclosed patogenic mutation in mtDNA unexpected related to the phenotype expanding repertoire of mtDNA mutations in human diseases

and suggests to look for variants in the mitochondrial genome when dealing with otherwise undetermined or novel phenotype.

Conclusions and Future Perspectives

NGS represent a successfully strategy to screen patients with suspected mitochondrial disease to define genetic diagnosis. Sometimes disclose unexpected molecular diagnosis in relation to phenotype.

Correlation genotype-phenotype in this cases will be usefull in the future to design an updated flow chart in diagnosis of mitochondrial disease.